UNIVERSITÀ
DI SIENA
1240

Dipartimento di Medicina, Chirurgia e Neuroscienze

Dottorato in Medicina Traslazionale e di Precisione

38° Ciclo

Coordinatore: Prof. Francesco Dotta

Novel Strategies for Detecting Circulating Biomarkers in Neurodegenerative Disorders

Settore scientifico disciplinare: *MED-26*

Candidata
Righi Delia
Dept. of Medicine, Surgery, and Neuroscience, University of Siena

Supervisore
Prof.ssa Federica Ginanneschi
Dept. of Medicine, Surgery, and Neuroscience, University of Siena

Co-supervisore
Prof. Domenico Plantone
Dept. of Medicine, Surgery, and Neuroscience, University of Siena

Anno accademico di conseguimento del titolo di Dottore di ricerca
2025/26

Università degli Studi di Siena

Dottorato in Medicina Traslazionale e di Precisione

38° Ciclo

Data dell'esame finale

N/A

Commissione giudicatrice

N/A

N/A

N/A

N/A

N/A

Supplente

N/A

Background

Both in terms of absolute numbers and as a percentage of the global disease burden, the prevalence of neurological disorders has sharply increased over the last decades. The aging of the world's population and general population growth are the two interrelated demographic trends that are primarily responsible for this increase. Age-related neurological conditions, such as neurodegenerative diseases like Alzheimer's disease, Parkinson's disease, and amyotrophic lateral sclerosis, as well as cerebrovascular diseases and other chronic neurological disorders, are becoming more common as life expectancy rises, partly due to improvements in public health and medicine [1].

The importance of preventive medicine has grown in this changing epidemiological environment. In addition to lowering the prevalence of neurodegenerative disorders, preventive measures are crucial for delaying their onset, reducing their rate of progression, and improving. A multifaceted strategy is necessary for effective prevention, including tertiary prevention (managing disease progression and complications), secondary prevention (early detection and intervention), and primary prevention (targeting risk factors prior to disease onset) [2].

However, several significant challenges hinder the development of effective prevention strategies. Therefore, the development of early detection methods is urgently needed in neurodegenerative diseases, as they often remain clinically asymptomatic in their initial stages [3]. Additionally, the diversity of these diseases—both in their underlying mechanisms and clinical manifestations—complicates the identification of universal risk factors and preventive strategies. To address these challenges, innovative approaches are needed to improve our ability to predict, diagnose, and treat neurodegenerative conditions. Finding and validating new circulating biomarkers is one of the most promising ways to advance early detection and prevention. Biomarkers are quantifiable markers of pathogenic conditions, biological processes, or therapeutic response. Circulating biomarkers, such as proteins and metabolites, can be found in blood or cerebrospinal fluid.

Blood matrix is composed of various blood cells suspended in plasma. Plasma is composed of approximately 55% of blood fluid in humans and constitutes glucose, proteins, hormones, minerals while serum is the fluid and solute component of blood without fibrinogens [4]. Cerebrospinal fluid (CSF) is the secretion fluid of the central nervous system (CNS), and approximately 80% is produced by the choroid plexus that occupies the ventricles of the brain, subarachnoid space, and spinal cord [5]. While both matrices are used, precision approach in neurodegenerative disorders, has prioritized blood-based biomarkers for their minimally invasive sampling and dynamic monitoring capabilities.

Aim of the thesis

In order to characterize the neurodegenerative pathway from its earliest stages through disease progression across a spectrum of neurodegenerative disorders, our research aims to identify and characterize biomarkers that track neurodegenerative processes from the earliest preclinical stages through advanced disease. A key focus is discovering circulating biomarkers, which could enable earlier intervention and pave the way for personalized medicine [6]. By detecting biomarkers before clinical symptoms appear, we can enhance prognostic accuracy and ultimately improve therapeutic outcomes. We aim to shift the paradigm of managing neurodegenerative diseases from reactive to proactive, as shown in **Figure 1.**

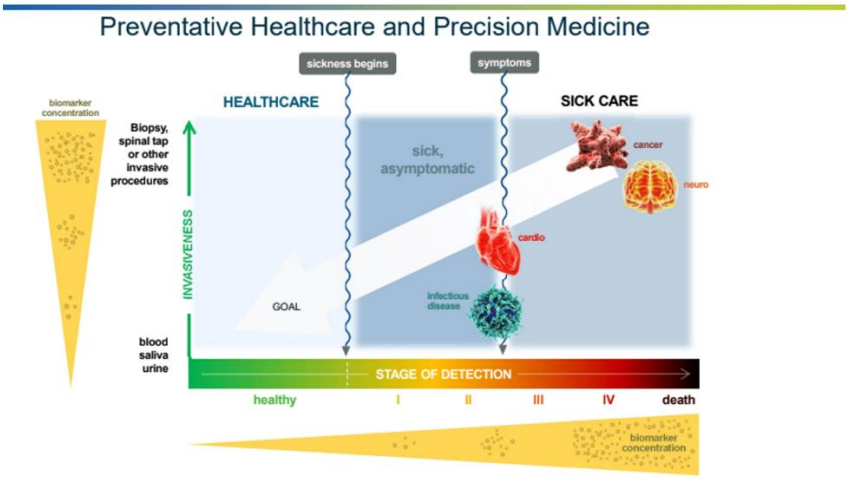

Figure 1. Identifying disease before symptom onset enables proactive disease management and enhances treatment outcomes through early intervention strategies.

The objective is to establish a robust framework for the early identification of diseases prior to the onset of symptoms. By focusing on pre-symptomatic detection, has the potential to transform disease management, enabling a shift from reactive to proactive strategies. This paradigm not only enhances the potential for early intervention but also significantly improves the prospects for successful treatment outcomes. Implementing such a framework would rely heavily on the development and utilization of advanced biomarkers and diagnostic tools, which can provide critical insights into the earliest stages of disease progression. This approach underscores the necessity of investing in cutting-edge research and technology to pave the way for innovative healthcare solutions. The focus of this PhD program was to investigate potential future biomarkers. By identifying these biomarkers, we aim to gain a deeper understanding of the pathways involved in neurodegeneration and neuroinflammation. This knowledge is crucial as it can lead to earlier detection and intervention, ultimately transforming the approach to managing and treating these complex conditions. Focusing on biomarkers offers a promising avenue for developing targeted therapies and improving patient outcomes, thereby making a significant impact on global healthcare efforts.[1]. Neurodegenerative diseases are characterized by a complex and heterogeneous pathological mechanisms, making early and accurate diagnosis challenging. Among the proteins analyzed, our study has focused particularly on neurofilament light chain (NfL), glial fibrillary acidic protein (GFAP), growth differentiation factor-15 (GDF-15), TAR DNA-binding protein 43 (TDP-43), and peripherin (PRPH). These molecules are capable of serving as biomarkers, and in last years have been attracted considerable interest due to their well-documented

associations with critical neurodegenerative and neuroinflammatory pathways. Each will be examined individually in the following sections**.**

To accomplish this, an interdisciplinary strategy, longitudinal research, and molecular analyses is needed to find biomarkers that can differentiate between neurodegenerative and neuroinflammatory processes, detect early pathological changes, and ultimately improve patient outcomes. This thesis is organized in chapters, each addressing a distinct aspect of biomarker research in neurodegenerative and neuroinflammatory disorders. Chapter 1 introduces the key biomarkers analyzed, examining their roles in neurodegeneration pathway. Chapter 2 evaluates the correlation between CSF and serum biomarker levels assessing whether serum measurements can serve as reliable surrogates for CSF concentrations. Chapter 3 compares two detection platforms, SiMoA and Ella, to determine reliability in biomarker detection. Chapter 4 explores the role of biomarkers in different disorders, analyzing their concentrations levels in different clinical settings. Finally, Chapter 5 presents an innovative study using a homebrew SiMoA-based assay. Collectively, these chapters provide a comprehensive and multidisciplinary perspective to enhance the early detection and monitoring of neurodegenerative diseases.

CHAPTER 1- BIOMARKERS

Accurate detection and prognostic evaluation of specific protein levels are essential for early diagnosis, disease monitoring, and therapeutic stratification. Over the past decade, there has been a marked increase in interest toward biofluid-based biomarkers, driven by their potential for minimally invasive assessment and clinical applicability. In this context, the systematic investigation and validation of biofluid biomarkers not only enhance our understanding of the underlying mechanisms of neurodegeneration and neuroinflammation but also pave the way for the development of non-invasive, cost-effective diagnostic and prognostic tools. Such tools are essential for improving patient outcomes and facilitating the translation of research findings into clinical practice. Among the most well-established and validated biomarkers are neurofilament proteins (Nf), which serve as fundamental structural components of the neuro-axonal cytoskeleton. When measured in biofluids, neurofilament proteins have emerged as robust and dependable indicators of neurodegenerative processes, offering critical insights into disease progression and neuronal injury [7] as shown in **Figure 2.**

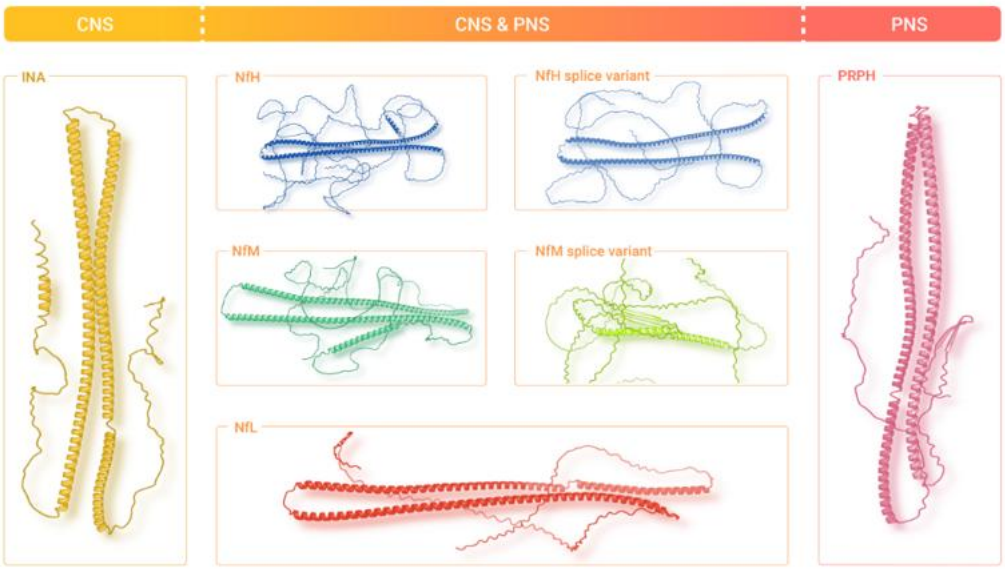

Figure 2. Summary of the Neurofilament variant. The figure shows the seven variants of Nf: Nf light (NfL), two variants of Nf medium (NfM), two variants of Nf heavy (NfH), α-internexin (INA), and PRPH (peripherin).

Neurofilaments' (Nf) genetic and epigenetic profiles highlight their critical function in oncology and neurodegenerative diseases. As shown in **Figure 2**, Nf present an heavy (NfH), medium (NfM), and light (NfL) chains, which are structurally and functionally different proteins that are expressed in the CNS and peripheral nervous system (PNS). These subunits are encoded at specific loci on the genome: NfH is found on Chromosome 22 (29480218.0.29491390), whereas NfM and NfL map to Chromosome 8 at positions (24913761.0.24919093) and (24950955.0.24956612) respectively, as shown in **Table 1**. In addition to supporting cytoskeletal integrity, their differential expression and post-translational changes are important indicators of axonal damage and the advancement of disease [7].

	NfH	NfM	NfL	INA	PRPH
Chromosome	22	8	8	10	12
Gene location	29,480,218–29,491,390	24,913,761–24,919,093	24,950,955–24,956,612	49,295,147–49,298,686	49,295,147–49,298,686
Length 1[a]	1020	916	543	499	470
Length 2[b]	924	540	–	–	–
Weight 1 (Mw)[c]	112477.56734 ± 7.23404	102470.81258 ± 6.54664	61400.80804 ± 3.95853	55389.99135 ± 3.54851	53650.26292 ± 3.46054
Weight 2 (kDa)[d]	105.6	102.5	61.5	55.4	53.7
Weight 3 (kDa)[e]	190–210	150	68	66	57
Charge[f]	−11	−64	−49	−14	−15
Phosphorylation	+++[g]	++	+	+	+
O-glycosylation	++	++	+	–	–
Genetic risk for	ALS/SMA, CMT	ALS, PD	ALS, CMT	PD, LBD	ALS

Table 1. Summarized all the differents Neurofilament variant, including characteristics as chromosome location, gene location, lenght of the protein, weight, charge, phosphorylation, O-glycosylation and genetic risk for.

The structural and functional properties of the neurofilament protein family are regulated by a variety of post-translational modifications, including phosphorylation, citrullination, glycosylation, and acetylation. Phosphorylation, which occurs at specific amino acid residues in the neurofilament subunits, primarily threonine, serine, and tyrosine, is the most obvious and physiologically significant of these alterations. This process is catalyzed by proline-directed kinases and mainly targets the C-terminal tail domain, which is rich in KSP (Lys-Ser-Pro) repeats. [8] Numerous factors, such as immunogenicity, solubility, proteolytic resistance, and axonal caliber, are impacted by phosphorylation in neurofilament dynamics.

By adding negative charges along the neurofilament sidearms, phosphorylation causes electrostatic repulsion and increases inter-filament spacing. [9]. This charge-mediated expansion directly modulates axonal diameter, an important determinant of nerve conduction velocity and neuronal integrity. During development, myelination and neurofilament phosphorylation correlate, suggesting a role in the axonal cytoskeleton's maturation and stabilization. Additionally, phosphorylated neurofilaments are more resilient to protease degradation. [5] which could be a factor in their buildup in diseased states. Additionally, phosphorylation modifies the immunogenicity of neurofilaments, which may impact autoimmune reactions in neurodegenerative and oncological settings[10], [11]. These changes are important in both physiological and pathological conditions because they not only improve cytoskeletal organization but also act as biomarkers for axonal damage and the advancement of disease.

At first, it was thought that neurofilaments (Nf) had a limited structural function in living things. Although this fundamental viewpoint is still relevant, later studies have significantly increased our comprehension of their functional diversity. It is now known that neurofilaments are multipurpose proteins that control a wide range of biological functions. Among these is adjusting the action potential conduction velocity influencing the axonal diameter [12] mediating aldosterone secretion [13],and directly influencing axonal caliber [14], [15]. Nf takes part in axonal flow and stasis in addition to structural contributions [16] and axonal transport [17]. Additionally, their epigenetic expression is disregulated in cancer cells, including breast cancer and sarcoma cells [18] [19].

Furthermore, neurofilaments have played a pivotal role in the evolution of the nervous system across species [15], interact with mitochondria [20] [21] and myelin proteins [22], and contribute to mechanical stability [23] and endoplasmic reticulum modulation [23]. Their functional repertoire extends to ontogenetic development [24] synaptic modeling [25]and the startle response through presynaptic terminal activity. Additionally, Nf influences the viscoelastic properties of cells [26]; [27],

underscoring their integral role in both neuronal function and cellular biomechanics, as shown in **Figure 3** [7]. This expanding body of evidence highlights the pleiotropic nature of neurofilaments in physiological and pathological contexts, in fact Nf isoforms align in parallel to form dimers, which then align antiparallelly to form tetramers, forming the neurofilament heteropolymer. After that, these tetramers come together to form filaments of a certain length.

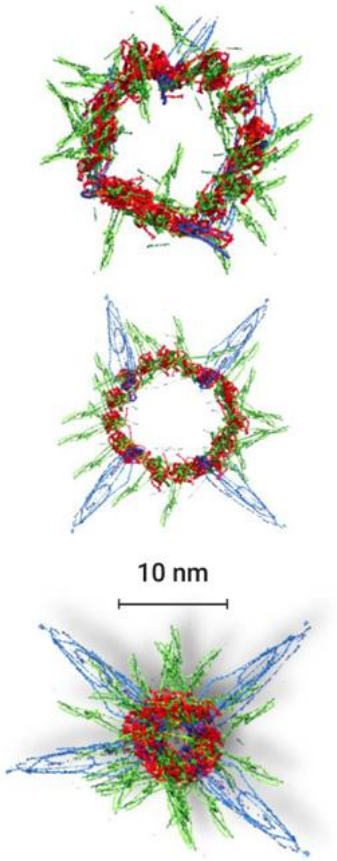

Figure 3 shows neurofilament as crucial structural elements of the cytoskeleton of the neuro-axon. Radial compaction (sagittal view) of the 16 nm diameter of the forming unit length Nf to the final diameter of 10 nm in three different stages (measurements has been done by Pymol; = 10.2 Å).

Neurofilament Light Chain (NfL)

NfL is one of the Nf family, has undergone a great deal of validation and is now widely recognized as a biomarker of neuronal integrity. NfL plays a crucial part in the pathophysiology of neurodegenerative diseases by reflecting axonal damage and neuronal injury. [28]. Since NfL is expressed in both CNS and the PNS, it is not disease-specific and can be found in a wide range of neurological disorders.[29]. NfL is a cytoskeletal protein that gives neurons structural stability. It is highly expressed in axons, dendrites, and neuronal soma [29]. Notably, NfL promotes radial axonal growth, especially in large myelinated axons. Low amounts of NfL are constitutively released from

axons under physiological conditions, most likely in an age-dependent manner, with higher concentrations observed in older individuals [29] Nevertheless, NfL release into the bloodstream dramatically increases after neuronal or axonal damage, whether brought on by inflammatory, neurodegenerative, or traumatic insults. After being released, NfL diffuses into the interstitial fluid, which then reaches the CSF and, eventually, the bloodstream, where its concentration is about 40 times lower than that of the CSF [29]. NfL has become a clinically significant biomarker for tracking the course and severity of disease because it can be detected in biofluids. Following the creation of the first immunoassays that could identify NfL in CSF, the use of NfL as a biomarker gained popularity in the 1990s. The methodical investigation of NfL concentrations in a variety of neurological disorders was made possible by this technological breakthrough. NfL has emerged as a crucial marker of neurological decline due to its association with disease severity, where higher levels are linked to faster progression and lower patient survival. [30] Also, since they accurately reflect the course of disease, NfL is being incorporated into diagnostic frameworks increasingly. In addition to the well-known astrocytic activation marker, GFAP, NfL has been added to the updated Alzheimer's disease (AD) guidelines as a biomarker of non-specific processes involved in AD pathophysiology [31]. NfL is clinically relevant, but it lacks disease specificity, as its levels rise in a variety of neurological conditions that impact the CNS and the PNS. This makes it more difficult for it to distinguish between different diseases, which makes it difficult to use as a prognostic or diagnostic biomarker for a particular disease.

Glial Fibrillary Acidic Protein (GFAP)

Another well-known biomarker is GFAP, which is an intermediate filament protein with a high degree of expression in astrocytes and has been recognized as a strong biomarker of astrocytic activation and injury [32].GFAP is a member of the family of Intermedite Filaments (IFs), that comprise the cytoskeleton of the majority of eukaryotic cells, along with microtubules and microfilaments. Their filamentous form is in beteween 8–12 nm thick microtubules 25 nm and thin actin microfilaments 7 nm. Together with vimentin, desmin and PRPH are classified as type III IFs protein [33]. The human GFAP gene, located on chromosome 17q21, includes nine exons and alternative splice variants, with mutations linked to Alexander disease (AxD)[34]. Nine exons and eight introns comprised the human GFAP gene. Alternative splicing results in transcripts of different lengths, including the novel exons 7a and 7b. GFAP α isoform is the predominant isoform expressed in CNS, the first to be identified and the most studied, along with seven other splice variants, except for GFAPβ, which has only been reported in the rat CNS. These variations include GFAPγ, which lacks most of exon 1 but has a segment of intron 1; GFAPδ, which has a conserved 41-amino-acid C-terminal tail and a novel exon 7a that replaces exons 8–9; and GFAPκ, which is comparable to GFAPδ but includes exon 7b, which is derived from intron 7 [35]. Expression is regulated by developmental, injury, and epigenetic factors, with increased levels during aging and gliosis. It’s mainly expressed in CNS astrocytes and some

peripheral glia, in particular, in non-myelinating Schwann cells of the PNS and in enteric glial cells within the enteric nervous system (ENS) [36].

GFAP isoforms suggest specialized functions in neural stem cells and reactive astrocytes. Its dynamic regulation highlights its importance in CNS disease. GFAP function mainly involved cell motility and migration. Moreover, GFAP is known to influence mitosis by modulating filament assembly within the cell. The assembly process of GFAP is controlled through the phosphorylation and dephosphorylation of its 'head' domain, which changes the domain's charge.

Mitosis is characterized by a rise in phosphorylated GFAP levels, along with the relocation of this modified protein to the cleavage. A characteristic alteration in the function of astrocytes in a variety of neurological conditions, including neurotrauma, ischemic stroke, and neurodegenerative disease, reactive astrogliosis impacts the course of disease as well as the recovery process [37]. Many CNS diseases show heightened GFAP levels including traumatic, degenerative, vascular, and autoimmune disorders of the CNS, typically considered a secondary response to neurodegeneration [38], [39], [40]. As it happens with NfL, also GFAP, once the astrocytes are damaged, GFAP is released in blood. In addition to serving as a biomarker of astrocytic injury, GFAP contributes to neuroinflammatory stimulation through the release of cytokines, inflammatory mediators, nitric oxide, and reactive oxygen species (ROS), thereby promoting redox status imbalance [41]. GFAP has been chosen as biomarker of astrogliosis and neuroinflammtion in different neurodegenerative disorders as AD, and recent finding suggests that maybe occur before other well-know pathogenesis [42]. Its detection in CSF, but also in blood following astrocytic damage makes GFAP a valuable tool for monitoring disease progression assessing treatment responses in clinical and research settings. The ability to detect GFAP in CSF and blood following astrocytic injury positions it as a valuable biomarker for monitoring disease progression and evaluating therapeutic responses in clinical and research contexts.

As NfL, GFAP challenges for biomarker specificity, as its levels elevate across a broad spectrum of CNS disorders, limiting its capacity to differentiate between distinct pathologies, making difficult to use it as biomarker of sensitivity.

Growth Differentiation Factor-15 (GDF-15)

GDF-15 is a systemic molecule that is becoming more and more significant in neurological disorders and serves as a link between different biological processes or pathogenic processes and cellular stress responses. GDF-15 belongs to the bone morphogenetic protein-like group's transforming growth factor (TGF)-β subfamily. Several cell types express GDF-15, which is also known as macrophage inhibitory cytokine (MIC)-1, non-steroidal anti-inflammatory drug-inducible gene (NAG)-1, placental transforming growth factor-beta (pTGFB), prostate-derived factor (PDF), and placental bone morphogenetic protein (PLAB) [43]. The N-terminus is cleaved and released as α≈30kDa disulphide

linked dimeric active protein form [44]. GDF-15 can be found in the blood, but its levels are different based on age and sex. Biologic age is related to several markers such as oxidative stress, protein glycation, inflammation and hormonal changes [45]. It is abundant in both the central and peripheral nervous systems, with particularly elevated concentrations in the choroid plexus. This region secretes GDF-15 into CSF, being also damaged neurons and microglial cells responsible for its production within the CNS [46].

GDF-15 inhibit the NF-kB pathway, it contributes to the promotion of angiogenesis, the enhancement of hippocampus neurogenesis, the improvement of synaptic activity, the reduction of cell apoptosis, and the modulation of inflammatory responses, especially in the regulation of innate immunity. It has been investigated in various neurological and non-neurological disease states, is responsive to mitochondrial stress, and increases with age and age-related pathologies. [47]. GDF-15 has a good diagnostic performance separating neurodegenerative disease from healthy controls, demonstrating a good high sensitivity of 0.90 and a specificity of 0.77. According to these results, GDF15 levels could be a useful biomarker for neurodegenerative diseases. Additionally, a number of studies have shown a correlation between elevated GDF15 levels and Lewy body dementia, AD, cognitive decline, and PD [48].

Its exact function its not completely understood, in fact, GDF-15 may be involved in inflammatory processes in addition to mitochondrial dysfunction. Notably, Machado and colleagues show that in a mouse model of Parkinson's disease, GDF15 has been demonstrated to be essential for the neuroprotection of dopaminergic neurons [49]. On the other hand, research has indicated that GDF15, is upregulated in response to lesion and systemic injury in CNS, behaving as anti-inflammatory cytokine network [50]. Additional studyes will need to elucidate the role of GDF15 in CNS and its implications for neurological disorders.

Tar DNA-Binding Protein (TDP-43)

TDP-43 is an intranuclear protein that is involved in RNA splicing, trafficking, stabilization, and, consequently, gene regulation expression. Cellular disfunction leads to inclusion bodies in the cytoplasm that contain truncated and phosphorylated versions of TDP-43. TDP-43 is a 43 kDa heterogeneous nuclear ribonucleoprotein (hnRNP) consisting of 414 amino acids, encoded by the *TARDBP* gene located on chromosome 1 at position 1p36.22. One of the main contributing factors to its pathogenic mechanisms may be TDP-43 dysregulation. Studies have shown that TDP-43 is autoregulated through a negative feedback loop in which it binds to its own mRNA transcript's 3' untranslated region, causing it to become unstable [51]. TDP-43 inclusions are the hallmark in amyotrophic lateral sclerosis (ALS) pathology and in a subset of frontotemporal lobar degeneration (FTLD), but in recent years Up to 57% of AD cases have been found to have TDP-43 inclusions, which primarily show a limbic distribution in both cases with and without concomitant hippocampus

sclerosis. The loss of function of TDP-43 is linked to neurodegeneration. Notaby, it has been demostrated by Vatsavayai and colleagues that in humans with C9ORF72-linked FTLD the lost of nuclear TDP-43 and the subsequent cytoplasmic aggregation appears even before symptoms [52]. In particular, neuronal atrophy can be induced by the mere lack of nuclear TDP-43 [53], indicating that this loss may be an early pathological event that contributes to neurodegeneration.

Moreover, TDP-43 is involved in secondary comorbid pathology in AD. In fact, disruption of TDP-43, which moves from the nucleus to cytoplasm, causes it to lose ist ability to perform vital physiological functions, as RNA splicing. However, as AD progresses, pathological events leads to TDP-43 aggregation insolublely. The loss of TDP-43's regular physiological functions and the acquisition of toxic qualities linked to its pathological forms could be the two mechanisms causing the ensuing neurodegeneration [54]. It's role in neurodegeneration has been largely assessed in different neurological disorders, but it's precise mechanism by which TDP-43 contribute to disease remain incompletely understood.

Peripherin (PRPH)

PRPH is an intermediate filament protein of class III that has recently garnered attention as a potential biomarker for axonal damage in the peripheral nervous system [55], [56]. This interest arises from its distinct expression pattern, which is predominantly found in the spinal cord ventral horn, alpha motor neurons, and primary afferent sensory neurons in the dorsal columns [57], [55]. Evidence in the literature supports the role of PRPH in neurite growth, potentially aiding in the recognition of axonal pathways after the migration phase of neural crest cells and following neuronal injury [58], [59]. It also plays a role in neurite stability, particularly in long myelinated neurons [60], [61]. Although the precise functions of PRPH are not fully understood.

PRPH expression is mainly localized in the ventral horn motor neurons of the spinal cord and is distributed in the sciatic nerve, autonomic ganglionic and preganglionic neurons, and sensory neurons [62]. Also, expression in the CNS is predominantly found in the brain stem, optic tract, and internal capsule. In particular, it was found in the nerve fibers and nuclei connected to cranial nerves V through XII. It is also found in the cell bodies and axons of the mesencephalic trigeminal nucleus, the pars compacta region of the nucleus ambiguus, and fibers that make up the descending spinal trigeminal tract, the solitary tract, and the trigeminal and facial nerves [63]. Moreover, PRPH positive fibers were observed in the inferior cerebellar peduncle and the folia of the intermediate zone of the cerebellum [64]. Additionally, Boitard et al., found PRPH expression in pancreatic islet beta- cells and interestingly, autoreactive B cells characterized by a specific immune response to PRPH have been demonstrated to

have a significant role in the non-obese diabetic mouse model, representing a heterogeneous population proliferating as diabetes develops [65], [66]

Various cytokines regulate PRPH expression and post- transcriptional modifications, such as Neuronal Growth Factor (NGF) [67], IL- 6 [68], and fibroblast growth factor (FGF) [69] In particular, Aletta and his colleagues, described how NGF has been shown to regulates PRPH phosphorylation, both in the presence and absence of protein kinases A and C, thereby influencing its solubility and dynamic properties, and ultimately, its function in network organization. [67]Moreover, Sterneck et al explores the mechanisms of IL-6 inducing PRPH expression in pheocromocitoma cells (P12). They discovered that IL-6 and NGF work sinergetically together enhancing tyrosine phosphorylation inducing PRPH expression in P12 cells[68]. Other post- transcriptional modifications were highlighted as acetylation, nitration and methylation but the significance is not entirely understood [70]; [7][71].

Moreover, variuos study demostrate that PRPH interact with different type of proteins including Ras-related protein Rab- 7a, a small GTPase, which is involved in late endocytotic compartments [72], or Adaptor protein complex 3 (AP- 3) [73], which is a multi-subunit protein plays a crucial role in intracellular trafficking, transporting membrane proteins to lysosomes and lysosome-related organelles, and Synaptosome Associated Protein 25 (SNAP- 25) interacting protein 30 (SIP30), which is a neuronal protein involved in receptor-dependent exocytosis involved in SNAP receptor- dependent exocytosis [74] . PRPH is associated with vesicular trafficking and axonal transport-related proteins, indicating its direct involvement in neurite outgrowth and axonal pathfinding. In particular, it may promote the formation and regeneration of axonal connections during neural crest migration and in response to neuronal damage, suggesting a potential role in neuronal repair and plasticity.

Moreover, PRPH is associated with the soluble form of amyloid-beta precursor protein (sAPP). After the protein cleavage, PRPH binds to the N-terminal of the protein, helping to locate sAPP. This indicates that PRPH neurofilaments are crucial for the localization of APP fragments [75]. Also, Susennon and colleagues, shows that PRPH protein aggregation is induced by protein kinase C (PKC) in cultured neuroblastoma cells. The formation of aggregates was coupled to an increased apoptosis, suggesting a possible interaction between these two events. [76]. Given its predominant localization in PNS, PRPH can be considered to have a significant potential as a biomarker for PNS-related disorders. However, further studies are essential to fully validate its clinical utility. Although, interest in neurological biomarkers continues to grow, significant challenges persist—particularly in the standardization of measurement techniques. Key unresolved issues include defining age-, sex-, and disease-specific cutoff thresholds to ensure precise and reliable biomarker quantification and interpretation.

CHAPTER 2- COMPARISON CSF/SERUM

The following study aims to investigate the correlation between CSF and serum levels of NfL, GFAP, and TDP-43 in AD patients to determine whether serum measurements can serve as reliable surrogates for CSF concentrations and to characterize their interrelationships in AD pathology. This project is currently unpublished.

Methods

Sample collection

CSF was collected through lumbar puncture at L3/L4/L4/L5 (8:00–10:00 a.m., after overnight fasting). 10–12 mL and centrifuged (2,000 rpm, 10 min, 4°C), aliquoted (0.5 mL), and stored at -80°C. While serum was collected after venipuncture into gel-separator tubes, centrifuged (3,000 rpm, 10 min, room temperature), aliquoted, and stored at -80°C.

NfL, GFAP and TDP-43 assay

The following project used the ultrasensitive SiMoA technology (SR-X instrument) to quantify biomarkers in both CSF and serum samples. Demographic and clinical characteristics were summarized using the number of patients, median values, and interquartile ranges (25th–75th percentiles) to provide a comprehensive overview of the study population. The normality of NfL, GFAP, and TDP-43 measurements—obtained via the Simoa platform—was assessed using the Shapiro–Wilk test. In instances where the assumption of normality was violated, data were logarithmically transformed (Log10) in accord with established methodological guidelines [77].

Statistical Analysis

A non-parametric, one-tailed Spearman correlation analysis, adjusted for age as a covariate, was conducted to evaluate the relationship between biomarker levels in CSF and serum. This approach was selected due to its robustness in handling non-normally distributed data. ANCOVA models were employed to compare levels of TDP-43, NfL, and GFAP between AD cohorts and HCs. For NfL and GFAP, age and sex were included as covariates, based on evidence from prior studies [78]. Binomial regression models were utilized to assess the discriminatory performance of serum NfL and GFAP (with age and sex as covariates) and TDP-43 in distinguishing between AD cohorts and HCs. This analysis aimed to evaluate the potential diagnostic utility of these biomarkers. When correlation analyses yielded statistically significant results, Passing–Bablok regression analysis—a non-parametric method—was performed to evaluate the agreement between biomarker measurements in CSF and serum.

The slope of the regression line was interpreted as an indicator of the relationship between variations in the two biofluids. Statistical significance was defined as a p-value < 0.05 for all analyses. All statistical analyses were conducted using Jamovi Software (The Jamovi Project, 2021) and RStudio, ensuring rigorous and reproducible data processing.

Results

In this retrospective study, AD patients were categorized into three distinct cohorts for analysis. The first cohort, designated as the NfL/GFAP cohort, included 87 AD patients, while the second, referred to as the TDP-43 cohort, comprised 105 AD patients. Within the TDP-43 cohort, both CSF and serum levels of TDP-43 were measured. Consequently, all 105 patients were included in analyses comparing serum TDP-43 concentrations with those of HCs, whereas only 85 patients with CSF TDP-43 levels above the LLOQ were considered for correlation analyses. For HCs, 50 individuals were included in comparison with the NfL/GFAP cohort, and 33 individuals were identified for the TDP-43 cohort. Additionally, a subsample of 63 AD patients, common to both cohorts, was selected for comprehensive correlation analyses of all biomarkers—NfL, GFAP, and TDP-43—in both CSF and serum. None of the patients in this subsample had CSF TDP-43 levels below the LLOQ. Demographic values of each cohort are presented in **Table 2.** Serum levels of NfL and GFAP in AD patients were significantly elevated compared to HCs, with both biomarkers demonstrating p-values < 0.001 (**Figure 4**).

	NfL/GFAP cohort	TDP-43 cohort	All biomarkers cohort	NfL/GFAP Healthy controls cohort	TDP-43 Healthy controls cohort
Number patients (Female/male)	87 (49/38)	105 (59/46)	63 (35/28)	50 (32/18)	33 (15/18)
Median Age (years, 25^{th}–75^{th} percentile)	75 (70–80)	75 (71–80)	75 (71–80)	68 (64–74)	58 (37–69).

Table 2. Descriptive analysis of demographic data in NfL/GFAP cohort, TDP-43 cohort and all biomarkers cohort.

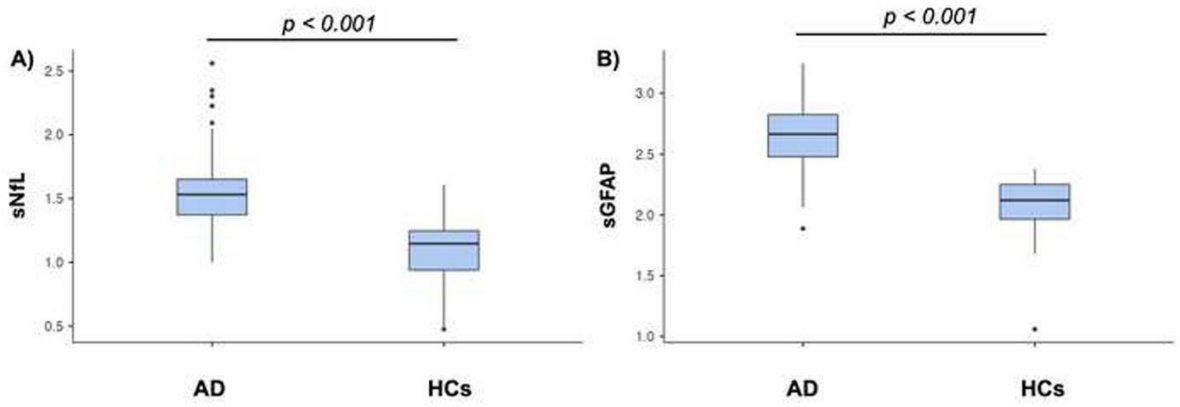

Figure 4. Box-plots of serum NfL and GFAP levels in AD patients and HCs. Panels A) comparison of serum NfL levels between AD and HCs, panel B) comparison of serum GFAP levels between AD and HCs. Box plots express the first (Q1) and third (Q3) quartiles by the upper and lower horizontal lines in a rectangular box, in which there is a horizontal line showing the median. The whiskers extend upwards and downwards to the highest or lowest observation within the upper (Q3+1.5 × IQR) and lower (Q1 - 1.5×IQR) limits. p-values indicate statistical significance between the different groups.

Strong and statistically significant positive correlations were observed between CSF and serum levels for both NfL ($r = 0.5$, $p < 0.001$) and GFAP ($r = 0.4$, $p < 0.001$). But no correlation was found between CSF and serum TDP-43 ($p = 0.378$). Additionally, CSF NfL correlated positively with CSF GFAP ($r = 0.5$, $p < 0.001$), while serum NfL showed a positive correlation with serum GFAP ($r = 0.5$, $p < 0.001$). A moderate but significant correlation was also detected between serum NfL and CSF GFAP ($r = 0.3$, $p = 0.006$). Age was found to be positively correlated with both CSF ($r = 0.3$, $p = 0.02$) and serum NfL ($r = 0.3$, $p = 0.008$), whereas no significant correlation was observed between age and CSF or serum GFAP levels. Passing–Bablok regression analysis revealed linear relationships between CSF and serum measurements, with slopes of 0.01 for NfL ($y = 21.6 + 0.01 \times x$) and 0.02 for GFAP ($y = 306 + 0.02 \times x$) (**Figure 5**). Binomial regression models confirmed the diagnostic utility of serum biomarkers, with serum NfL (AIC 111.8) and GFAP (AIC 67.6) both demonstrating statistical significance ($p < 0.001$). Serum NfL explained 42–58% of the variance, exhibiting a specificity of 81%, sensitivity of 82%, and an area under the curve (AUC) of 0.90, while serum GFAP accounted for 58–80% of the variance, with an AUC of 0.96, specificity of 90%, and sensitivity of 92% (**Figure 6)**.

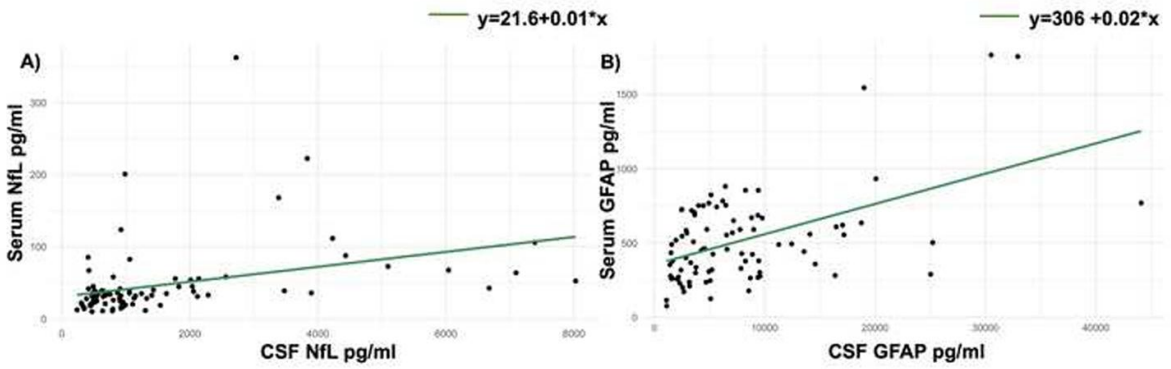

Figure 5. Passing-Bablok regression analysis of biomarkers. Panel A) shows the regression line for NfL (y=21.6+0.01*x), while panel B) shows the regression line for GFAP (y=306+0.02*x). The scatter plots with regression lines illustrate the agreement between CSF and serum measurements.

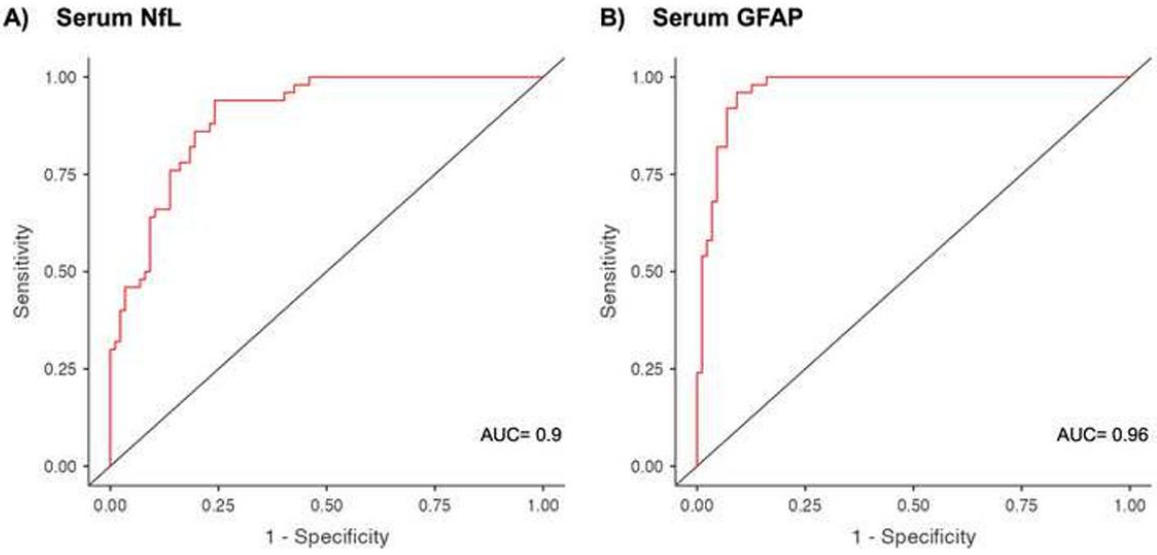

Figure 6. ROC curves for serum biomarker performance in distinguishing AD patients from HCs. (A) ROC curve for NfL, with an area under the curve (AUC) of 0.90, specificity of 81%, sensitivity of 82%. (B) ROC curve for GFAP, with an AUC of 0.96, specificity of 90%, and sensitivity of 92%. The curves illustrate the diagnostic accuracy of serum NfL and GFAP levels in differentiating AD patients from HCs, with sensitivity plotted against 1 – specificity.

Discussion

Our results show a moderate correlation between serum and CSF levels of NfL and GFAP, with CSF concentrations substantially higher as 33-fold for NfL and 15-fold for GFAP as compared to their serum counterparts. On the other hand, TDP-43 did not exhibit a similar pattern, suggesting distinct kinetic

pathways. The presence of NfL, and GFAP, are attributed to mechanisms such as blood-brain barrier (BBB) transport, glymphatic clearance, and renal excretion. Previous studies, including those by Andersson et al. [79], Halbgebauer et al. [80], and Wojdała et al. [81] have similarly documented strong correlations between CSF and serum/plasma NfL in AD patients, although the magnitude of concentration disparities differed (with a Rho of Spearman of 0.7) as did the specific characteristics of the study cohorts. While GFAP correlations between CSF and serum are less documented, existing literature in multiple sclerosis (MS) and neuromyelitis optica spectrum disorder (NMOSD) [82], [83] suggests a 51.5-fold higher CSF GFAP concentration than in serum, might be due to the influence of blood volume, degradation processes, and BBB dynamics on biomarker distribution.

The lack of correlation for TDP-43 between CSF and serum underscores its limited utility as a surrogate marker for CNS pathology. This aligns with findings from Kasai et al. [84] and Álvarez-Sánchez et al. [85], where TDP-43 serum levels in AD patients did not differ significantly from HCs, contrasting with its elevated levels in frontotemporal dementia (FTD). Feneberg et al. [86] suggested that CSF TDP-43 is predominantly blood-derived, with CSF levels approximately 200-fold lower than serum levels when assessed by Western blot technique.

Serum NfL and GFAP reflects the rate of active neurodegeneration, with binomial regression models demonstrating high diagnostic accuracy (AUC > 0.90), sensitivity (>80%), and specificity (>80%), consistent with prior reports by Wojdała et al. [87]. These results remained robust under internal validation using 5,000-iteration bootstrap resampling.

No comparable studies in the literature were found regarding the predictive role of serum TDP-43 in AD. Conversely, Kasai and colleagues previously documented the limited detection performance of TDP-43 immunoassays, particularly for CSF TDP-43. In their study, CSF TDP-43 alone exhibited a sensitivity and specificity ranging from 75.86% to 80.49% and 74.36% to75.86%, respectively, for amyotrophic lateral sclerosis (ALS) [88].

Passing–Bablok regression analysis indicated that while serum and CSF NfL/GFAP levels are correlated, they are not interchangeable, with serum levels showing minimal responsiveness to CSF fluctuations (slopes of 0.01 for NfL and 0.02 for GFAP). While correlation confirms a linear relationship, Passing–Bablok was employed specifically to assess the inter-matrix agreement and potential systematic bias between CSF and serum, which is a standard procedure for method comparison. This underscores the necessity for highly sensitive assays and cautious interpretation of serum biomarkers. Study limitations include the retrospective design, and the absence of evaluations for BBB integrity, renal function, or body mass index, all of which may influence biomarker dynamics. Future research should prioritize prospective designs, expanded cohorts, and comprehensive assessments of confounding factors to refine the clinical applicability of these biomarkers in AD diagnosis, stratification, and monitoring.

CHAPTER 3- COMPARATIVE ANALYSIS BETWEEN ELLA and SIMOA

In this context, this following paragraph aims to present a comparative analysis of two advanced diagnostic platforms, Simoa and Ella. The focus is on evaluating their performance in detecting biomarker concentrations, with a detailed comparison of specificity and sensitivity. This approach aims to provide a robust framework for enhanced biomarker detection accuracy, offering potential solutions for more reliable clinical and research applications. This project has been already published [89].

Because of variations in the ultrasensitive method, the measurement of neurological biomarkers such as NfL, GFAP, and TDP-43 varies from study to study. The Single Molecule Array (SiMoA) and Ella are the two main commercial platforms for measuring neurological biomarkers in blood. SiMoA is a digital immunoassay technology that uses arrays of microwells and non-competing monoclonal antibodies to detect and quantify individual molecules with extremely high sensitivity. Ella is an immunoassay platform that uses microfluidic cartridges to quantify soluble biomarkers in a high-throughput, fully automated manner. In order to evaluate the correlation and dependability of the two techniques for detecting NfL levels in peripheral neuropathy, we wish to compare the effectiveness of SiMoA and Ella in measuring serum NfL levels in symptomatic and presymptomatic Hereditary Transtyrethin Amyloidosis (v for variant) (ATTRv) subjects.

Ella Platform

We used the Ella platform (ProteinSimple, San Jose, CA, USA) to conduct the straightforward Plex cartridge-based assay. The factory-provided standard curve in the cartridge was used to calibrate the Ella. All samples were measured at a 1:2 dilution on the same day according tot he manufacturer‘s instructions (**Figure 4**). Three distinct glass nanoreactors (GNRs) make up the immunoassay experimental setup, which is carried out entirely inside a single cartridge well as previously explained. In this case, the antigen sample and the detection antibody (a mixture of the biotinylated antibody and the SA-DyLight650) were introduced through the GNRs' inlet channels, immobilizing the capture antibody across the GNRs (as illustrated in **Figure 7**). Three steps make up the cartridge-based immunoassay: first, add 25 µl of the sample or samples to the well or wells; second, insert the cartridge into the Ella device; and third, load, wash, and detect the sample. Three individual data points per sample, or each of the three GNRs in the well, were produced by each experimental run. Additionally, instead of using multiple manipulations to get a data point with ELISAs, the incubations are completed in a single step. Furthermore, the standards can be "barcoded" to the Ella cartridge, giving you the flexibility to process more samples quickly.

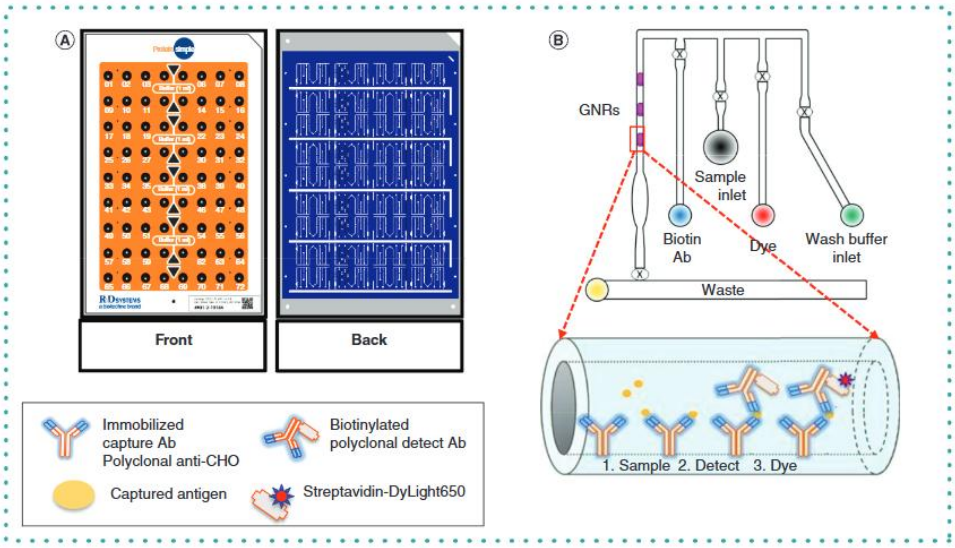

Figure 7. Cartridge layout and design. (A) The size of the cartridge is 72 × 1, where 72 represents the number of cells and 1 represents the number of analytes coated inside the GNRs. Triangular wells hold the buffer reagent used to prewet the lyophilized antibody, while round wells hold prediluted samples. A barcoded CHO HCP antigen standard for quantitative comparison with the cartridge lot is located in the lower right corner of the cartridge. (B) Top Panel: the arrangement of one of the 72 microfluidic channels is depicted in this figure. Each channel has waste outlets in yellow, GNRs in purple dashes, and inlets for samples (black), biotin antibody (blue), SA-DyLight650 (red), and wash buffer (green). Lower Panel: Immunoassay are shown.

Simoa Platform

SR/X The Biomarker Detection System (Quanterix) semi-automated ultrasensitive SR-X instrument was used to perform the assay. On 96 well plates, samples were dispersed at random after being diluted 1:4. The kit's quality control (QC) samples show concentrations within the specified range, and the coefficient of variance between plates was kept to less than 10%. Alphanumeric codes were used for blinded analysis of every sample. Only after QC-verified NfL concentrations were reported to the database manager the diagnostic codes were disclosed. Concentrations were recorded in the database and expressed in pg/mL (4). **Figure 8.**

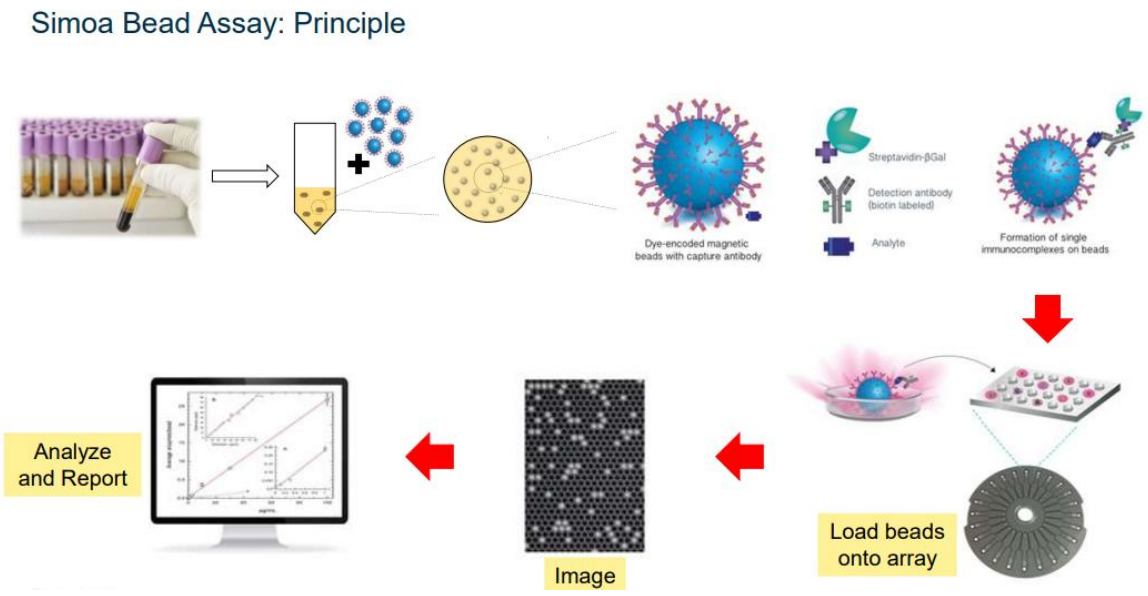

Figure 8. Basic principle of SR/X SIMOA Assay technology.

Simoa technology uses arrays of reaction chambers the size of femtoliters to detect single proteins in a novel way. It is based on earlier research by Rissin and Walt [6] that used arrays to examine the kinetics of individual enzyme molecules. The objective is to identify individual protein molecules that have been tagged with an enzyme by using the capacity to trap and detect single enzyme preparations. The process starts with 2.7 µm beads forming a sandwich antibody complex.

The enzyme used to tag these complexes is comparable to that used in conventional bead-based ELISAs. The ratio of protein molecules to beads is likewise very low at very low protein concentrations; it is usually less than 1:1 and typically has a Poisson distribution. This proves that the immunocomplexes are single-beads. Beads are loaded into a series of femtoliter (fL)-sized wells for the detection of Simoa. Each bead is enclosed in a femtoliter-sized reaction chamber by a fluorogenic enzyme substrate that seals the array. A high local concentration of fluorescent product is produced by the beads containing a single enzyme-labeled immunocomplex. Time-lapse fluorescence images are used for imaging, and the beads with a single enzyme (referred to as "on" wells) and those without (referred to as "off" wells) are separated for image analysis. The protein concentration in the test sample is determined by counting the number of wells that contain both a fluorescent product and a bead in relation to the total number of wells that contain beads. SiMoA creates a very high local concentration of the fluorescent product molecules by localizing fluorophores in very small volumes, which allows it to detect incredibly low concentrations of enzyme labels.

The sensitivity of SiMoA is approximately 70.000 times better than traditional ensemble measures [6]. Finding low sub-femtomolar protein concentrations in serum has clinical implications because it may allow for earlier disease diagnosis and treatment. In summary, the SiMoA-based digital ELISA

technique offers much greater sensitivity than any of the previously described techniques and allows us to detect clinically significant proteins in serum at or below sub-femtomolar concentrations with excellent diagnostic utility.

Results

Comparing the detection effectiveness of two platforms—Simoa and Ella—was the goal of this study. By assessing serum NfL levels in both symptomatic and presymptomatic ATTRv individuals, we were able to concentrate especially on patients with diseases of the peripheral nervous system.

The Wilcoxon signed-rank test was applied to compare NfL concentrations obtained using the two methods. The Spearman correlation coefficient was calculated to analyze the association between the serum NfL concentrations obtained using the methods in the same sample series. A 95% confidence interval was reported on the correlation as well. To assess the mean difference and the 95% limits of agreement between the NfL concentrations obtained using the SiMoA and Ella methods, the Bland–Altman method was utilized. This Bland–Altman method was then repeated on the NfL concentrations obtained from both methods. The data was organized based on a cut-off applied to the NfL concentrations from the Ella method and was defined as the mean of the medians obtained for both methods. The percentage over- or underestimation based on each assessment was calculated as [(mean bias/NfL concentrations mean of the two methods) × 100].

The regression approach considered was Passing–Bablok. Passing–Bablok is a non-parametric method used to assess the comparability of measurement methods. The non-parametric method is particularly helpful when all of the data does not meet the normality conditions. Within the comparability of methods of Passing–Bablok regression, there are two parameters to consider, the slope of the regression line and the intercept of the regression line. The slope represents an index of the relationship of the variances of the two methods, whereas the intercept expresses a systematic difference between the two methods at lower concentrations. The non-normal distribution of NfL measurements obtained on the SiMoA and Ella platforms was assessed with the Shapiro–Wilk test. However, the data was subjected to a logarithmic transformation (Log10), when the normality assumption was not met, as for prior studies. The logarithmic transformation was used specifically to compare concentration values between presymptomatic and symptomatic ATTRv subjects. The difference in serum NfL levels across groups were evaluated using ANCOVA models, adjusted for age.

Statistical significance was defined as p value less than 0.05. Statistical analyses were conducted using Jamovi Software and MedCalc Software. These analyses were completed collectively to provide a thorough comparison of the Ella and SiMoA methods to measure NfL concentrations, additively assessing agreement, correlation, and possible biases.

The cohort had serum NfL concentrations of 15.9 pg/mL (25th-75th percentile 8.62-43.7 pg/mL) for the SiMoA platform and 27.5 pg/mL (25th-75th percentile 9.46-68.7 pg/mL) for the Ella platform. As seen in **Table 3** the 55 symptomatic and 55 presymptomatic subjects included several distinct demographic details and TTR variants.

	Whole cohort	Pre-symptomatics subjects	Symptomatics subjects
Sex (Female/tot)	41/110	28/55	12/55
Age (median, 25th Percentile – 75th percentile)	64 (47–72)	47 (42,5–58)	71 (66,5–75)
Mutation (number, mutation type, number of females)		30 V30M, 16F 14 F64L, 6F 3 I64L, 3F 3 V122I, 0F 3 E89Q, 2F 1 A109S, 1 F 1 E62K, 0F	27 V30M, 3F 16 F64L, 6F 4 I64L, 0F 3 V122I, 0F 2 E89Q, 2F 1 A109S, 0 F 1 A120S, 1F 1 V32R, 0F

Table 3. Descriptive characteristics of patients' demographic data and TTR variants.

Overall, the Ella concentrations were significantly greater than the SiMoA concentrations (W=1024.0; p<0.001), as generated by the 55 symptomatic and 55 presymptomatic subjects (**Figure 9**).

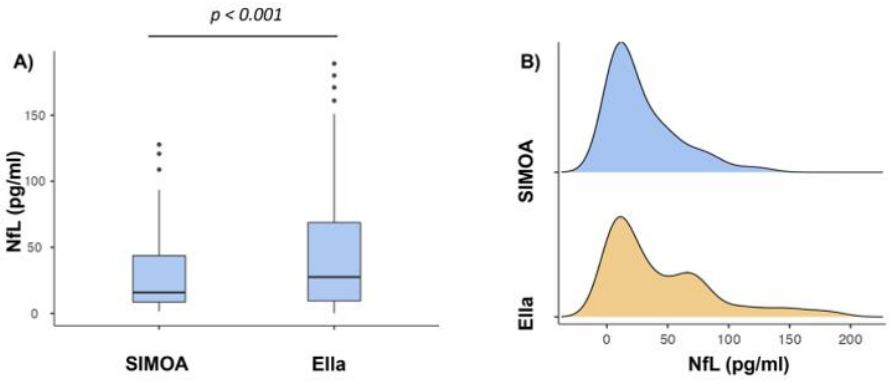

Figure 9. Boxplots and histograms with density curves. (A) Box plots express the first (Q1) and third (Q3) quartiles by the upper and lower horizontal lines in a rectangular box, in which there is a horizontal line showing the median. The whiskers extend upwards and downwards to the highest or lowest observation within the upper (Q3 + 1.5 × IQR) and lower (Q1–1.5 × IQR) limits. p values indicate statistical significance between the different groups. (B) histograms with density curves showing the comparison of NfL concentrations distribution measured by SiMoA and ELLA methods.

A strong positive correlation was found for serum NfL concentrations determined by SiMoA and Ella across all ATTRv cohort (r=0.8, p<0.001). The Bland–Altman analysis found a mean bias 15.4 pg/mL (p<0.001), indicating Ella method results in 42% higher concentrations as compared to the SiMoA method. The limits of agreement were determined as -41.1 pg/mL (95% CI [-50.4, -31.7]), and +72.0

pg/mL (95% CI [62.6, 81.3]) with 95% of observations prevented between these limits as shown in **Figure 10**.

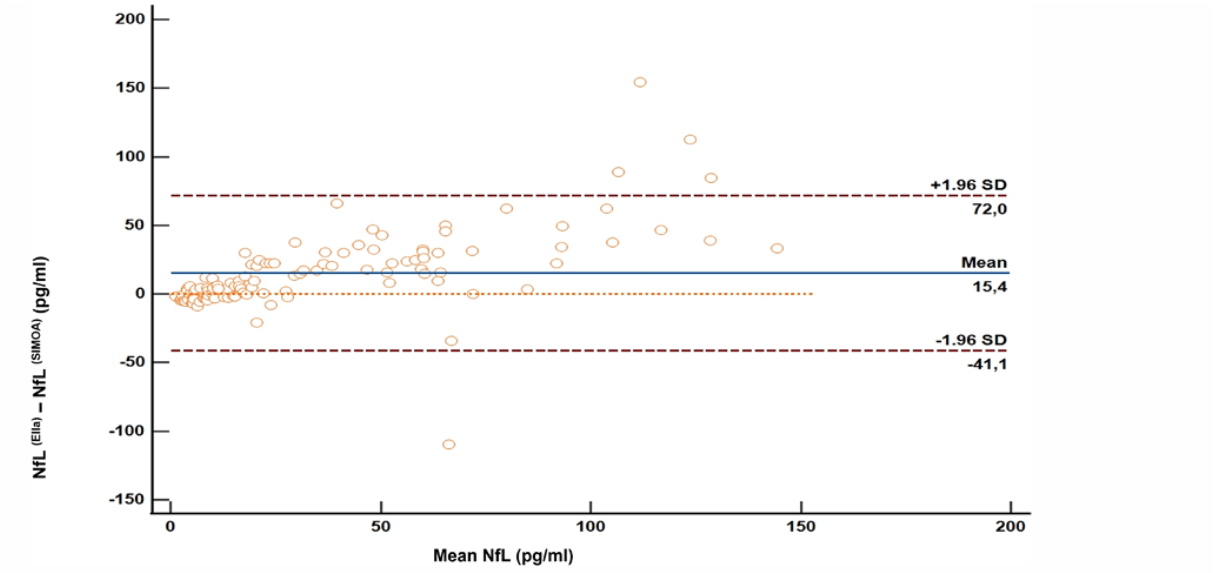

Figure 10. Bland–Altman plots illustrating the agreement between the two measurement methods. The X- axis represents the mean values of the two methods, while the Y- axis represents their differences. The blue central line indicates the mean bias, the upper and lower dashed lines cor respond to the limits of agreement (±1.96 SD).

The regression analysis between the two methods produced the following equation, y = 3.404 + 0.581x. Where x is NfL concentration measured by Ella, while y is NfL concentration measured by SiMoA. An intercept at 3.404 pg/mL suggests that SiMoA would report a 3.404 pg/mL measure at the same time when Ella would measure 0.000 pg/mL. This means there is a systematic bias for low concentrations of NfL. The slope indicates every unit increase in NfL measured by Ella, SiMoA would measure an increase of 0.581 units. This indicates that Ella tends to overestimate concentrations of NfL, especially at higher concentrations. In addition, the linearity test showed there was no significant deviation from linearity of the two datasets (p=0.44), which is appropriate for concluding on method agreement **Figure 11.**

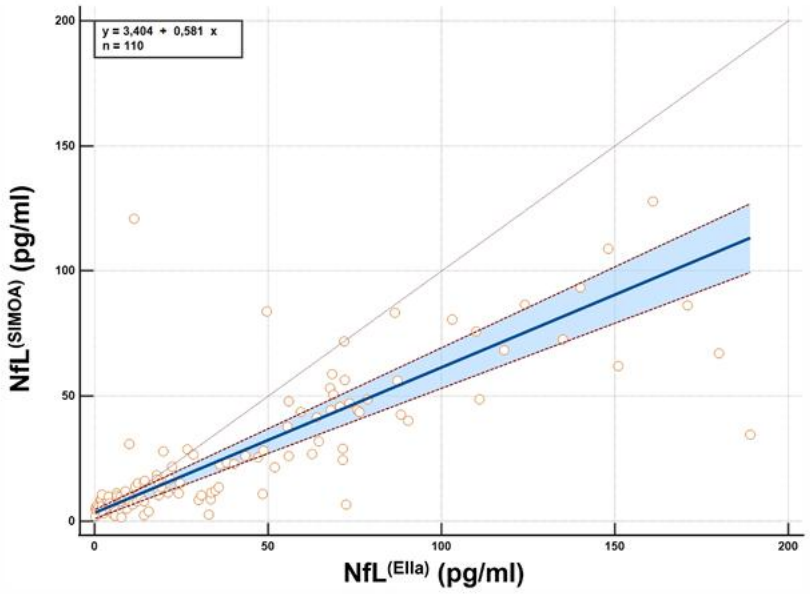

Figure 11.

Passing Bablock regression plot comparing NfL mea surements between Ella and SiMoA methods. The x- axis represents NfL concentrations measured by Ella (pg/mL), and the y- axis represents NfL concentrations measured by SiMoA (pg/mL). The blue line indicates the linear regression fit, with the shaded area representing the confi dence interval. The equation of the regression line is y = 3.4 + 0.58x.

Moreover, the study indicated that serum NfL levels were significantly higher in symptomatic ATTRv than presymptomatic ATTRv, for both Ella and SiMoA ($p<0.001$). In reporters, the median log10 serum NfL value for presymptomatic subjects was 0.99 (25th–75th 0.62–1.22) compared to 1.84 (25th–75th 1.69–1.95) for symptomatic subjects based on Ella. In SiMoA subjects, the median log10 serum NfL value for presymptomatic subjects was 0.97 (25th–75th 0.74–1.11) and symptomatic subjects was 1.64 (25th–75th 1.41–1.78). The significant differences are further illustrated in **Figure 12**.

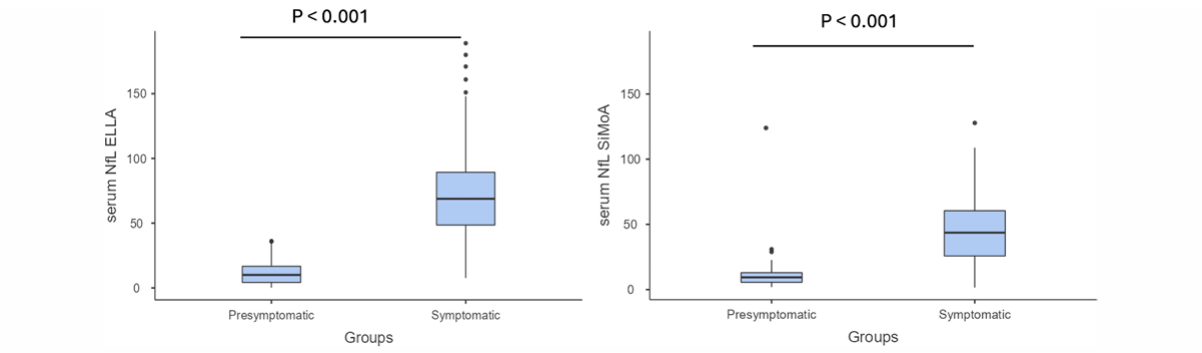

Figure 12. Comparison of serum NfL levels between presymptomatic subjects and symptomatic ATTRv patients using both Ella and SiMoA. Box plots express the first (Q1) and third (Q3) quartiles by the upper and lower horizontal lines in a rectangular box, in which there is a horizontal line showing the median. The whiskers extend upwards and downwards to the highest or lowest observation within the upper (Q3 + 1.5 × IQR) and lower (Q1 − 1.5 × IQR) limits. p Values indicate statistical significance between the different groups.

Discussion

Generally, the research shows strong agreement between the two measurement techniques and large discrepancy in the absolute measurements and possible bias at the different concentrations. The performance of two immunoassay platforms, SiMoA and Ella, for determining serum NfL concentration in presymptomatic subjects with TTR variants and symptomatic ATTRv subjects with polyneuropathy is compared in this study. Serum NfL levels are crucial for tracking the course of the disease, identifying symptomatic and presymptomatic individuals, and diagnosing peripheral nervous system disorders such as ATTRv polyneuropathy.

The results of this study showed a strong positive correlation ($r = 0.8$, $p < 0.001$) between the two methods, indicating that both SiMoA and Ella are valid for comparison with NfL serum concentrations. The Passing-Bablok regression, on the other hand, was computed and yielded a slope of 0.58, suggesting that the methods are linear but decrease with increasing serum NfL concentrations. The higher increment factor observed with the Ella platform in comparison to earlier studies may be explained by the non-linearity effect observed when examining the serum NfL concentrations on Ella [90], [91], [92], [93].

According to these results, NfL concentrations in serum as assessed by Ella had higher detectability for NfL compared to SiMoA with a 40% difference, which is greater than the 15%-25% difference previously identified between the two analytical platforms in a cohort of multiple sclerosis patients.[94].

The intercept of the regression line was 3.404 pg/mL indicating a systematic bias and an overestimation by SiMoA in the lower ranges of detection. It is reasonable to assume that this bias could arise from SiMoA's higher sensitivity at lower ranges and the different lower limits of detection of the two platforms. The two methodologies distinctly classified presymptomatic ATTRv subjects from symptomatic subjects ($p < 0.001$ both) by utilizing differences in both lower limits and calibrators which influences detection sensitivity. Ella uses bovine, naturally derived NfL while SiMoA uses recombinant, human NfL possibly highlighting systematic bias based on different antibody affinities [94].

To sum up, Ella and SiMoA are both accurate and dependable indicators of serum NfL, but we have shown that they cannot be used interchangeably. Because a similar concentration of NfL may be evaluated differently depending on the method or platform used, we must always keep in mind the methodology used to quantify NfL when interpreting the results. It is also crucial to consider the possible effects of varying Ella (1:2) and SiMoA (1:4) dilution factors on the outcomes as well as the variability measured in the serum concentration. Although they might influence our findings, we think they wouldn't significantly affect the outcomes that are regularly achieved in clinical practice. Both platforms can distinguish between patients who seem to have neuroaxonal damage and those who do not. In order to resolve these disparities and contribute to the most precise and comparable NfL quantification from clinical settings and patient groups, future research should concentrate on creating a method to create standardized conversion factors.

There are limitations to our study. We had patients with elevated NfL concentrations in the study, which provided a representative concentration range for this population, but we were unable to reach the upper detection limits of the two methods. For generalizability, more research is required on other neurological conditions.

Because our analysis is cross-sectional, it lacks longitudinal data, which is essential for observing changes in NfL concentrations over time, particularly as the disease progresses or during treatment cycles. Notably, we also failed to assess matrix effects and spike recovery rates for the SiMoA and Ella platforms, two significant sources of interference that could affect measurements and ought to be examined in subsequent research.

Variability was caused by the fact that measurements were taken by various operators in several laboratories. A conversion factor between the two approaches will be required to supply improved diagnostic biomarkers for clinical settings in the future. This idea will make it possible to assess NfL as a diagnostic biomarker that is frequently applied in a clinical setting. Based on these previously mentioned performance factors, we felt more confident going forward with the SiMoA platform given the factor differences between these two platforms, most notably the more sensitive, efficient, and reliable measures of serum NfL concentrations from the SiMoA platform, based on our data.

CHAPTER 4 - PROJECTS using SIMOA technology

The following projects exemplify the application of ultrasensitive SiMoA technology (SR-X instrument) to quantify biomarkers in CSF and serum samples, focusing on their clinical relevance in neurodegenerative and neuroinflammatory diseases, such as Alzheimer’s disease (AD) and hereditary transthyretin amyloidosis (ATTRv), as well as in cohorts of obese patients to detect neurodegeneration and neuroinflammation. In each of the following projects, we detected biomarkers using SiMoA technology, as detailed in the Methods sections below.

This study aims to examine CSF levels of IL-6, GDF-15, TDP-43, GFAP, and NfL in a cohort of AD patients, exploring their reciprocal associations and relationships with core AD biomarkers (Aβ, tau, and p-tau levels) as well as cognitive impairment, as assessed by the Mini-Mental State Examination (MMSE). By evaluating how these biomarkers interact within the context of AD pathology, particularly in mechanisms such as neuroinflammation and mitochondrial stress, this analysis will provide critical insights into their role in cognitive decline and their potential as diagnostic or prognostic tools. This project has been already published [95].

Along with long-standing hypotheses for AD pathology as the 'amyloid cascade' and 'tau propagation', novel interesting hypotheses on AD pathogenesis have gained recognition. Among these, the "immune activation“ [96] and ‘mitochondrial dysfunction’[97] appear highly promising, as they succeed in explaining specific aspects of the neu rodegenerative process and may constitute therapeutical targets in future.

Research on GDF-15 in AD has largely focused on blood concentrations, with only a few studies focusing on CSF concentrations of GDF-15 in AD patients and its association with important inflammatory markers. One previous study, however, did not find difference in CSF concentrations of GDF-15 between AD patients and healthy controls, although it did note a significant positive correlation between GDF-15 gene expression and IL-6 gene expression in the cortex of AD patients The important role of TDP-43 in RNA processing has previously been established and has also been recognized to involved in immunity and neuroinflammation [98]. NfL concentration is a strong biomarker of neuronal degeneration with elevated CSF and serum levels in a variety of neurological diseases. CSF GFAP has also been recognized as a potential biomarker of AD [32]. The proposed study will examine the CSF levels of IL-6, GDF-15, TDP-43, GFAP, and NfL, their reciprocal associations, and associations with core AD biomarkers (amyloid, tau, p-tau levels) as well as cognitive impairment (assessed by MMSE) in a cohort of AD subjects. The analysis will shed light on how these biomarkers may work in the context of AD pathology, particularly in mechanisms of disease such as neuroinflammation and mitochondrial stress, and their link to cognitive decline.

Methods

Study Design and Population

This cross-sectional pilot study, conducted between January 2022 and June 2023, enrolled a cohort of AD patients presenting with memory complaints at the cognitive disorders clinics of the University of Siena and the University of Genova. All participants met the 2018 National Institute on Aging and

Alzheimer's Association diagnostic criteria for AD and exhibited preserved Activities of Daily Living, indicating early-stage disease with functional independence. CSF biomarkers analyzed for diagnosis included Aβ1-42, Aβ1-40, total tau (t-Tau), and phosphorylated tau at position 181 (P-Tau181), with a CSF Aβ1-42 cut-off of 450 pg/mL. In cases where Aβ1-42 exceeded this threshold, the Aβ42/Aβ40 ratio and amyloid PET results (when available) were considered for diagnosis.

Exclusion Criteria Patients were excluded if they presented with:

- Evidence of alternative causes of cognitive decline (e.g., subdural hematoma, brain tumors).
- Immunosuppressant or immunomodulatory treatment within the previous 3 months.
- Infectious diseases within the previous 6 months.
- Severe psychiatric comorbidities.
- Pregnancy or lactation.
- Terminal neoplastic diseases with a life expectancy of less than 6 months.
- History of autoimmune disease.
- Family history of autosomal dominant AD, genetic dementia, or monogenic neurological diseases.
- History of cerebrovascular disease (e.g., stroke).

Ethical Considerations The study adhered to the principles of the Declaration of Helsinki, Good Clinical Practice guidelines of the International Conference on Harmonization (ICH), and national and international ethical standards. It was approved by the Local Ethics Committee of Regione Toscana Area Vasta Sud Est (protocol number 24397), and all participants provided written informed consent.

CSF sample collection

CSF samples were obtained via lumbar puncture between 8 and 10 a.m. after overnight fasting. Samples were collected in sterile polypropylene tubes and shaken gently in order to eliminate gradient effects. Following standardized pre-analytical guidelines established by the Alzheimer's Association, samples were analyzed for core AD biomarkers, including Aβ 1-42, total Tau (t-Tau), and phosphorylated Tau (p-Tau181), using LUMIPULSE® G600II. The LUMIPULSE system utilizes monoclonal antibody coated beads to discriminate pathological from non-pathological targets. CSF samples were centrifuged and stored at -80°C for additional analysis.

NfL and GFAP assay

The concentrations of NfL and GFAP were determined in patients CSF samples using com mercially available immunoassay kits for NfL and GFAP – Simoa™ assay Neurology 2-Plex B (GFAP, NfL)

Assay Kit (Catalog #103520; Quanterix, Billerica, MA, USA). The assays were conducted on the semi-automated ultrasensitive SR-X Biomarker Detection System (Quanterix). Samples were diluted at a ratio of 1:40 and randomly distributed on 96-well plates. Quality control (QC) samples, provided with the kit, exhibited concentrations within the predefined range and the coefficient of variance across the plates was maintained below 10%. All samples were ana lyzed blindly under alpha-numeric codes, and diagnostic codes were disclosed only after QC-verified NfL and GFAP concentrations were reported to the database manager. Concentrations were measured in pg/mL and documented in the database.

TDP-43 assay

The concentrations of TDP-43 were quantified in patients CSF samples using the commercially available immunoassay kit (Catalog #103293; Quanterix). The assays were conducted on the semi-automated ultrasensitive SR-X Biomarker Detection System (Quanterix). Samples were diluted at a ratio of 1:4 and randomly distrib uted on 96-well plates. QC samples, provided with the kit, exhibited concentrations within the predefined range, and the coefficient of variance across the plates was maintained below 10%. The Simoa TDP-43 assay incorporates antibodies targeting amino acids 203–209 and the C-terminal region. This assay, as per the manufacturer, is designed to identify both full-length and patho logically truncated forms of the TDP-43 protein.

GDF-15 assay

GDF-15 assay GDF-15 levels in each patient CSF sample were assessed using the GDF-15 Human ELISA kit (Bio-Techne, USA R&D Systems, Inc. Minneapolis, USA). The readings were obtained on an iMark Absorbance Microplate Reader (Bio Rad, Milan, Italy), following the manufacturer's instructions. Samples were diluted at a ratio of 1:2 and randomly distributed on the plates. Concentrations were measured in pg/mL and recorded in the database.

IL-6 assay

Concentrations of IL-6 in the CSF were deter mined using a multiplex bead-based flow cytom etry assay (LEGENDplex HU Essential Immune Response Panel; BioLegend, San Diego, CA, USA). The FACSCanto II flow cytometer and LEGENDplex™ version 8.0 software (BioLegend) were utilized for sample analysis. Samples were diluted at a ratio of 1:2 and ran domly distributed on the plates. Concentrations were measured in pg/mL and recorded in the data base. Before analysis, the cytometer underwent calibration using set-up beads according to the manufacturer's protocol.

Statistical analysis

Statistical analyses consisted of a summarizing data, and non-parametric partial correlation analyses adjusting for age, sex, and educational level. A mediation analysis was performed with R software to

investigate relationships between the biomarkers and cognitive measures. The cohort was divided into groups based on Aβ 1-42 levels. A value of p less than 0.05 was considered significant.

Results

CSF samples of the 52 AD patients were collected, and the analytes were assessed at the laboratory of the Centre of Precision and Translation Medicine, University of Siena, Italy. Demographic and clinical features of patients are summarized in **Table 4**.

Variables	Whole cohort
#patients	52
Sex, #F	34/52
Age (median, minimum-maximum)	74.3 (54–84.6)
MMSE score (median, minimum-maximum)	24.0 (11.3–30)

MMSE, Mini-mental State Examination.

Table 4. Descriptive table of demographic and neurocognitive data.

The median age of patients with AD was 74.3 years (minimum-maximum 54–84.6) and 35% were male. When looking at the patients from each centre independently, a statistically significant group difference was identified in severity of cognitive impairment using MMSE scores. In **Table 5** we present median values and the 25th and 75th percentiles of the CSF concentrations of all analytes that were tested. We did not find a significant correlation between baseline levels of CSF tau and cognitive impairment in our cohort. While comparing the CSF levels of the biomarkers studied, we identified that GDF-15 levels were higher in the 'low Aβ group (20F, median age 74.0years, minimum-maximum 54–83.2) than in the 'high Aβ' group (13F, median age 74.8years; minimum-maximum 65.2–84.6), as shown in **Figure 13.**

Variable	Whole group
Aβ 1-42 pg/ml (median, minimum-maximum)	330 (97–952)
Tau pg/ml (median, median, minimum-maximum)	682 (283–2000)
pTau pg/ml (median, median, minimum-maximum)	107 (47.7–341.9)
TDP-43 pg/ml (median, median, minimum-maximum)	29 (0.6–163.9)
NfL pg/ml (median, median, minimum-maximum)	147 (5.9–722)
GDF15 pg/ml (median, median, minimum-maximum)	439 (23.4–739)
GFAP pg/ml (median, median, minimum-maximum)	653 (196.9–987.5)
IL-6 pg/ml (median, median, minimum-maximum)	1.55 (0–13.9)

Aβ 1-42, beta-amyloid 1-42; GDF-15, growth differentiation factor-15; GFAP, glial fibrillary acidic protein; IL-6, interleukin-6; NfL, neurofilament light chain; pTAU, TAU phosphorylated; TDP-43, transactive response DNA binding protein.

Table 5. Descriptive Table of analytes.

Correlation of the concentrations of the analytes in AD patients:

MMSE score showed a positive correlation with the CSF Aβ 1-42 concentrations ($r = 0.48$; $p < 0.001$), and a negative correlation with CSF GDF-15 concentrations ($r = -0.41$; $p = 0.003$). CSF IL-6 concentrations showed a positive cor relation with CSF NfL concentrations ($r = 0.30$; $p = 0.037$) and a negative correlation with CSF TDP-43 concentrations ($r = -0.31$; $p = 0.028$). Additionally, TDP-43 concentrations showed a positive correlation with GFAP ($r = 0.33$, $p = 0.018$).

Figure 13.

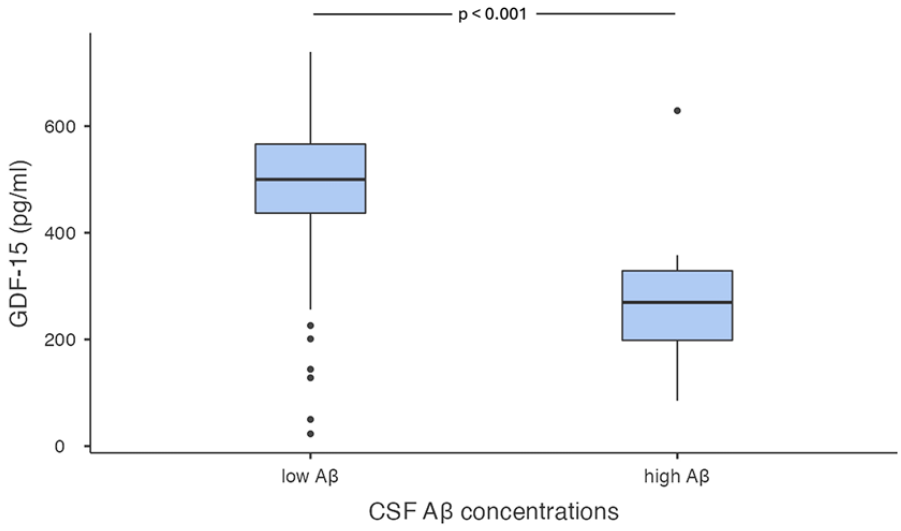

Figure 13. CSF levels of GDF-15 values in the 'low Aβ' and the 'high Aβ' groups of patients with Alzheimer's disease. Box plots express the first (Q1) and third (Q3) quartiles by the upper and lower horizontal lines in a rectangular box, in which there is a horizontal line showing the median. The whiskers extend upwards and downwards to the highest or lowest observation within the upper (Q3 + 1.5 × IQR) and lower (Q1 − 1.5 × IQR) limits. p Values indicate statistical significance between the different groups.

Mediation analysis:

Regarding mediation analysis, we tested whether the relationship between Aβ 1-42 and MMSE was mediated by the effect of IL-6 ($p = 0.525$), TDP 43 ($p = 0.543$), GFAP ($p = 0.461$), none of which showed a mediation effect. Further analysis of the potential mediation of the relationship between Aβ 1-42 and MMSE via GDF-15 was also not stastistically significant ($p = 0.376$). When examining the components of this indirect effect, the rela tionship between Aβ 1-42 and GDF-15 was statis tically significant ($p < 0.001$), while the relationship between GDF-15 and MMSE was not ($p = 0.359$). Regarding the direct effect of Aβ 1-42 on MMSE, a significant effect was observed ($p = 0.003$). Lastly, the total effect (including both direct and indirect effects) of Aβ 1-42 on MMSE was highly significant ($p < 0.001$; **Figure 14**). Moreover, when we explored the relation between GDF-15 and MMSE via Aβ 1-42, mediation analysis showed that the indirect effect of GDF-15 on MMSE mediated by Aβ 1-42 was significant ($p = 0.021$). Examining the components of the indirect effect, a significant effect was found from GDF-15 to Aβ 1-42 ($p < 0.001$) and from Aβ 1-42 to MMSE ($p = 0.003$). The direct effect of GDF-15 on MMSE was not significant ($p = 0.359$). However, the total effect of GDF-15 on MMSE, including both the direct and indirect effects, was significant ($p = 0.021$). These findings suggest that the asso ciation between GDF-15 and MMSE is primarily mediated by Aβ 1-42 (**Figure 14**).

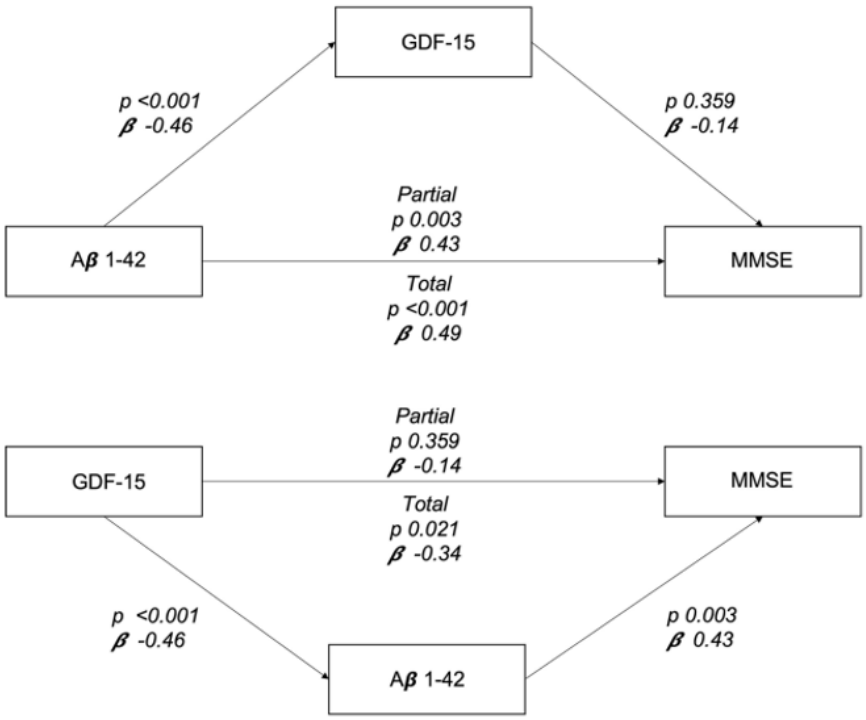

Figure 14.

Mediation models representing Aβ 1-42 and GDF-15 as the mediator variable or as independent variable, MMSE score as the dependent variable. β coefficients are reported and p values are indicated.

Discussion

This research aimed to investigate the links between the markers of inflammation (specifically IL-6 and mitochondrial dysfunction) and misfolded proteins and markers of neurodegeneration of neural and astrocyte cells using CSF markers in the AD population. One notable finding was the inverse relationship between CSF GDF-15 levels and MMSE scores. Although expression of GDF-15 increases as people age and with a number of age-related diseases, the CSF levels of GDF-15 did not significantly vary between the AD patients and controls [99]

Within the AD group, levels of GDF-15 associated significantly with cognitive impairment as measured by MMSE scores, but this was mainly influenced by an indirect pathway via CSF Aβ 1-42. Current directions suggest increased GDF-15 levels may be a predictive marker for future cognitive impairment [100]. Therefore, GDF-15 is currently regarded as a risk marker for neurodegeneration in AD rather than a more straightforward marker for the disease in question.

These results imply that more research is required to examine the connections between Aβ 1-42 deposition, mitochondrial stress, and cognitive impairment in AD. Aβ's direct effects on cognitive processes are still poorly understood, although a number of indirect pathways have been proposed. These include the effects of amyloid on neural metabolism and tau protein phosphorylation [101].

The fact that AD patients with low Aβ concentrations had higher levels of CSF GDF-15 than those with high Aβ concentrations is another noteworthy finding. Evidence from in vitro studies indicates that GDF-15 may improve microglial cells' ability to remove Aβ [102], and studies on AD animal models show that GDF-15 increases the migration and proliferation of hippocampus stem cells [103]. Therefore, our study's results may be interpreted as the brain parenchyma's attempt to reduce Aβ deposition and aggregation.

Unlike other gene expression studies, the study found no positive correlation between GDF-15 and IL-6 levels. This disparity might result from different approaches because this study looked at CSF concentrations, whereas earlier research concentrated on gene expression in cortical tissue [100].

Nonetheless, there was a negative correlation between CSF levels of TDP-43 and IL-6 in our AD patient cohort, which is consistent with TDP-43's link to neuroinflammation. It has been demonstrated that TDP-43 regulates the production of IL-6 in pericytes, which is an important player in neuroinflammation. This regulation may rely on the promotion of IL-6 mRNA decay and be at least partially independent of NF-κB translocation. [104], [105].

It has been demonstrated, nevertheless, that TDP-43 and NF-κB interact, with TDP-43 influencing NF-κB signaling, most likely by competitively binding to the nuclear translocation importin α3 (KPNA4) through its nuclear localization signal [106].

Morever, the relationship between IL-6 and neurodegeneration in AD is complex, supporting previous findings that IL-6 is an effective indicator of neuronal damage in AD [107]. Previous research has shown a negative correlation between blood IL-6 levels and hippocampal grey matter volume, and chronic inflammation markers are linked to elevated CSF NfL levels [108] .

While chronic overexpression of IL-6 can worsen neurodegeneration and promote neuroinflammation, studies suggest that IL-6 may provide protection by improving Aβ clearance through microglial activation [109]. By triggering multiple signaling pathways, such as the Janus kinase/Signal Transducer and Activator of Transcription pathway, the Mitogen-Activated Protein Kinase/Extracellular signal-Regulated Kinase pathway, the Phosphoinositide 3-Kinase/Protein Kinase B/Mechanistic Target of Rapamycin pathway, and, lastly, the Nuclear Factor kappa-light-chain-enhancer of activated B cells (NF-κB) pathway that results in neuronal damage, IL-6 appears to impact the progression of AD both systemically and within the brain [110], [111], [112].

A possible function of TDP-43 in promoting reactive gliosis, a phenomenon seen in neurodegenerative conditions involving TDP-43, is suggested by the positive correlation between CSF TDP-43 and GFAP levels [113]. It is still unknown, though, if astrogliosis is a targeted reaction to TDP-43 pathology or a nonspecific reaction to neuronal loss. Our AD cohort's lack of a relationship between initial CSF tau levels and cognitive impairment is consistent with other research [114], [115], [116], suggesting that measurements made at one point in time may not adequately capture cognitive decline in AD.

These results support the idea that mitochondrial stress and neuroinflammatory markers are linked to neurodegeneration and cognitive impairment in AD, even though the study admits a number of limitations, such as a cross-sectional design and a relatively small sample size, which limit the ability to track longitudinal changes in biomarkers and cognitive decline. To examine their precise functions and potential value as biomarkers for tracking the course of disease, further longitudinal research is necessary.

PROJECT 2- ELEVATED SERUM CONCENTRATIONS OF GFAP IN HEREDITARY TRANSTHYRETIN AMYLOIDOSIS SINCE PRE-SYMPTOMATIC STAGES

This study focus on the evaluation of sGFAP and sNfL levels in symptomatic and pre-symptomatic ATTRv patients, as well as in healthy controls (HCs), with a focus on sex-related variations and their association with disease progression. By elucidating the dynamics of GFAP, this research aims to deepen our understanding of ATTRv pathophysiology and inform the development of enhanced diagnostic and therapeutic approaches. This project has been alrealdy published [116].

Methods

Patients

Patients with confirmed pathogenic TTR variants, including both symptomatic ATTRv patients and pre-symptomatic subjects, are the focus of this multicenter cross-sectional cohort study. Italian reference centers with a wealth of experience in diagnosing and treating ATTRv were used to recruit participants. Expert neurologists performed thorough evaluations on all enrolled symptomatic and pre-symptomatic subjects, including neurological, genetic, and demographic tests. Based on the specific TTR gene mutation, the typical age of onset for that mutation, and the age of onset in other family members, the predicted age of disease onset (PADO) for the 55 pre-symptomatic ATTRv subjects was calculated. The term "Years from PADO" refers to the difference between the pre-symptomatic subjects' current age and the PADO. A group of HCs who showed no signs of neurological, cardiac, renal, or autoimmune diseases provided the control samples. Approved by the Fondazione Policlinico Agostino Gemelli IRCCS's Comitato Etico Territoriale Lazio Area 3, the study followed the guidelines in the 1964 Declaration of Helsinki.

Serum sample collection

Peripheral blood was drawn using separating gel in additive-free vacutainers for the collection of serum samples. The serum was then centrifuged and kept at -80 degrees Celsius.

NfL and GFAP assay

SiMoA commercially available immunoassay kits (Catalog #103520; Quanterix, Billerica, MA, USA) operating on the semi-automated ultrasensitive SR-X Biomarker Detection System (Quanterix) were used to measure the levels of NfL and GFAP. On 96-well plates, samples were distributed at random after being diluted 1:4. The kit's quality control (QC) samples show concentrations within the specified range, and the coefficient of variance between plates was kept below 10%. Alphanumeric codes were used for blinded analysis of every sample. Only after the database manager received reports of QC-verified NfL and GFAP concentrations were the diagnostic codes made public. The concentrations were recorded in the database and expressed in pg/mL. The analyses were carried out at the University of Siena's Centre for Precision Medicine and Translation lab in Italy.

Statistical Analysis

Every participant in the study had a thorough medical examination. The Neuropathy Impairment Score (NIS) was used to evaluate the severity of the disease in patients who showed signs of polyneuropathy. Descriptive analyses, normality testing, and the use of ANCOVA models were among the statistical techniques used to assess variations in sGFAP and sNfL levels while controlling for sex and age. Two-tailed Spearman's correlation was used to examine correlations between sNfL, sGFAP, age, years from PADO, and the NIS clinical score. A p-value of less than 0.05 was deemed significant. Jamovi software was used for the analyses (The Jamovi Project, 2021).

Results

The ATTRv cohort, which includes 111 participants with confirmed pathogenic TTR gene variants and a median age of 64 years, was enrolled in this study. The cohort, which was split into 56 symptomatic patients and 55 pre-symptomatic subjects, included 41 females and 70 males. A cohort of 183 HCs, 109 of whom were female and 74 of whom were male, with a median age of 50 years, was also included in the study. In both groups, there were found no age differences between males and females. Demographic’s data are reported in **Table 6.**

	HCs	ATTR pre-symptomatic subjects	ATTR patients
Sex (F/tot)	109/183	28/55	13/56
Age (median, 25th–75th percentile)	50 (32–61)	47 (42,5-58)	71 (66,75-75)
Mutation (number of subjects, median age, number of female subjects)		V30M (30; 45 years; 16 F) F64L (14; 50.5 years; 6 F) I68L (3; 44 years; 3 F) V122I (3; 59 years; 0 F) E89Q (3; 47 years; 2 F) A109S (1; 45 years; 1 F) E62 K (1; 59 years; 0 F)	V30M (28; 69.5 years; 4 F) F64L (16; 74 years; 6 F) I68L (4; 73 years; 0 F) V122I (3; 70 years; 0 F) E89Q (2; 71.5 years; 2 F) A109S (1; 78 years; 0 F) A120S (1; 72 years; 1 F) V32R (1; 65 years; 0 F)
sGFAP levels (median, 25 th–75 th percentiles)	75.5 pg/ml, 43.7–125.0 pg/ml	105.50 pg/ml, 68.92–195.42 pg/ml	238.35 pg/ml, 138.99–342.88 pg/ml
sNfL levels (median, 25 th–75 th percentiles)	7.54 pg/ml, 5.59–10.80 pg/ml	9.36 pg/ml, 5.59–12.97 pg/ml	43.68 pg/ml, 25.99–63.32 pg/ml

Table 6. Detailed demographics of ATTRv patients, pre-symptomatic subjects and healthy controls (HCs), as well as TTR gene mutations, sNfL and sGFAP concentrations.

Within the ATTRv cohort, various TTR gene mutations were identified, including V30M, F64L, I68L, V122I, E89Q, A109S, V32R, A120S, and E62K, summarized in **Table 6**, together withspecific median concentrations and percentiles of sGFAP and sNfL in male and female HCs, pre-symptomatic ATTRv subjects, and ATTRv patients.

There was no significant difference between ATTRv patients and pre-symptomatic subjects, but sGFAP levels were significantly higher in both groups than in HCs ($p<0.001$ for both comparisons, Bonferroni-adjusted). Similarly, there was no significant difference between pre-symptomatic subjects and HCs ($p<0.001$ for both comparisons, Bonferroni-adjusted), but sNfL levels were significantly higher in ATTRv patients than in both pre-symptomatic subjects and HCs **Figure 15.** To address the age discrepancy, an age-matched subgroup of HCs older than 59 years was identified. This subgroup included 50 HCs with a median age of 68.5 years The median age of the 50 HCs in this subgroup was 68.5 years. Comparisons revealed that ATTRv patients had higher levels of both sNfL and sGFAP than this age-matched subgroup of HCs.

The median concentrations, as well as 25 th and 75 th percentiles, of sGFAP and sNfL in female and male HCs, presymptomatic ATTRv subjects and ATTRv patients are reported in **Table 7.**

	Female HCs	Male HCs	Female ATTR pre-symptomatic subjects	Male ATTR pre-symptomatic subjects	Female ATTR patients	Male ATTR patients
sGFAP levels (median, 25 th–75 th percentiles)	88.6 pg/ml, 44.4–133.0 pg/ml	59.8 pg/ml, 40.3–111.0 pg/ml	119.44 pg/ml, 79.59–205.99 pg/ml	89.05 pg/ml, 67.19–174.10 pg/ml	253.11 pg/ml, 176.60–346.27 pg/ml	209.70 pg/ml, 138.06–328.52 pg/ml
sNfL levels (median, 25 th–75 th percentiles)	7.5 pg/ml, 6.5–10.9 pg/ml	7.8 pg/ml, 5.5–10.3 pg/ml	9.02 pg/ml, 5.92–13.66 pg/ml	9.49 pg/ml, 5.59–12.21 pg/ml	43.70 pg/ml, 26.19–58.90 pg/ml	43.65 pg/ml, 25.80–70.19 pg/ml

Table 7. The table shows the specific median concentrations and percentiles of sGFAP and sNfL in male and female HCs in females and males in HCs, presymptomatic ATTRv subjects and ATTRv subjects.

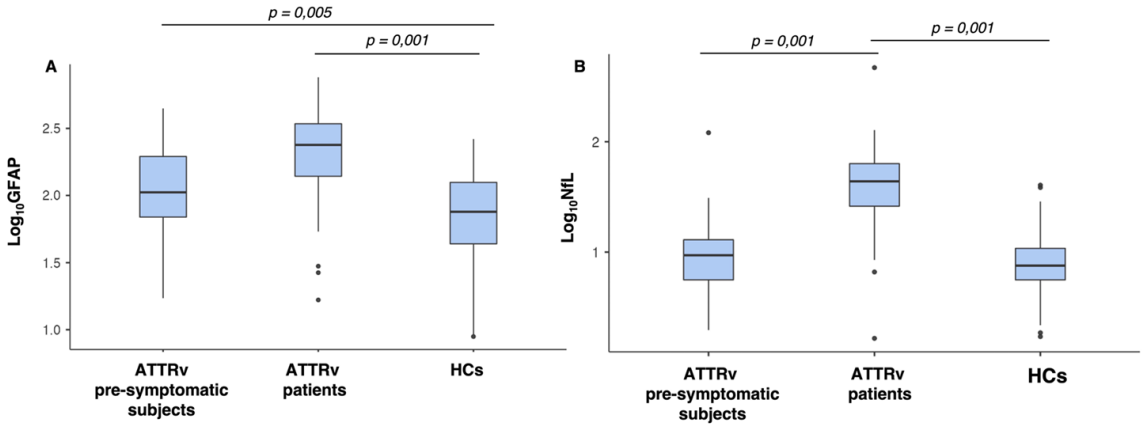

Figure 15. Comparison of sGFAP and sNfL levels (expressed as Log10 GFAP and Log10-NfL, respectively) across the three groups. Box plots express the first (Q1) and third (Q3) quartiles by the upper and lower horizontal lines in a rectangular box, in which there is a horizontal line showing the median. The whiskers extend upwards and downwards to the highest or lowest observation within the upper (Q3 + 1.5 × IQR) and lower (Q1 − 1.5 × IQR) limits. p Values indicate statistical significance between the different groups.

To evaluate the differences in sGFAP and sNfL levels between males and females in the healthy controls (HCs) cohort, an ANCOVA was performed. While there were no discernible sex differences in sNfL levels, the results showed that female HCs had significantly higher sGFAP values than male HCs (p=0.011, Bonferroni-adjusted) **Figure 15.**

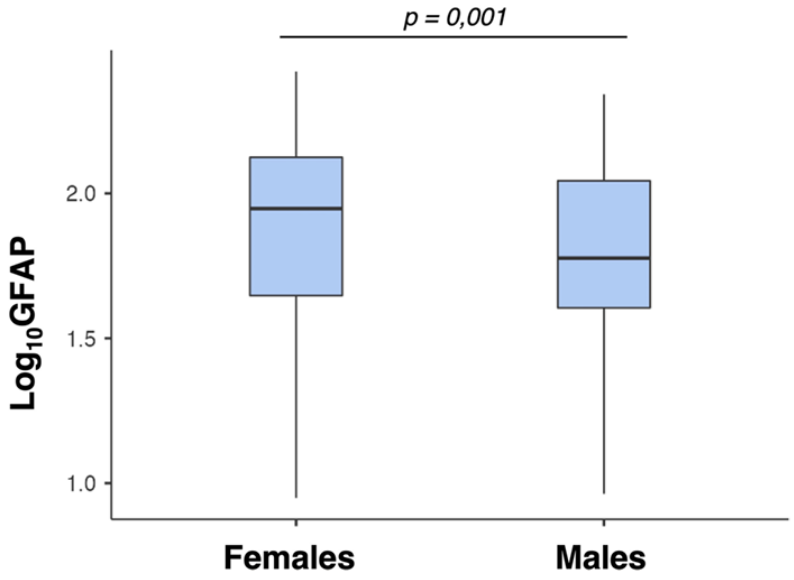

Figure 15.

Comparison of sGFAP levels (expressed as Log10-GFAP) between females and males in the HCs cohort. Box plots express the first (Q1) and third (Q3) quartiles within a given dataset by the upper and lower horizontal lines in a rectangular box, in which there is a horizontal line showing the median. The whiskers extend upwards and downwards to the highest or lowest observation within the upper (Q3+ 1.5 × interquartile range) and lower (Q1− 1.5 × interquartile range) limits. p values indicate statistical significances (<0.05) between the different group.

Furthermore, there were no discernible differences in the Neuropathy Impairment Score (NIS), a multivariate analysis that took into account age, gender, and the severity of the disease in ATTRv patients. Significant associations between biomarkers and clinical or demographic factors were found using Spearman correlation analysis. NIS scores were positively correlated with both Log10-NfL and Log10-GFAP (Rho 0.47, p<0.001 and Rho 0.28, p=0.04, respectively) **Figure 16.** When stratified by sex, age was found to be significantly correlated with both Log10-NfL (Rho 0.62, p<0.001) and Log10-GFAP values (Rho 0.45, p<0.001) in the HCs group. These correlations were confirmed for both males (Log10-NfL: Rho 0.66, p< 0.001; Log10-GFAP: Rho 0.48, p< 0.001) and females (Log10-NfL: Rho 0.61, p< 0.001; Log10-GFAP: Rho 0.48, p< 0.001).

Age also had a significant correlation with Log10-NfL (Rho 0.65, p<0.001) and Log10-GFAP (Rho 0.43, p<0.001) in the ATTRv cohort. Additionally, there was a significant correlation between Log10-NfL and Log10-GFAP in the ATTRv cohort (Rho 0.68, p<0.001) and the HCs group (Rho 0.53, p<0.001).

There was no discernible relationship between years from PADO and sNfL and sGFAP concentrations in pre-symptomatic ATTRv subjects. Nonetheless, during the pre-symptomatic stage, there was a positive correlation between age and sGFAP (p=0.03, rho 0.25).

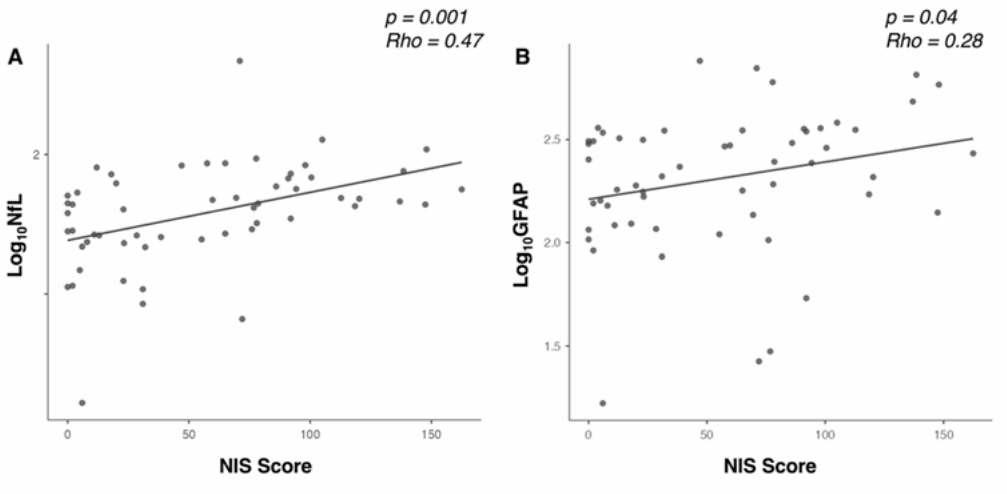

Figure 16.

Correlation between sNfL and sGFAP levels (expressed as Log10-NfL and Log10-GFAP, respectively) with NIS scores.

Discussion

The current study emphasizes how important sGFAP and sNFL are to ATTRv. While elevated sNfL levels were only observed in symptomatic patients, our data showed elevated sGFAP levels in both pre-symptomatic subjects and symptomatic patients when compared to HCs. This implies that sGFAP elevation identifies the disease at preclinical stages, whereas an increase in sNfL is associated with the occurrence of neurological symptoms.

sGFAP is mainly known as a marker for astrocytic damage and activation in the CNS, but might also originate from the PNS and the enteric nervous system (ENS). According to recent studies, astrocytic activation in ATTRv may begin in the pre-symptomatic stage [118], potentially due to amyloid buildup in the central nervous system before polyneuropathy develops. This activation expands in scope as the disease progresses and corresponds with the CNS's progressive stages of TTR-amyloidosis [119]. Initially, transthyretin (TTR) deposition is observed in the leptomeninges and subarachnoid meningeal vessels, with significant involvement in the brainstem and spinal cord.

Amyloid deposition spreads to subpial cortical areas and increases in frequency in perforating cortical vessels as the disease advances to the second stage. The disease progresses to subependymal areas and basal ganglial vessels close to the ependymal lining in the last stage. Notably, astrocytosis is linked to subpial TTR amyloid deposits, highlighting the importance of astrocytic activation and damage in ATTRv pathology [120]. **Figure 16** which displays the relationship between sNfL and sGFAP levels (represented as Log10-NfL and Log10-GFAP, respectively) and NIS scores, suggests that these processes may play a substantial role in the observed increase in serum GFAP concentrations. demonstrating a significant positive relationship between both biomarkers and clinical impairment.

Additionally, we hypothesized that the PNS and/or ENS could be the source of the rise in sGFAP levels in pre-symptomatic individuals. In these systems, GFAP expression is well-established, particularly in enteric glial cells and Schwann cells [121]. Myelin-forming Schwann cells downregulate GFAP, which is first expressed in immature Schwann cells [122], [123]. Non-myelinating Schwann cells, on the other hand, still express GFAP and function similarly to astrocytes. In cases of dedifferentiation or mild, subclinical nerve injury, these non-myelinating Schwann cells may release GFAP into the bloodstream.

Elevated serum GFAP levels may also be caused by glial cells in the ENS that express GFAP. Important trophic and neuromodulatory tasks are carried out by these sub-epithelial glia, such as mediating neurotransmitter signaling, controlling gut motility, and supporting intestinal neurons and epithelial cells. It makes sense to speculate that early changes in the ENS among carriers of TTR variants may be a factor in the observed increase in sGFAP levels, given the high frequency of gastrointestinal symptoms in ATTRv [124].

Additionally, patients with ATTRv had higher sNfL levels than pre-symptomatic subjects. Since both the CNS and the PNS contribute to its serum concentration, sNfL is well known as a biomarker of neuroaxonal damage [7], [125]. The study demonstrates the ability to differentiate between symptomatic ATTRv polyneuropathy patients and pre-symptomatic subjects [32]. Despite the fact that sNfL is frequently used to track the clinical development of ATTRv polyneuropathy, there is insufficient proof to conclusively link the PNS to its full concentration. Similar to GFAP biomarker, ATTRv's pathological involvement of the central nervous system has been well-documented for sNfL [126], [127]. Although the precise percentage is unknown, it is reasonable to speculate that some of the sNfL may come from the CNS given the patient cohort's observed elevation of GFAP levels.

To more precisely identify and describe the causes of sNfL elevation, future studies should investigate neurofilament isoforms with regional specificity. Serum levels of this isoform have already been investigated because PRPH seems to be a promising biomarker of neuroaxonal damage involving the PNS.

Our study's key finding is that female HCs have higher levels of sGFAP than male HCs. This finding is in line with earlier studies showing that women without cognitive impairment had higher plasma GFAP concentrations than men [128]. Sex-based differences in astrocyte number, differentiation, and function have been the subject of extensive research Sex-specific mechanisms in neuroinflammation and blood-brain barrier permeability are also important [129], [130], [131], [132], as evidenced by the different ways that inflammation impacts the blood-brain barrier in the sexes and the varying expression of tight junction proteins and inflammatory markers [133]. Given that sex seems to be an important covariate that needs to be taken into account for precise measurement interpretation, these findings have important ramifications for the statistical analysis of scientific studies looking into sGFAP.

Furthermore, the fact that there were no appreciable variations in sGFAP levels between pre-symptomatic individuals and symptomatic patients may indicate that sGFAP functions more as a marker of the existence of the disease than its advancement. This is corroborated by the fact that there was no discernible relationship between sGFAP levels and years from the PADO during the pre-symptomatic stage.

However, this absence of a significant difference between pre-symptomatic individuals and symptomatic patients deserves a deeper analysis. As mentioned, it could be mainly explained by the lack of statistical power and the presence of confounding factors. Specifically, the sample size could have inhibites the statisticals' tool capability to detect the slightest differences in sGFAP concentrations that could exist while passing from the preclinical to the symptomatic stage of the disease. Longitudinal research is crucial to determine the role of sGFAP as either a state or a stage marker. In fact, the longitudinal design would have been able to overcome the issue of interindividual variability and sex-related confounders, allowing a better understanding of the precise moment when sGFAP concentrations. A longitudinal design would have been highly valuable to establish whether sGFAP could be used not only for early diagnosis but also as a sensitive marker of disease progression.

Nonetheless, a number of factors might have contributed to this finding, such as our study's small sample size, which might have limited the statistical power to identify minute variations between these groups. The unequal distribution of sexes, with a greater percentage of females in the pre-symptomatic group than in the symptomatic patients, is another possible contributing factor. Given that sGFAP levels are generally higher in females, this sex imbalance may obscure potential differences attributable to disease progression.

Future studies with larger and more balanced cohorts should explore these factors to better understand the dynamics of sGFAP levels across the stages of ATTRv.

A potental limitation of the present study is the age gap among the cohorts of HCs, pre-symptomatic subjects, and patients. The age difference between the HC cohorts, pre-symptomatic subjects, and patients is a potential limitation of the current study. In particular, the subjects in the other cohorts were younger than the patients. We performed all pertinent analyses of sGFAP and sNfL levels while adjusting for age as a covariate in order to overcome this limitation. Additionally, we eliminated age-related differences by choosing a subgroup of older, healthy controls who were age-matched with the ATTRv patients in order to validate our findings.

The concentrations of sNfL and sGFAP have a positive correlation with neurological impairment as determined by the NIS, which highlights their potential use as biomarkers for determining the severity of the disease. Using a different assessment technique, our group's earlier research has shown a correlation between sNfL levels and clinical disability. Similarly, Notturno et al. have reported on the association between sGFAP and clinical measures of disability in the peripheral neuropathy cohort [134]. To the best of our knowledge, this study is the first to show that patients with ATTRv have this correlation.

According to our study, both symptomatic and pre-symptomatic ATTRv subjects had higher levels of sGFAP than healthy controls, suggesting that the CNS, PNS, and ENS may be involved in the disease even in its early stages. In addition to sNfL, which indicates clinical involvement, this demonstrates the value of sGFAP as an early detection biomarker for ATTRv. The complex pathophysiology of ATTRv is reflected in the elevation of GFAP, which indicates involvement from both the central and peripheral nervous systems. Additional investigation into GFAP isoforms may enhance biomarker specificity and offer more profound understanding of disease mechanisms.

Furthermore, sex should be taken into account in biomarker analysis, possibly reflecting variations in glial physiology, as evidenced by the observed sex differences in sGFAP levels among HCs. Our results lend credence to the use of sGFAP and sNfL as separate ATTRv biomarkers. Future longitudinal research is required to monitor the evolution of biomarkers as the disease progresses and how well treatments work.

Project 3- Longitudinal analysis of sNfL and sGFAP Biomarkers in Patients with Obesity: Impact of Bariatric Surgery

This study aimed to comprehensively analyze the concentrations of sNfL and sGFAP in individuals with severe obesity, compare these levels to those observed in HCs, and evaluate the impact of weight-reduction interventions, specifically bariatric surgery, on these biomarkers. Additionally, the study sought to assess the impact of estimated glomerular filtration rate (eGFR) and other biochemical parameters on sNfL and sGFAP concentrations, providing insights into their behavior in the context of obesity-related renal function modifications. This project is currently unpublished.

Methods

Anthropometric Measurements and Excess Weight Calculation

Height and weight were measured using a stadiometer and steelyard scale, respectively. BMI was calculated as weight (kg) divided by height squared (m^2). The percentage of excess weight loss (%EWL) was determined as the proportion of excess weight lost relative to the pre-surgical excess weight, where excess weight was defined as the difference between pre-surgical weight and ideal body weight, estimated using standard reference equations based on height and sex. Body surface area (BSA) was calculated using the Mosteller formula: BSA (m^2) = $\sqrt{}$[(height (cm) ×weight (kg)) / 3600].

HOMA Index Calculation

The HOMA Index was calculated by the following formula: [fasting insulin (mU/L) × fasting glucose (mmol/L)] / 22.5, as per the Matthews model (Matthews et al., 1985), to assess insulin resistance.

Estimation of non-indexed eGFR

The estimated glomerular filtration rate (eGFR) was calculated using the CKD-EPI equation (Levey et al., 2009) n, incorporating serum creatinine, age and sex. To obtain the non-indexed eGFR, the standard eGFR value (adjusted for 1.73 m^2 BSA) was corrected based on the patient‘s actual body surface area, calculated using the Mosteller formula (RD, 1987). This approach provides a more accurate assessment of renal function, particularly in individuals with obesity.

Measurement of sNfL and sGFAP Concentrations

The concentrations of sNfL and sGFAP were measured using the commercially available Neurology 2-Plex B (GFAP, NfL) Assay Kit (Catalog #103520; Quanterix, Billerica, MA, USA). The assay was performed on the semi-automated, ultrasensitive SR-X Biomarker Detection System (Quanterix). Samples were diluted 1:4 and randomly plated on 96-well plates. Quality control (QC) samples provided with the kit had concentrations within the predefined range, and the inter-plate coefficient of variation was maintained below 10%. All samples were analyzed in a blinded manner using alphanumeric codes, with diagnostic codes revealed only after QC-verified NfL and GFAP concentrations were reported. Concentrations were measured in picograms per milliliter (pg/mL) and recorded in the database. The analyses were conducted at the laboratory of the Centre for Precision Medicine and Translation, University of Siena, Italy. Samples were stored at -80°C in the Endocrinology Unit. sNfL and sGFAP levels were assessed at baseline in both the study population and the control group. In patients with obesity, sNfL and sGFAP levels were also evaluated at a 12-month follow-up after bariatric surgery.

Statistical Analysis

Continuous variables were tested for normality using the Shapiro-Wilk test and reported in **Table 8**. Categorical variables are presented as absolute frequencies and percentages. sNfL and sGFAP concentrations were log10 transformed as previously described [77]. Moreover, we calculated sNfL Z scores using the online application provided by Benkert et al., 2022 [135] based on a reference database of 4532 healthy persons (Serum Neurofilament Light Chain Reference App; Serum Neurofilament Light Chain Reference App) and sGFAP Z score as already described in literature [136]. Comparisons were performed using Z-scores for sNfL and sGFAP values and Student's t-test for continuous variables, the paired Wilcoxon signed-rank test for comparing pre- and post-surgery eGFR, and the Chi-square test or Fisher's exact test for categorical variables. The Δ% between variables before and after bariatric surgery was calculated as the relative difference between the final and initial values, expressed as a percentage of the initial value. Correlations between sNfL and sGFAP levels and clinical/biochemical parameters were assessed using Spearman's rank correlation, age and BMI were used as control variables, except when already included in the formulas (e.g., eGFR). A linear regression model was used to assess the prediction value of eGFR levels, BMI and sex were used as covariates. A p-value of less than 0.05 was deemed significant. Jamovi software was used for the analyses (The Jamovi Project, 2021).

Results

Study population

Sixty-two morbid obese patients were recruited [Median body mass index (25th-75th percentile): 45.2 (42.14-50.50); 42 females (F) (67.74%), age (25th-75th percentile) 45.5 years (38.5-51.8)]. Thirty-three underwent RYGB, while twenty-nine underwent sleeve gastrectomy. Additionally, the study included a cohort of 137 age- and sex-matched HCs with a median age (25th-75th percentile) of 51 years (31-64), consisting of 89 F. The characteristics of these two cohorts are summarized in **Table 8.**

Characteristics	Obese Group	HCs Group
Age (years)	Mean 45.1 ± 9.94 Range 23* 68	Mean 49.8 ± 18.7 Range 21- 93
Sex n (%)	Females n=42 (67.74%) Males n= 20 (32.26%)	Females n=89 (64.96%) Males n= 48 (35.04%)
BMI	Mean 46.8 ± 6.46 Range 37.6-67.6	Mean 23.6 ± 1.29 Range 20.1-24.9
BMI Categories		
Grade II (n, %) **BMI 35-39.9 kg/m^2**	4 (6.4.)	
Grade IIIA (n, %) **BMI 40-44.9 kg/m^2**	22 (35.5)	
Grade IIIB (n,%) **BMI 45-49.9 kg/m^2**	20 (32.3)	
Grade IIIC (n,%) **BMI >50 kg/m^2**	16 (25.8)	
Surgery procedures		
RYGB (n,%)	33 (53.2)	
Sleeve Gastrectomy (n,%)	29 (46.8)	

Table 8. Demographic, clinical and antrophometric parameters in the study Obese population at the enrollment (n=62 patients and HC (137).

Pre-surgical findings

We found significantly higher sGFAP Z scores (median 1.48; IQR 1.68; p< 0.001) and sNfL Z score [median 0.57; interquartile range (IQR) 2.13; p = 0.03] in obese subjects compared to HCs (GFAP Z score median – 0.53, IQR 2.04 **Figure 17-A**; NfL Z score median – 0.08, IQR 1.89; **Figure 17-B**.

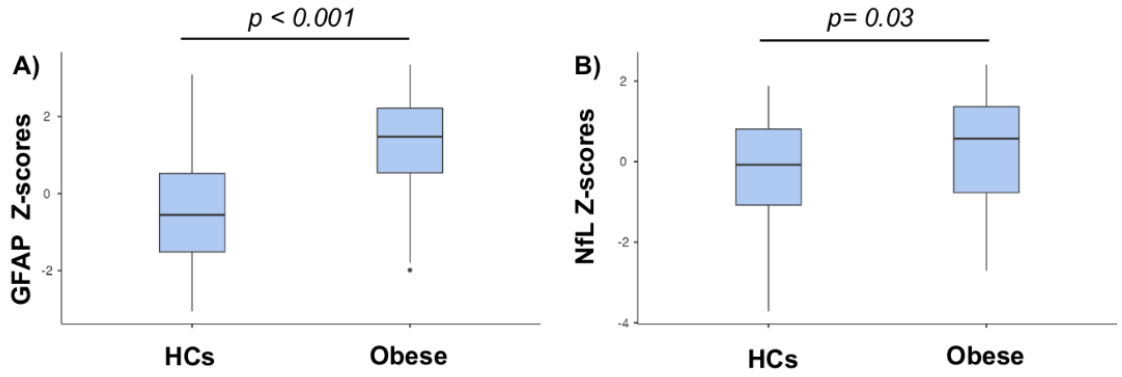

Figure 17 A-B. Comparison between of z-scores of serum neurofilament light chain (sNfL) (A), and

serum glial fibrillary acidic protein (sGFAP) (B) between obese patients and HCs before surgery. Box plots express the first (Q1) and third (Q3) quartiles within a given dataset by the upper and lower horizontal lines in a rectangular box, in which there is a horizontal line showing the median. The whiskers extend upwards and downwards to the highest or lowest observation within the upper (Q3+ 1.5 × interquartile range) and lower (Q1− 1.5 × interquartile range) limits. p values indicate statistical significances (<0.05) between the different groups.

sGFAP Z scores showed a positive correlation with age (r = 0.30, p = 0.018) and a negative correlation with both eGFR (r = -0.29 p=0.027) and BSA (r=-0.31, p=0.012). sNfL concentrations also positively correlated with age (r=0.58, p<0.001) and negatively with eGFR (r=−0.34, p=0.011). sGFAP and sNfL concentrations were positively correlated in both obese subjects (r = 0.42; p< 0.001) and in HCs (r = 0.47; p< 0.001). Finally, a linear regression analysis showed that pre-surgery eGFR values significantly predicted pre-surgery concentrations of both sNfL (R 2 = 0.18; p [overall model test]= 0.01; β = –0.0042; p -coefficient model = 0.002) and sGFAP (R 2 = 0.16; p [overall model test] = 0.03; β =0.0035; p-coefficient model= 0.003) (**Figure 18A-B**).

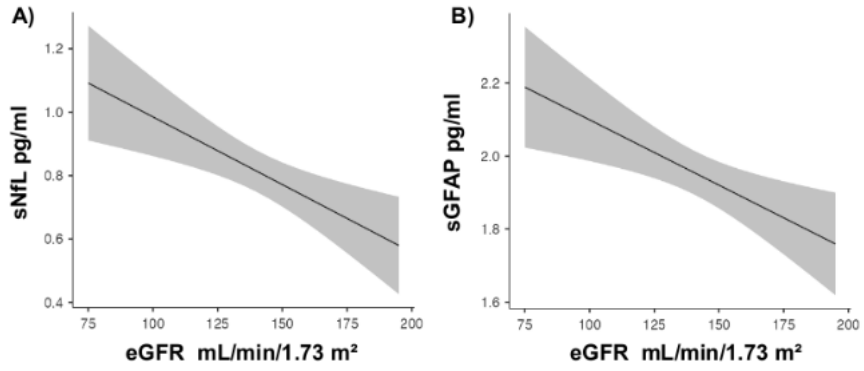

Figure 18 A-B. Marginal means plots are shown. Panel a) illustrates the linear relationship between sNFL pre-surgery and eGFR, while panel b) shows the linear relationship between sGFAP pre-surgery and eGFR.

Post-surgical findings

We documented significant reductions in both anthropometric and biochemical parameters following bariatric surgery (**Table 9**). In detail, the reduction of weight after surgery was considerable (p< 0.001), and, consequently, BMI also showed a pronounced decrease (p<0.001). Furthermore, both the %EW (p< 0.001) and BSA (p< 0.001) sdeclined, as well as % EWL (median 71.2 %, 25th-75th

percentiles 53.3%-83.4). No significant difference was found by comparing patients based on the type of surgical intervention performed (Sleeve Gastrectomy vs. RYGB). Finally, post-bariatric surgery eGFR values were significantly lower compared to pre-surgery eGFR values ($p < 0.001$, **Figure 19).**

	Pre-surgical (T0)	Shapiro-Wilk p-value (T0)	Post-surgical (T1)	p-value
Weight (Kg)		0.109		
Mean	130 ± 22.8		85.2 ± 19.6	< 0.001
Range	88.8 - 178		48.4 – 147	
Median	130		83.8	
BMI (Kg/m2)		<0.001		< 0.001
Mean	46.8 ± 6.56		30.7 ± 6	
Range	37.6 – 67.6		20.2 – 49.7	
Median	45.2		29.5	
EW%		0.011		< 0.001
Mean	106 ± 33.8		36.8 ± 28.2	
Range	22.8 – 206		- 8.62 – 108	
Median	98		30.3	
EWL%				
Mean	N/A		69.2 ± 21	N/A
Range			- 2.74 – 112	
Median			71.2	
BSA (m2)	2.35±0.27	<0.001	2.02±0.26	< 0.001
Mean	1.90-3.24		1.4-2.5	
Range	2.32		2.02	
Median				
eGFR (mL/min)	138±26.01	0.994	123±24.5	< 0.001
Mean	75.6-192		67.2-181	
Range	140		124	
Median				

Table 9. Pre and post-surgical anthropometrical parameters in obese group. The present table shows Body Mass Index (BMI), the percentage of Excess Weight (EW%), the percentage of Excess Weight Loss (EWL%), Body Surface Area (BSA), and the estimated Glomerular Filtration Rate (eGFR).

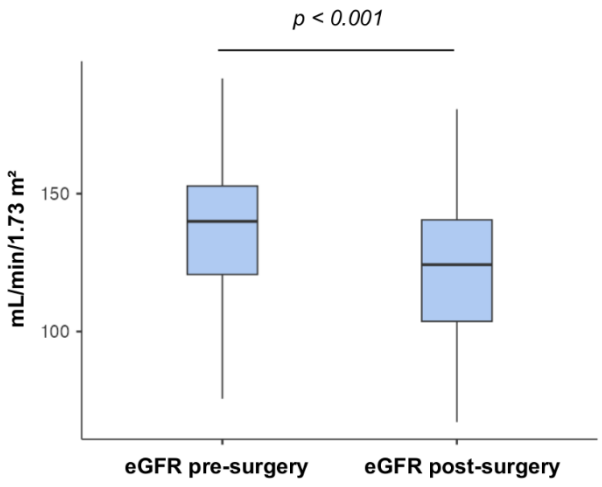

Figure 19. Comparison of z-scores of estimated Glomerular Filtration Rate (eGFR) in obese patients in pre-surgery and post-surgey setting. Box plots express the first (Q1) and third (Q3) quartiles within a given dataset by the upper and lower horizontal lines in a rectangular box, in which there is a horizontal line showing the median. The whiskers extend upwards and downwards to the highest or lowest observation within the upper (Q3+ 1.5 × interquartile range) and lower (Q1− 1.5 × interquartile range) limits. p values indicate statistical significances (< 0.05) between the different group.

After bariatric surgery, both sGFAP Z-scores (median 1.41; IQR 1.95; p< 0.001) and sNfL Z-scores (median 0.81; IQR 2.61p = 0.001) remained elevated in the obese group compared to the HCs group (GFAP Z score median – 0.53, IQR 2.04, **Figure 20 A**; NfL Z score median – 0.08, IQR 1.89; **Figure 20 B**). Moreover, we found a significant reduction in sGFAP Z Scores after surgery (p= 0.028) compared to pre-surgical values, but in contrast, sNfL values did not change (p = 0.25) by comparing pre- and post-surgical concentrations.

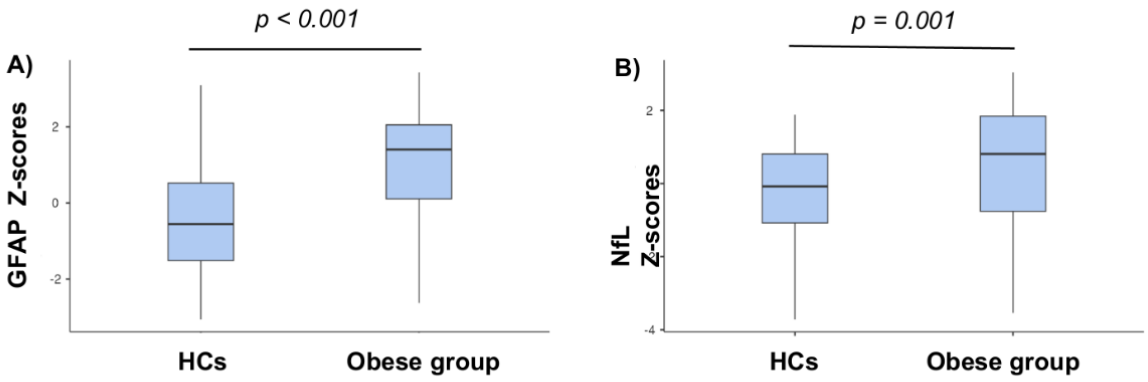

Figure 20 A-B. Comparison of z-scores of serum neurofilament light chain (sNfL) between obese patients and healthy controls (HCs) after surgery. Box plots express the first (Q1) and third (Q3) quartiles within a given dataset by the upper and lower horizontal lines in a rectangular box, in which there is a horizontal line showing the median. The whiskers extend upwards and downwards to the highest or lowest observation within the upper (Q3+ 1.5 × interquartile range) and lower (Q1− 1.5 × interquartile range) limits. p values indicate statistical significances (<0.05) between the different groups.

Linear regression analysis revealed that post-surgery eGFR values significantly predicted post-surgery sNfL levels. Post-surgery sNFL levels continued to have a significant positive correlation with age (r = 0.37, p = 0.003) and a negative correlation with post-surgery eGFR (r =-0.48, p< 0.001) and BSA (r – 0.36 p = 0.004). Regarding sGFAP levels a significant correlation was observed only with BSA (r – 0.26, p = 0.04). A statistically significant correlation was found between Δ% sNfL and Δ% BMI (r=-0.29, p=0.02). The correlation between anthropometric changes and Δ% eGFR revealed a significant correlation between Δ% eGFR and Δ% BSA (r=0.58, p< 0,001) (**Figure 21**). No significant other difference nor correlation was found.

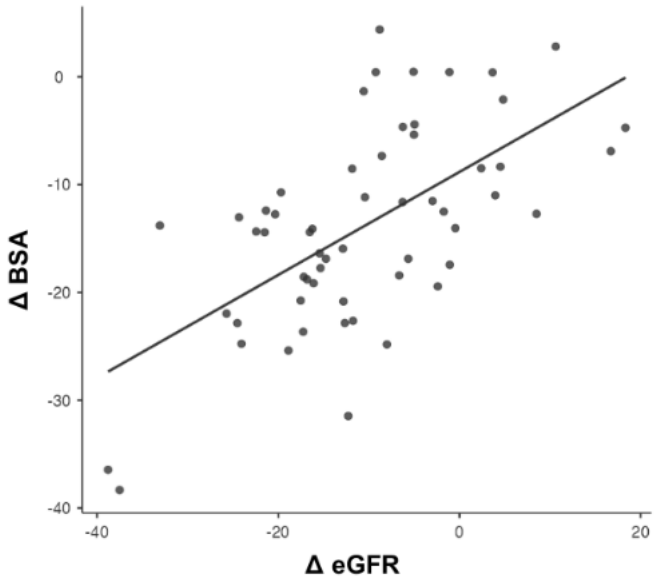

Figure 21. The scatter plot illustrates the positive correlation between the Δ body surface area (BSA, y-axis) and the Δ eGFR (x-axis).

Discussion

Our study shows new insights into how severe obesity and subsequent weight loss affect the levels of sGFAP and sNfL, as well as their connection to kidney function and BMI. Our study underline that patients with severe obesity have higher levels of hidden nerve damage and astrocyte activation than healthy controls. Bariatric surgery leads to significant changes in body measurements and kidney function, which also influences the behavior of biomarkers.

The first important finding in our study is the demonstration of subclinical neuroaxonal and glial damage in obese patients, which persists for up to one year after bariatric surgery. Obesity can cause damage to the nervous tissue through various mechanisms. Among these, the development of low-grade inflammation should be listed first.

Low-grade systemic inflammation is a critical factor, as it reflects a chronic inflammatory state. In obesity, the chronic release of pro-inflammatory cytokines promotes a state of systemic oxidative stress, triggering microglial activation, leading to the subclinical neuroinflammation reflected by elevated NfL and GFAP levels. In obesity, the chronic release of pro-inflammatory cytokines from dysfunctional adipocytes drives a state of systemic oxidative stress that triggers microglial activation, axonal injury, increasing blood-brain barrier permeability, thereby eliciting the subclinical neuroinflammation reflected by elevated GFAP and NfL levels. Consequently, inflammation is not merely a concomitant factor but one of driver of the entire neuro-metabolic cascade.

This is linked to the bloodstream's release of pro-inflammatory cytokines and adipokines, which may increase the blood-brain barrier's permeability. One of the first stages of a number of neurodegenerative diseases is this increased permeability. It is important to note that in animal models of obesity [137], [138], [139], the inflammatory pattern is associated with reduce synaptic plasticity, impaired neurogenesis [140], [141] and neuronal toxicity as well as increased expression of GFAP by astrocytes [142]. Furthermore along with the accumulation of fat mass, leptin levels increase while adiponectin decreases. Leptin appears to play a role in several aspects of obesity-related cerebral parenchymal damage, mainly by encouraging neuroinflammation. Additionally, long-term excessive consumption of foods high in carbohydrates and saturated fats in obese people can change cerebral glucose consumption, which can impact insulin secretion [143]. Furthermore, the second significant finding confirms that the levels of sNfL and sGFAP in obese patients are significantly influenced by renal function. Renal hyperfiltration represent a distinctive charatteristics of obesity [144] and it can be hypothesized that the normalization of the eGFR induced by weight loss in turn decreases the renal clearance of these biomarkers. This hypothesis is further supported by the significant relationship we found between Δ% eGFR and Δ% BSA, suggesting that a greater reduction in BSA was associated with a greater post-surgical decline in eGFR. Moreover, it should be that only sGFAP levels demonstrated a significant decrease following the weight-loss intervention, whereas sNfL levels exhibited an upward trend, but the increse was not-statistically significant. Despite this reduction, sGFAP levels remained elevated compared to those observed in HCs. A possible explanation could be related to the different half-lives and blood kinetics of these two biomarkers. In particular, sNfL is known to peak between 7 and 10 days after CNS injury and to exhibit a blood half-life of up to one to two months, making it a good suit for detecting cumulative or subacute neuroaxonal damage [144], [145].On the other hand, sGFAP rises rapidly, within 1 hour of CNS damage, peaks at 20–24 hours, and returns to baseline within 72 hours, reflecting acute astroglial activation [146], [147], [148].

The different behaviour of serum concentrations of these two biomarkers, when comparing during pre- and post- levels, could be due to the differing impact that the normalization of the hyperfiltration renal state has on them. sGFAP can be seen as a more "rapidly responding" biomarker compared to sNfL, primarily due to their different blood kinetics [144]. Another possible explanation for these findings could involve the differences in the underlying pathological processes driving the release of these biomarkers. While neuroaxonal damage, represented by sNfL, may be a more chronic or cumulative process that is less immediately affected by short-term interventions, astrocyte activation, represented by sGFAP levels, may be easily reversible in response to metabolic improvements following weight loss. This distinction could contribute to the differenzial behavior observed between the two circulating biomarkers after surgery. Finally, it should also be acknowledged that, to detect significant differences in the blood concentrations of these biomarkers in the obese population, it is necessary to standardize the values by using Z-scores accounting for age, BMI, and assay characteristics, as we did. In order to improve compatibility of result all similar studies must take these factors into account.

This study presents both strengths and limitations. By evaluating both sGFAP and sNfL in obese subjects, it provides valuable insights into astrocytic activation and neuroaxonal integrity in this condition, shedding light on how metabolic dysfunction and bariatric surgery influence these processes. The longitudinal design, with pre- and post-surgical measurements, enables a dynamic evaluation of biomarker changes over time, enhancing our understanding of the metabolic and renal influences on their levels.

However, this study also has some limitations. The reliance on blood-based biomarkers does not fully capture the neuroinflammatory or neurodegenerative processes occurring within the brain. The inclusion of neuroimaging data (e.g., MRI, PET scans) could have strengthened the findings by providing a direct assessment of structural and functional brain changes. Moreover, while renal function was considered, other potential contributors to biomarker variability, such as insulin resistance, lipid metabolism, and systemic inflammation (e.g., cytokine levels), were not extensively analyzed. These factors could provide further mechanistic insights into the observed changes. Another limitation of the study is the indirect assessment of renal clearance using the CKD-EPI formula, which prevents correlation analyses with age and Z-scores. Additionally, the study examines biomarker trends up to 12 months post-surgery, but longer follow-up is needed to determine whether these neurobiological changes persist, stabilize, or evolve further over time. Finally, the inclusion of a detailed neuropsychological assessment of these patients in the study protocol, both in the pre- and post-surgery phases, could have provided clinical significance to these biomarker modifications.

Regarding clinical utility, these biomarkers provide a non-invasive tool to stratify 'at-risk' patients and monitor therapeutic efficacy. Since our data indicates that damage persists after surgery, these markers can be used to assess whether weight loss effectively translates into a reduction of central neuroinflammation over time.

Although the observed increase in serum sNfL concentrations was not statistically significant, it may still reflect persistent neuroaxonal damage following weight loss. As previously discussed, NfL exhibits distinct blood kinetics and a prolonged half-life of up to one to two months, in contrast GFAP rises soon after CNS injury. Importantly, it must be emphasized that this increase lacks statistical significance, and further investigation is warranted to clarify its clinical relevance.

CHAPTER 5- PROJECT using HOMEBREW SIMOA technology

PROJECT 1- Serum PRPH concentration levels in hereditary Transthyretin amyloidosis

This study aims to investigate serum PRPH concentrations as a novel, PNS-specific biomarker in ATTRv, addressing the critical unmet need for biomarkers that can distinguish PNS damage from CNS involvement. Assessing serum PRPH levels in symptomatic and presymptomatic ATTRv patients, alongside sNfL, and comparing findings with healthy controls. This study seeks to provide complementary diagnostic and pathophysiological insights to sNfL, ultimately improving early detection and clinical management of ATTRv. This project is currently unpublished.

Methods

ATTRv patients

This multicenter, cross-sectional cohort study focuses on the subject with TTR variants, encompassing both symptomatic ATTRv patients and pre-symptomatic carriers. Participants were recruited from leading Italian reference center specializing in the diagnosis and management of ATTRv, with all enrolled subjects—both symptomatic and pre-symptomatic—undergoing comprehensive assessments by expert neurologists, including neurological, genetic, and demographic evaluations. A healthy control (HC) group, free of neurological, cardiac, renal, or autoimmune conditions, was included for comparative analysis. The study was conducted in accordance with the Declaration of Helsinki (1964) and received ethical approval from the Comitato Etico Territoriale Lazio Area 3 at Fondazione Policlinico Agostino Gemelli IRCCS.

The predicted age of onset of symptomatic disease (PADO) has been estimated for all the pre-symptomatic ATTRv subjects, considering the specific TTR gene mutation, the typical age of onset for that mutation and the age of onset in other members of the proband's family, as previously recommended [150]. The difference of the age of the pre-symptomatic ATTRv subjects and the PADO was, therefore, calculated and named "Years from PADO". All enrolled subjects underwent an extensive medical evaluation. For patients with evidence of polyneuropathy, disease severity was assessed using the Neuropathy Impairment Score (NIS) [151]. Peripheral blood samples were

collected in additive-free vacutainers with separating gel to obtain serum for analysis, centrifuged at 3000 rpm for 10 minutes at room temperature and stored at -80 degrees.

Serum Bovine Albumin (BSA) removal procedure

The chosen capture antibody, 8G2 (Merck P5117), according to the datasheet, is expected to contain 1% BSA. BSA is a protein used in antibody preparations in liquid format as a stabilizer; it improves the solubility of the antibody in the buffer and reduces the nonspecific absorption. Given that bovine serum albumin (BSA) has a molecular weight of 66.5 kDa, its substantial size can potentially interfere with the subsequent binding between the antibody and the antigen. For this reason, to utilize the antibody effectively in our assay development, we remove the BSA using the Pierce Antibody Clean-Up Kit from Thermo Scientific™ (Waltham, MA, USA). This step ensures that the antibody is free from BSA interference, optimizing its performance in the assay.

Single-molecule biomarker detection is made possible by the Simoa SR-X platform, which is a breakthrough in ultra-sensitive immunoassay technology. Its "homebrew"compatible design enables labs to create unique assays for new or uncommercial biomarkers, extending the scope of research and diagnostic capabilities beyond those of commercial kits.

Developing Homebrew Assay

In developing Homebrew Immunoassay for PRPH, the choice of capture and detector antibodies is pivotal for optimizing assay performance. Initially, we evaluated MAB 1527 (Sigma-Aldrich, Merck) and A-3 anti-peripherin (Santa Cruz Biotechnology) as potential capture antibodies, and 8G2 (Sigma-Aldrich, Merck) and A-3 anti-peripherin (Santa Cruz Biotechnology) as detector antibody. Based on the best performance obtained, we ultimately selected 8G2 monoclonal antibody (Sigma-Aldrich, Merck) as capture and A-3 anti-peripherin (Santa Cruz Biotechnology) as detector antibodies. The antibodies were conjugated to beads or biotinylated according to the Simoa Homebrew Assay Development Guide (Quanterix) for compatibility with semi-automated ultrasensitive SR-X Biomarker Detection System (Quanterix, Billerica, MA, USA). (https://portal.quanterix.com/folder-viewer/Homebrew).

Protocol for Capture Antibody

The capture antibody was first buffer exchanged into Bead Conjugation Buffer using Amicon Ultra0.5 50 kDa centrifugal filters (Merck Millipore). The antibody was concentrated, and its final volume was carefully adjusted to achieve a concentration of 0.2 mg/mL in a total volume of 300 µL of Bead Conjugation Buffer. Paramagnetic carboxylated beads (Quanterix) were used, firstly added with cross-linker agent 1-ethyl-3-(3-dimethylaminopropyl) carbodiimide (EDC) at 0.3 mg/mL concentration. The paramagnetic beads were then resuspended to a final concentration of 1.4 × 10 9 beads/mL in the

capture antibody solution. The reaction was allowed to proceed for 120 minutes at 2–8°C under gentle agitation using a HulaMixer (Thermo Fisher Scientific), which ensured continuous bead suspension and uniform conjugation. After conjugation, the beads were washed to remove excess EDC and unbound antibody. A blocking solution was then added to the beads to minimize non-specific binding, and the mixture was incubated for 45 minutes at 2–8°C. Following this, the beads underwent three additional washes to remove any residual blocking solution and unbound components. Finally, the conjugated beads were resuspended and maintained at 4°C until further use.

Protocol for Detection Antibody preparation:

The detection antibody was prepared by performing a buffer exchange into Biotinylation Reaction Buffer (Quanterix) using Amicon Ultra-0.5 50 kDa centrifugal filters (Merck). The starting concentration of the antibody was adjusted at 130 ug with Biotinylation Reaction Buffer. The antibody solution was then subjected to consecutive washing steps, the concentration of the recovered antibody was then adjusted to 1 mg/mL using the same buffer. For biotinylation 8.9 mM NHS-PEG4-Biotin (Thermo Fisher Scientific) and Biotinylation Reaction Buffer were used. The antibody was biotinylated at a 40× challenge ratio. The mixture was vortexed, briefly centrifuged, and incubated for 30 minutes at room temperature to allow biotin conjugation. Amicon filter buffer exchange was performed to remove unbound compounds. The final concentration of the Ab was measured by NanoDrop One (Thermo Fisher Scientific).

Procedure:

The measurement of PRPH valuesonducted using the semi-automated ultrasensitive SR-X Biomarker Detection System (Quanterix, Billerica, MA, USA). Serum samples were diluted 1:4 with Sample Diluent A, provided by Quanterix. The capture antibody use is the 8G2 antibody (Sigma-Aldrich, Merck), from which 1% BSA has been previously removed using Antibody Clean/up Kit (Thermo Scientific™ Waltham, MA, USA), and then conjugated with paramagnetic beads (Quanterix, Billerica, MA, USA) at a concentration of 0.02 µg/mL. The A-3 anti-peripherin antibody (Santa Cruz) is used as the detector, byotinilated with NHS-PEG4-biotin (A3959: Thermo Scientific™ Waltham, MA, USA). After dilution, 150 µL of each sample was dispensed per well. Following the two-step protocol, 20 µL of capture antibody conjugated to paramagnetic beads, no helper beads were used, and 20 µL of detector antibody, at a concentration of 1µg/mL, were added to each well. The plate was then incubated for 30 minutes at 30°C with shaking at 800 rpm.

Following the two-step assay, the plate was washed using SIMOA microplate washer (Quanterix, Billerica, MA, USA). Streptavidin-β-galactosidase (SβG) was subsequently added at a concentration of 25 pM. After two additional wash steps and a 1-minute incubation on the plateshaker at 800 rpm,

the plate was ready for analysis. The SR-X instrument was used to read the plate, generating results through both analog and digital measurements.

The calibration curve was optimized range 0 to 3300 pg/mL, consisting of eight points generated using a 1:3 serial titration with full-length human recombinant peripherin protein (NM_006262, Origene). Lower limit of detection (LLOD) was calculated as 2.5 times the standard deviation (STD) added to the mean average enzymes per bead (AEB) derived from six blank replicates. This yielded an LLOD of 0.0038 pg/mL, which was subsequently adjusted to 0.015 pg/mL following a 1:4 sample dilution **Figure 22.**

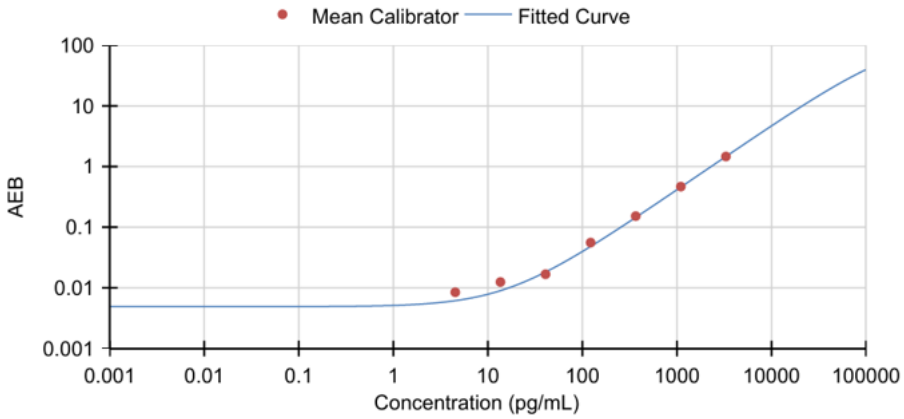

Figure 22. In this graph we show an example of calibration curve. Concentration points (from Cal B 4.11 pg/mL to Cal H 3300 pg/mL) in X axis was reported. In Y axis AEB was reported. R^2 of 0.9961 was shown.

In the Homebrew assay, the important parameters to consider are:

1. **Bead Conjugation Percentage:** This parameter indicates the extent to which the capture antibody is bound to the paramagnetic beads. This parameter indicates the number of Ab bound to the beads, thereby reflecting the potential binding sites available per bead.

2. **Active Bead Equivalent (AEB):** This measures the number of paramagnetic beads considered active in a well of the immunoassay plate. The AEB is primarily based on the total number of beads present in a well and the fraction of beads that have successfully linked to an immunocomplex. The AEB is based on the fraction ON (fON) it's the number of active beads present in the well, and the total number of beads present in the well.

The assay was considered optimized when the signal-to-noise (S/N) ratio of the beads in Calibrator B exceeded that of Calibrator A by at least 2.5-fold, with a consistently high S/N ratio maintained up to Calibrator H. The percentage of the coefficient of variation (CV%) is a statistical metric used to assess the relative variability of data, particularly when comparing datasets with different units or

widely varying means. A CV of less than 20% indicates low variability in relation to the mean and guarantees consistent and reproducible data, which is necessary for results to be considered statistically significant (**Figure 23).**

Sample Name	AEB	Conc.	Errors	# Beads	fON	Mean	STD	CV %	S/N
Cal A	0.000738	0		35,121	0.00737				
Cal A	0.000752	0		42,215	0.00748	0.000745	9.9E-06	0.013288	1
Cal B	0.006519	4.5		30,625	0.006498				
Cal B	0.007782	4.5		29,154	0.007752	0.007151	0.000893	0.124897	9.597987
Cal C	0.016148	13.6		40,766	0.016018				
Cal C	0.017717	13.6		38,323	0.017561	0.016933	0.001109	0.065522	22.72819
Cal D	0.064427	40.7		30,579	0.062396				
Cal D	0.06907	40.7		34,163	0.066739	0.066749	0.003283	0.049186	89.5953
Cal E	0.150412	122.20		42,142	0.139647				
Cal E	0.136124	122.20		34,432	0.127265	0.143268	0.010103	0.070519	192.306
Cal F	0.37241	366.70		41,627	0.310928				
Cal F	0.326353	366.70		36,951	0.27845	0.349382	0.032567	0.093214	468.9685
Cal G	0.691268	1,100.00		37,212	0.499059				
Cal G	0.741985	1,100.00		38,100	0.523832	0.716627	0.035862	0.050043	961.9148
Cal H	3.114734	3,300.00		37,942	0.70671				
Cal H	3.262434	3,300.00		27,089	0.774447	3.188584	0.10444	0.032754	4279.979

Figure 23. A run data example is displayed in the figure. Specifically, all of the crucial parameters for achieving good dosage results are reported, starting from the left: the run name, the calibrators, the Active Bead Equivalent (AEB), the theoretical concentrations, the number of beads per well, the fraction of active beads/total number of beads (fON), the mean, the Standard deviation (STD), the % Coefficient of Variation (CV%), and the Signal to Noise ratio (S/N).

NfL analysis

Serum concentrations of NfL were determined in patients' samples using commercially available immunoassay kits for NfL and GFAP – SiMoA™ assay Neurology 2-Plex B (GFAP, NfL) Assay Kit (Catalog #103520; Quanterix, Billerica, MA, USA). The assays were conducted on the semi-automated ultrasensitive SR-X Biomarker Detection System (Quanterix). Serum samples were diluted at 1:4 and randomly distributed on 96-well plates. Quality control (QC) samples, provided with the kit, exhibited concentrations within the predefined range and the coefficient of variance across the plates was maintained below 10%.

Statistical Analysis

Descriptive analyses and demographic data were summarized using the number of patients and median values with interquartile ranges (25th–75th percentile). The distribution of continuous variables was assessed with the Shapiro–Wilk test. sNfL values were logarithmically transformed (Log10) in accordance with established methodologies [77]

Non-parametric two-tailed Spearman correlations were performed to evaluate the relationships between all continuous variables in the HC and ATTRv cohorts. Nonparametric one-way Kruskal–Wallis analysis of variance (ANOVA) was used to compare PRPH levels among the HC cohort and the ATTRv presymptomatic and symptomatic groups. ANCOVA, with age included as a covariate, was performed to assess differences in sNfL levels among the same groups.

Binomial regression models were subsequently applied to evaluate the predictive performance of models including serum PRPH alone, as well as in combination with sNfL and age, in distinguishing the HC cohort from the ATTRv groups. Receiver Operating Characteristic (ROC) curve analyses were performed to assess the discriminative ability of each biomarker, with calculation of the area under the curve (AUC), sensitivity, and specificity. For regression models, model fit was assessed using Nagelkerke's R^2 (R^2N) and the Akaike Information Criterion (AIC). Cut-off values were selected from univariate models using Youden's J statistics. Statistical significance was defined as $p < 0.05$. All statistical analyses were conducted using Jamovi software (The Jamovi Project, 2021).

Results

Two cohorts of subjects were enrolled. The first, referred to as the ATTRv cohort, included 96 individuals divided into two groups: 49 presymptomatic ATTRv and 47 symptomatic ATTRv subjects. The second cohort consisted of 42 HCs, referred to as the HC cohort. Demographic data and descriptive analyses of the biomarkers are presented in **Table 10**.

Correlation analysis

No significant correlation was found between age and PRPH levels in either cohort (ATTRv or HCs). In the ATTRv cohort, PRPH levels did not correlate with sNfL levels, even when presymptomatic and symptomatic groups were analyzed separately. Similarly, no significant correlation was observed between PRPH levels and either the predicted age of onset (PADO) or the "years from PADO" in the presymptomatic ATTRv group. Moreover, no significant correlation was found between PRPH levels and the NIS score in the symptomatic ATTRv group. sNfL levels showed a significant positive correlation with age in the HCs cohort ($r = 0.6$, $p<0.001$) and in the presymptomatic ATTRv group ($r = 0.5$, $p< 0.001$), whereas no correlation with age was found in the symptomatic ATTRv group. sNfL levels were positively correlated with the NIS score in the symptomatic ATTRv group ($r = 0.4$, $p = 0.002$) and with "years from PADO" in the presymptomatic ATTRv group ($r = –0.4$, $p = 0.006$).

Comparison analysis

Kruskal-Wallis ANOVA model showed a significant difference in PRPH levels between disease status ($X^2 =34$, $p< 0.001$). Specifically, higher PRPH levels were significantly associated with both presymptomatic ($p< 0.001$) and symptomatic ATTRv groups ($p< 0.001$) compared with healthy

controls (HCs), whereas no significant difference in serum PRPH levels was observed between presymptomatic and symptomatic ATTRv subjects (**Figure24**).

ANCOVA model revealed significant differences in sNfL levels between disease status (F=57.66, p<0.001). Higher sNfL levels were significantly associated with symptomatic ATTRv patients compared with both presymptomatic ATTRv subjects (p <0.001) and HCs (p <0.001). In contrast, no significant difference in sNfL levels was observed between ATTRv presymptomatic subjects and HCs (**Figure 25**).

Binomial logistic regression

A binomial logistic regression model assessing the association between serum PRPH levels and disease status (ATTRv vs. HC) showed a significant overall model fit ($p < 0.001$; $R^2_n = 0.33$; AIC = 128.3), indicating that PRPH significantly contributed to group classification, with a sensitivity of 76% and specificity of 76% (AUC = 0.83) in discriminative performance. **Figure 25**. Youden's index analysis identified 16.03 pg/mL of peripherin as the optimal cut-off to discriminate between the ATTRV cohort and HCs (sensitivity 76%, specificity 77%, Youden's Index 0.54).

	HCs Cohort	**ATTRv whole cohort**	**ATTRv Symptomatic group**	**ATTRv Presymptomatic group**
Number patients (Female/male)	42 (14/28)	96 (38/58)	47 (12/35)	49 (26/23)
Median Age (years, 25th–75th percentile)	44.5 (34.2 – 53)	63 (46.5 – 71.3)	70 (66 – 75)	47 (43 – 57)
Mutation (number of subjects, median age, number of female subjects)			V30M (24; 69 years; 4 F) F64L (13; 70 years; 5 F) I68L (3; 74 years; 0 F) V122I (3; 70 years; 0 F) E89Q (2; 71.5 years; 2 F) A120S (1; 72 years; 1 F) V32R (1; 65 years; 0 F)	V30M (28; 45 years; 15 F) F64L (13; 51 years; 6 F) I68L (2; 45.5 years; 2 F) V122I (1; 59 years; 0 F) E89Q (3; 47 years; 2 F) A109S (1; 45 years; 1 F) E62K (1; 59 years; 0 F)
NIS scores (median, 25th–75th percentile)	NA	NA	47 (11.5 – 82.3)	NA

PADO (median, 25th–75th percentile)	NA	NA	NA	56 (54 – 64)
Years from PADO (median, 25th–75th percentile)	NA	NA	NA	11 (1– 16)
Serum Perpherin pg/mL (median, 25th–75th percentile)	7.8 (2.57 – 19.7)	38 (16.6 – 62.9)	44 (19 – 66.8)	37.2 (16.1 – 62.7)
Serum NfL pg/mL (median, 25th–75th percentile)	7.6 (5.5 – 9.52)	15.4 (7.8 – 43.9)	43.7 (25.8 – 64.6)	8.6 (5.1 – 12.4)

Table 10. Demographic data and descriptive analysis of serum sNfL, PRPH in healthy control cohort (HCs), in ATTRv whole cohort, ATTRv Syntomatic group and ATTRv pre-syntomatic group. Years from "Predicted age of onset of symptomatic disease"(PADO).

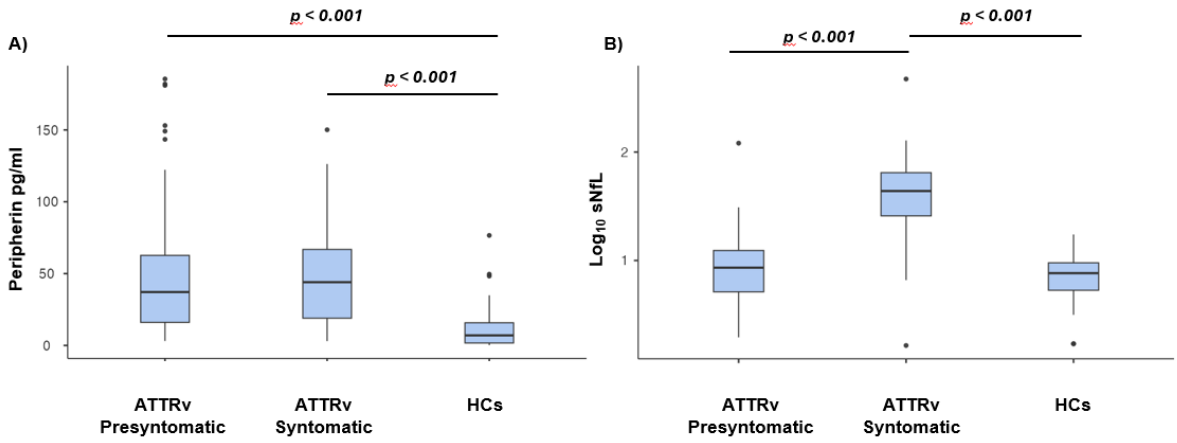

Figure 24. Serum levels of PRPH (A) and the sNfL (B) across healthy controls (HCs), presymptomatic ATTRv, and symptomatic ATTRv subjects. Box plots express the first (Q1) and third (Q3) quartiles by the upper and lower horizontal lines in a rectangular box, in which there is a horizontal line showing the median. The whiskers extend upwards and downwards to the highest or lowest observation within the upper (Q3+1.5 × IQR) and lower (Q1 - 1.5×IQR) limits. P values indicate statistical significance between the different groups.

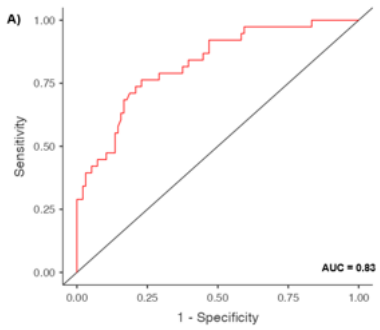

Figure 25. This graph shows PRPH ROC curves. In particular, ROC curve illustrates the diagnostic performance for the ATTRv group versus the HCs cohort of the binomial regression model 1 (peripherin alone) with a sensitivity/specificity of 76%/76% and an area under the curve (AUC) of 0.83.

Discussion

To the best of our knowledge, this represents the first study to measure PRPH levels in the blood of patients with hereditary ATTRv and the third study to explore PRPH as a biomarker of PNS damage. Our findings demonstrate that PRPH is a valuable blood biomarker in ATTRv, with elevated serum concentrations detectable as early as the presymptomatic stage and remaining high as patients progress to symptomatic stages.

PRPH is a class III intermediate filament protein predominantly expressed in the PNS, particularly in motor and sensory neurons, where it plays a critical structural role [152], [153], [154]. It interacts with other structural proteins, such as NfL [155], [156]. The identification of a biomarker specific to the PNS, such as PRPH, is of relevance. The introduction of disease-modifying therapies for ATTRv necessitates increasingly precise diagnostic tools capable of enabling effective early diagnosis and accurate monitoring of neurological damage. Compared to other neurological diseases involving both the central and peripheral nervous systems, ATTRv presents the challenge of distinguishing the "central" component of sNfL from the "peripheral" one. In this perspective, having a biomarker specific to the PNS offers a significant advantage.

A key result of our study is that serum PRPH concentrations serve as a robust biomarker for both presymptomatic and symptomatic ATTRv patients. We hypothesize that PNS damage, for which PRPH is a specific biomarker, begins before clinical onset. The lack of correlation between serum PRPH and sNfL levels suggests that these biomarkers follow distinct kinetics and reflect different

mechanisms of damage in disease pathogenesis. Specifically, sNfL is a biomarker of clinical onset, severity, and progression, whereas PRPH may be a superior biomarker for the preclinical stage. However, although serum PRPH levels reflect early PNS damage in ATTRv, they do not correlate with disease progression indices, such as years from PADO in presymptomatic patients or clinical severity in symptomatic patients. Therefore, PRPH may serve as a marker of neuronal stress and regeneration, as suggested by murine studies [157], rather than as a marker of irreversible neuroaxonal damage.

The absence of a correlation between serum PRPH concentrations and age has been previously reported [158], [159]. Unlike sNfL, this finding is significant for establishing universal cut-off values for serum PRPH concentrations, which could simplify clinical practice. In contrast, sNfL levels in serum and cerebrospinal fluid require age adjustment.

Another notable result is the lack of correlation between serum PRPH and NfL levels, consistent with the two prior studies that quantified PRPH. We hypothesize that this lack of correlation may be due to the broader distribution of NfL compared to PRPH, as well as their distinct kinetics, with PRPH potentially exhibiting a more rapid response [157].

Our study has several strengths and limitations. Regarding the methodology, our "homebrew" assay using the Simoa platform closely follows the protocol described by Keddie et al., although it is not entirely identical and employs a different instrument (SR-X instead of HD-X). Specifically, we used the same antibody pair, which, in our experience, yields the best performance. The reproducibility of our method is ensured by our detailed description of the procedures.

A second strength is the large sample size for a rare disease such as ATTRv, as well as the timing of blood sampling—conducted prior to the initiation of any treatment in all patients—and the comprehensive clinical characterization of the cohort.

The primary limitation is the cross-sectional design of the study, which precludes hypotheses about the longitudinal kinetics of serum PRPH or its response to treatment.

Furthermore, these concentrations were assessed in a single laboratory at the University of Siena. While this ensured satisfactory data reliability, confirmed by low intra-operator variability, future studies should include inter-laboratory comparisons to provide greater technical validation of the homebrew assay described here, to assess potential variability in PRPH measurements across different experimental settings.

Secondly, as we already specified in the first chapter, despite the fact that peripherin is found in higher amounts in peripheral axons, it is also present in the CNS, including in the corpus callosum, optic tracts, internal capsule, brainste m, and cerebellum, where it might be involved in the restoration and maintenance of neuronal fibers after axonal damage[63]. Therefore, we cannot exclude the possibility of a contribution from CNS axonal damage to the measured peripherin levels.

To sum up, our study provides compelling evidence that serum PRPH is a promising biomarker for early detection and monitoring of PNS damage in ATTRv. While further longitudinal research is needed to fully elucidate its kinetics and clinical utility, these findings lay the groundwork for future investigations and potential integration of PRPH into diagnostic and prognostic protocols for ATTRv.

Conclusions

This thesis explores the potential of circulating biomarkers in addressing the challenges posed by neurodegenerative and neuroinflammatory disorders. In response to the escalating global burden of neurodegenerative disease, an issue of increasing relevance and central importance to public health in the coming years, this thesis systematically investigated and validated circulating biomarkers. These biomarkers serve as critical indicators of neuroaxonal and glial damage in neurodegenerative and neuroinflammatory conditions, which are hallmark features of neurological diseases. One first focus of this thesis was to test whether the new elisa technology, whether Ella or SiMoA technologies, will be the most relevant technology for detecting those biomarkers. Additionally, we examined the correlation between CSF and serum levels, emphasizing the importance of utilizing less invasive serum-based matrices as an alternative to CSF for clinical applications. This approach enhances therapeutic stratification, diagnostic pathways, disease monitoring, and routine clinical practice. Of particular significance is the final project, which centered on the development of a novel assay for peripherin, a protein with potential as a biomarker reflecting PNS damage. This innovation addresses a critical gap in distinguishing PNS involvement from CNS pathology. Finally, this research underscores the importance of integrating biomarker data with clinical, imaging, and genetic information to enable a proactive approach to disease management. By accounting for factors such as sex-specific differences, renal function, and other confounding variables, this work highlighted the advancement of personalized medicine and targeted therapies, ultimately enhancing diagnostic accuracy and patient outcomes in neurological disorders. This thesis is not without limitations. To address potential biases and enhance generalizability, future research should incorporate multi-center studies with larger cohorts, enabling cross-laboratory validation and more robust applications. Additionally, the integration of neuroimaging and comprehensive neuropsychological assessments could provide deeper insights into the structural and functional correlations of biomarker changes. Exploring the interplay between biomarkers, metabolic dysfunction, and systemic inflammation—particularly in obesity and ATTRv—may uncover novel pathways for intervention.

This thesis contributes to demonstrating the clinical utility of novel biomarkers, including NfL, GFAP, GDF-15, TDP-43, and PRPH, in detecting early pathological changes, monitoring disease progression, and evaluating therapeutic responses. In the first chapter, we described the importance of comparing biomarker concentrations in CSF and serum, highlighting how non-invasive techniques, as blood sampling can effectively identify and characterize neurodegeneration and neuroinflammation across

various neurological disorders. The second chapter describes the use of advanced analytical platforms, such as Ella and Simoa, which achieve femtomolar sensitivity. This enhanced sensitivity is a critical requirement for detecting low-abundance biomarkers in biofluids. In preceding chapters, we have established that CSF and serum NfL levels are recognized as biomarkers of neurodegenerative damage across multiple diseases.

Additionally, we demonstrated that in ATTRv, sGFAP elevation identifies the disease at presymptomatic stages, reflecting early neuroaxonal injury. This opens the door to considering sGFAP, not only as a biomarker of CNS damage, as previously established, but also as a potential indicator of PNS injury. Beyond the well-established NfL and GFAP, which are gaining growing recognition for assessing neuroaxonal and neuroglial damage and predicting neurodegenerative disease progression, we analyzed additional biomarkers, including TDP-43 and GDF-15, in various research projects. Specifically, no correlation was observed between TDP-43 levels in blood and CSF samples. The limitations in detecting and quantifying TDP-43, as reported in recent literature, appear to be linked to the methodology employed. Indeed, Seed Amplification Assay (SAA) technology is now preferred over Simoa for TDP-43 detection, as evidenced by recent studies [159], [160].Furthermore, we investigated GDF-15 as a potential biomarker of neurodegeneration in AD. Through mediation analysis, we correlated GDF-15 levels with MMSE, positioning it as a promising risk marker for recognizing neurodegeneration in AD. Additional research is required to clarify the potentiality of this novel biomarker in neurodegenerative disorders. Further studies will be needed to assess the importance of this potential biomarker in neurodegenerative disorders. Finally, we focused on PRPH, a recently identified fluid biomarker. Using the previously mentioned technology, we developed a "homebrew" assay to experimentally detect PRPH in a cohort of patients with peripheral neuroaxonal damage. As research continues to refine these tools, their integration into routine clinical practice will be pivotal for precision medicine in neurodegenerative disorders.

References

[1] V. L. Feigin *et al.*, “The global burden of neurological disorders: translating evidence into policy,” *Lancet Neurol.*, vol. 19, no. 3, pp. 255–265, Mar. 2020, doi: 10.1016/S1474-4422(19)30411-9.

[2] K. S. Steinbeck, “The importance of physical activity in the prevention of overweight and obesity in childhood: a review and an opinion,” *Obesity Reviews*, vol. 2, no. 2, pp. 117–130, May 2001, doi: 10.1046/j.1467-789x.2001.00033.x.

[3] A. Chudzik, A. Śledzianowski, and A. W. Przybyszewski, “Machine Learning and Digital Biomarkers Can Detect Early Stages of Neurodegenerative Diseases,” *Sensors*, vol. 24, no. 5, p. 1572, Feb. 2024, doi: 10.3390/s24051572.

[4] ROSENTHAL TB., “The effect of temperature on the pH of blood and plasma in vitro.,” *J Biol Chem.* .

[5] W. M. Pardridge, “CSF, blood-brain barrier, and brain drug delivery,” *Expert Opin. Drug Deliv.*, vol. 13, no. 7, pp. 963–975, Jul. 2016, doi: 10.1517/17425247.2016.1171315.

[6] D. M. Rissin and D. R. Walt, “Digital Concentration Readout of Single Enzyme Molecules Using Femtoliter Arrays and Poisson Statistics,” *Nano Lett.*, vol. 6, no. 3, pp. 520–523, Mar. 2006, doi: 10.1021/nl060227d.

[7] A. Petzold, “The 2022 Lady Estelle Wolfson lectureship on neurofilaments,” *J. Neurochem.*, vol. 163, no. 3, pp. 179–219, Nov. 2022, doi: 10.1111/jnc.15682.

[8] P. Grant and H. C. Pant, “Neurofilament protein synthesis and phosphorylation,” *J. Neurocytol.*, vol. 29, no. 11–12, pp. 843–872, Nov. 2000, doi: 10.1023/A:1010999509251.

[9] J. B. Jones and C. R. Safinya, “Interplay between Liquid Crystalline and Isotropic Gels in Self-Assembled Neurofilament Networks,” *Biophys. J.*, vol. 95, no. 2, pp. 823–835, Jul. 2008, doi: 10.1529/biophysj.107.127415.

[10] S. W. L. V. Carden MJ, “The structure, biochemical properties, and immunogenicity of neurofilament peripheral regions are determined by phosphorylation state.,” *J Biol Chem.*.

[11] P. A. C. Cloos and S. Christgau, “Post-Translational Modifications of Proteins: Implications for Aging, Antigen Recognition, and Autoimmunity,” *Biogerontology*, vol. 5, no. 3, pp. 139–158, Jun. 2004, doi: 10.1023/B:BGEN.0000031152.31352.8b.

[12] S. N. Lawson, M. J. Perry, E. Prabhakar, and P. W. McCarthy, “Primary sensory neurones: Neurofilament, neuropeptides and conduction velocity,” *Brain Res. Bull.*, vol. 30, no. 3–4, pp. 239–243, Jan. 1993, doi: 10.1016/0361-9230(93)90250-F.

[13] C. Maniero *et al.*, “NEFM (Neurofilament Medium) Polypeptide, a Marker for Zona Glomerulosa Cells in Human Adrenal, Inhibits D1R (Dopamine D1 Receptor)–Mediated Secretion of Aldosterone,” *Hypertension*, vol. 70, no. 2, pp. 357–364, Aug. 2017, doi: 10.1161/HYPERTENSIONAHA.117.09231.

[14] J. B. Jones and C. R. Safinya, “Interplay between Liquid Crystalline and Isotropic Gels in Self-Assembled Neurofilament Networks,” *Biophys. J.*, vol. 95, no. 2, pp. 823–835, Jul. 2008, doi: 10.1529/biophysj.107.127415.

[15] R. J. Lasek, M. M. Oblinger, and P. F. Drake, “Molecular Biology of Neuronal Geometry: Expression of Neurofilament Genes Influences Axonal Diameter,” *Cold Spring Harb. Symp. Quant. Biol.*, vol. 48, no. 0, pp. 731–744, Jan. 1983, doi: 10.1101/SQB.1983.048.01.076.

[16] C. Balaratnasingam, W. H. Morgan, L. Bass, G. Matich, S. J. Cringle, and D.-Y. Yu, “Axonal Transport and Cytoskeletal Changes in the Laminar Regions after Elevated Intraocular

Pressure," *Investigative Opthalmology & Visual Science*, vol. 48, no. 8, p. 3632, Aug. 2007, doi: 10.1167/iovs.06-1002.

[17] R. A. Nixon and K. B. Logvinenko, "Multiple fates of newly synthesized neurofilament proteins: evidence for a stationary neurofilament network distributed nonuniformly along axons of retinal ganglion cell neurons.," *J. Cell Biol.*, vol. 102, no. 2, pp. 647–659, Feb. 1986, doi: 10.1083/jcb.102.2.647.

[18] M. F. Calmon *et al.*, "Epigenetic silencing of neurofilament genes promotes an aggressive phenotype in breast cancer," *Epigenetics*, vol. 10, no. 7, pp. 622–632, Jul. 2015, doi: 10.1080/15592294.2015.1050173.

[19] N. M. Hasan *et al.*, "Epigenetic signatures differentiate uterine and soft tissue leiomyosarcoma," *Oncotarget*, vol. 12, no. 16, pp. 1566–1579, Aug. 2021, doi: 10.18632/oncotarget.28032.

[20] B. J. Gentil, S. Minotti, M. Beange, R. H. Baloh, J. Julien, and H. D. Durham, "Normal role of the low-molecular-weight neurofilament protein in mitochondrial dynamics and disruption in Charcot-Marie-Tooth disease," *The FASEB Journal*, vol. 26, no. 3, pp. 1194–1203, Mar. 2012, doi: 10.1096/fj.11-196345.

[21] P.-P. Zhu *et al.*, "Transverse endoplasmic reticulum expansion in hereditary spastic paraplegia corticospinal axons," *Hum. Mol. Genet.*, vol. 31, no. 16, pp. 2779–2795, Aug. 2022, doi: 10.1093/hmg/ddac072.

[22] S. M. Dashiell, S. L. Tanner, H. C. Pant, and R. H. Quarles, "Myelin-associated glycoprotein modulates expression and phosphorylation of neuronal cytoskeletal elements and their associated kinases," *J. Neurochem.*, vol. 81, no. 6, pp. 1263–1272, Jun. 2002, doi: 10.1046/j.1471-4159.2002.00927.x.

[23] S. Kim, R. Chang, C. Teunissen, Y. Gebremichael, and A. Petzold, "Neurofilament stoichiometry simulations during neurodegeneration suggest a remarkable self-sufficient and stable in vivo protein structure," *J. Neurol. Sci.*, vol. 307, no. 1–2, pp. 132–138, Aug. 2011, doi: 10.1016/j.jns.2011.04.023.

[24] J. S. Pachter and R. K. H. Liem, "The differential appearance of neurofilament triplet polypeptides in the developing rat optic nerve," *Dev. Biol.*, vol. 103, no. 1, pp. 200–210, May 1984, doi: 10.1016/0012-1606(84)90021-6.

[25] T. , & H. G. A. Bullock, "Structure and function in the nervous systems of invertebrates.," 1965.

[26] H. Herrmann, H. Bär, L. Kreplak, S. V. Strelkov, and U. Aebi, "Intermediate filaments: from cell architecture to nanomechanics," *Nat. Rev. Mol. Cell Biol.*, vol. 8, no. 7, pp. 562–573, Jul. 2007, doi: 10.1038/nrm2197.

[27] N. Srinivasan and S. Kumar, "Ordered and disordered proteins as nanomaterial building blocks," *WIREs Nanomedicine and Nanobiotechnology*, vol. 4, no. 2, pp. 204–218, Mar. 2012, doi: 10.1002/wnan.1160.

[28] A. Yuan and R. A. Nixon, "Neurofilament Proteins as Biomarkers to Monitor Neurological Diseases and the Efficacy of Therapies," *Front. Neurosci.*, vol. 15, Sep. 2021, doi: 10.3389/fnins.2021.689938.

[29] G. Disanto *et al.*, “Serum Neurofilament light: A biomarker of neuronal damage in multiple sclerosis,” *Ann. Neurol.*, vol. 81, no. 6, pp. 857–870, Jun. 2017, doi: 10.1002/ana.24954.

[30] M. Benatar *et al.*, “Neurofilaments in pre-symptomatic ALS and the impact of genotype,” *Amyotroph. Lateral Scler. Frontotemporal Degener.*, vol. 20, no. 7–8, pp. 538–548, Oct. 2019, doi: 10.1080/21678421.2019.1646769.

[31] C. R. Jack *et al.*, “Revised criteria for diagnosis and staging of Alzheimer’s disease: Alzheimer’s Association Workgroup,” *Alzheimer’s & Dementia*, vol. 20, no. 8, pp. 5143–5169, Aug. 2024, doi: 10.1002/alz.13859.

[32] M. Khalil *et al.*, “Neurofilaments as biomarkers in neurological disorders,” *Nat. Rev. Neurol.*, vol. 14, no. 10, pp. 577–589, Oct. 2018, doi: 10.1038/s41582-018-0058-z.

[33] I. Szeverenyi *et al.*, “The Human Intermediate Filament Database: comprehensive information on a gene family involved in many human diseases,” *Hum. Mutat.*, vol. 29, no. 3, pp. 351–360, Mar. 2008, doi: 10.1002/humu.20652.

[34] M. Brenner, A. B. Johnson, O. Boespflug-Tanguy, D. Rodriguez, J. E. Goldman, and A. Messing, “Mutations in GFAP, encoding glial fibrillary acidic protein, are associated with Alexander disease,” *Nat. Genet.*, vol. 27, no. 1, pp. 117–120, Jan. 2001, doi: 10.1038/83679.

[35] D. F. Condorelli *et al.*, “Structural features of the rat GFAP gene and identification of a novel alternative transcript,” *J. Neurosci. Res.*, vol. 56, no. 3, pp. 219–228, May 1999, doi: 10.1002/(SICI)1097-4547(19990501)56:3<219::AID-JNR1>3.0.CO;2-2.

[36] D. Plantone *et al.*, “Elevated serum concentrations of GFAP in hereditary transthyretin amyloidosis since pre-symptomatic stages,” *J. Neurol.*, vol. 272, no. 5, p. 340, May 2025, doi: 10.1007/s00415-025-13072-6.

[37] E. M. Hol and M. Pekny, “Glial fibrillary acidic protein (GFAP) and the astrocyte intermediate filament system in diseases of the central nervous system,” *Curr. Opin. Cell Biol.*, vol. 32, pp. 121–130, Feb. 2015, doi: 10.1016/j.ceb.2015.02.004.

[38] N. J. Ashton *et al.*, “A multicentre validation study of the diagnostic value of plasma neurofilament light,” *Nat. Commun.*, vol. 12, no. 1, p. 3400, Jun. 2021, doi: 10.1038/s41467-021-23620-z.

[39] A. Pichet Binette *et al.*, “Confounding factors of Alzheimer’s disease plasma biomarkers and their impact on clinical performance,” *Alzheimer’s & Dementia*, vol. 19, no. 4, pp. 1403–1414, Apr. 2023, doi: 10.1002/alz.12787.

[40] I. C. Fontana, A. Kumar, and A. Nordberg, “The role of astrocytic α7 nicotinic acetylcholine receptors in Alzheimer disease,” *Nat. Rev. Neurol.*, vol. 19, no. 5, pp. 278–288, May 2023, doi: 10.1038/s41582-023-00792-4.

[41] M. T. Heneka, J. J. Rodríguez, and A. Verkhratsky, “Neuroglia in neurodegeneration,” *Brain Res. Rev.*, vol. 63, no. 1–2, pp. 189–211, May 2010, doi: 10.1016/j.brainresrev.2009.11.004.

[42] I. C. Fontana, A. Kumar, and A. Nordberg, “The role of astrocytic α7 nicotinic acetylcholine receptors in Alzheimer disease,” *Nat. Rev. Neurol.*, vol. 19, no. 5, pp. 278–288, May 2023, doi: 10.1038/s41582-023-00792-4.

[43] J. Wischhusen, I. Melero, and W. H. Fridman, “Growth/Differentiation Factor-15 (GDF-15): From Biomarker to Novel Targetable Immune Checkpoint,” *Front. Immunol.*, vol. 11, May 2020, doi: 10.3389/fimmu.2020.00951.

[44] M. R. Bootcov *et al.*, “MIC-1, a novel macrophage inhibitory cytokine, is a divergent member of the TGF-β superfamily,” *Proceedings of the National Academy of Sciences*, vol. 94, no. 21, pp. 11514–11519, Oct. 1997, doi: 10.1073/pnas.94.21.11514.

[45] M. Wesseling, J. H. C. de Poel, and S. C. A. de Jager, “Growth differentiation factor 15 in adverse cardiac remodelling: from biomarker to causal player,” *ESC Heart Fail.*, vol. 7, no. 4, pp. 1488–1501, Aug. 2020, doi: 10.1002/ehf2.12728.

[46] K. Unsicker, B. Spittau, and K. Krieglstein, “The multiple facets of the TGF-β family cytokine growth/differentiation factor-15/macrophage inhibitory cytokine-1,” *Cytokine Growth Factor Rev.*, vol. 24, no. 4, pp. 373–384, Aug. 2013, doi: 10.1016/j.cytogfr.2013.05.003.

[47] J. Reyes and G. S. Yap, “Emerging Roles of Growth Differentiation Factor 15 in Immunoregulation and Pathogenesis,” *The Journal of Immunology*, vol. 210, no. 1, pp. 5–11, Jan. 2023, doi: 10.4049/jimmunol.2200641.

[48] X. Xue, L. Tao, D. Su, C. Guo, and H. Liu, “Diagnostic utility of GDF15 in neurodegenerative diseases: A systematic review and meta-analysis,” *Brain Behav.*, vol. 12, no. 2, Feb. 2022, doi: 10.1002/brb3.2502.

[49] V. Machado *et al.*, “Growth/differentiation factor-15 deficiency compromises dopaminergic neuron survival and microglial response in the 6-hydroxydopamine mouse model of Parkinson’s disease,” *Neurobiol. Dis.*, vol. 88, pp. 1–15, Apr. 2016, doi: 10.1016/j.nbd.2015.12.016.

[50] S. N. Breit *et al.*, “The TGF-β superfamily cytokine, MIC-1/GDF15: A pleotrophic cytokine with roles in inflammation, cancer and metabolism,” *Growth Factors*, vol. 29, no. 5, pp. 187–195, Oct. 2011, doi: 10.3109/08977194.2011.607137.

[51] Y. M. Ayala *et al.*, “TDP-43 regulates its mRNA levels through a negative feedback loop,” *EMBO J.*, vol. 30, no. 2, pp. 277–288, Jan. 2011, doi: 10.1038/emboj.2010.310.

[52] S. C. Vatsavayai *et al.*, “Timing and significance of pathological features in *C9orf72* expansion-associated frontotemporal dementia,” *Brain*, vol. 139, no. 12, pp. 3202–3216, Dec. 2016, doi: 10.1093/brain/aww250.

[53] A. L. Nana *et al.*, “Neurons selectively targeted in frontotemporal dementia reveal early stage TDP-43 pathobiology,” *Acta Neuropathol.*, vol. 137, no. 1, pp. 27–46, Jan. 2019, doi: 10.1007/s00401-018-1942-8.

[54] A. Meneses, S. Koga, J. O’Leary, D. W. Dickson, G. Bu, and N. Zhao, “TDP-43 Pathology in Alzheimer’s Disease,” *Mol. Neurodegener.*, vol. 16, no. 1, p. 84, Dec. 2021, doi: 10.1186/s13024-021-00503-x.

[55] R. Romano, V. S. Del Fiore, and C. Bucci, “Role of the Intermediate Filament Protein Peripherin in Health and Disease,” *Int. J. Mol. Sci.*, vol. 23, no. 23, p. 15416, Dec. 2022, doi: 10.3390/ijms232315416.

[56] M. A. Thompson and E. B. Ziff, “Structure of the gene encoding Peripherin, an NGF-regulated neuronal-specific type III intermediate filament protein,” *Neuron*, vol. 2, no. 1, pp. 1043–1053, Jan. 1989, doi: 10.1016/0896-6273(89)90228-6.

[57] D. G. Leonard, J. D. Gorham, P. Cole, L. A. Greene, and E. B. Ziff, “A nerve growth factor-regulated messenger RNA encodes a new intermediate filament protein.,” *J. Cell Biol.*, vol. 106, no. 1, pp. 181–193, Jan. 1988, doi: 10.1083/jcb.106.1.181.

[58] J.-M. Beaulieu, J. Kriz, and J.-P. Julien, “Induction of peripherin expression in subsets of brain neurons after lesion injury or cerebral ischemia,” *Brain Res.*, vol. 946, no. 2, pp. 153–161, Aug. 2002, doi: 10.1016/S0006-8993(02)02830-5.

[59] C. M. Troy, N. A. Muma, L. A. Greene, D. L. Price, and M. L. Shelanski, “Regulation of peripherin and neurofilament expression in regenerating rat motor neurons,” *Brain Res.*, vol. 529, no. 1–2, pp. 232–238, Oct. 1990, doi: 10.1016/0006-8993(90)90832-V.

[60] B. T. Helfand, M. G. Mendez, J. Pugh, C. Delsert, and R. D. Goldman, “A Role for Intermediate Filaments in Determining and Maintaining the Shape of Nerve Cells,” *Mol. Biol. Cell*, vol. 14, no. 12, pp. 5069–5081, Dec. 2003, doi: 10.1091/mbc.e03-06-0376.

[61] R. C. Larivière, A. Ribeiro-da-Silva, and J. -P. Julien, “Reduced number of unmyelinated sensory axons in peripherin null mice,” *J. Neurochem.*, vol. 81, no. 3, pp. 525–532, May 2002, doi: 10.1046/j.1471-4159.2002.00853.x.

[62] A. Yuan *et al.*, “Peripherin Is a Subunit of Peripheral Nerve Neurofilaments: Implications for Differential Vulnerability of CNS and Peripheral Nervous System Axons,” *Journal of Neuroscience*, vol. 32, no. 25, pp. 8501–8508, Jun. 2012, doi: 10.1523/JNEUROSCI.1081-12.2012.

[63] T. Fang *et al.*, “Peripherin: A proposed biomarker of traumatic axonal injury triggered by mechanical force,” *European Journal of Neuroscience*, vol. 58, no. 5, pp. 3206–3225, Sep. 2023, doi: 10.1111/ejn.16111.

[64] M. Barclay, P. G. Noakes, A. F. Ryan, J.-P. Julien, and G. D. Housley, “Neuronal expression of peripherin, a type III intermediate filament protein, in the mouse hindbrain,” *Histochem. Cell Biol.*, vol. 128, no. 6, pp. 541–550, Nov. 2007, doi: 10.1007/s00418-007-0340-4.

[65] G. Song, Y. Cui, N. Zhong, and J. Han, “Proteomic characterisation of pancreatic islet β-cells stimulated with pancreatic carcinoma cell conditioned medium,” *J. Clin. Pathol.*, vol. 62, no. 9, pp. 802–807, Sep. 2009, doi: 10.1136/jcp.2009.065391.

[66] C. Boitard *et al.*, “Peripherin: an islet antigen that is cross-reactive with nonobese diabetic mouse class II gene products.,” *Proceedings of the National Academy of Sciences*, vol. 89, no. 1, pp. 172–176, Jan. 1992, doi: 10.1073/pnas.89.1.172.

[67] S. M. G. LA Aletta JM, “Phosphorylation of the peripherin 58-kDa neuronal intermediate filament protein. Regulation by nerve growth factor and other agents.,” *J Biol Chem.*.

[68] E. Sterneck, D. R. Kaplan, and P. F. Johnson, “Interleukin-6 Induces Expression of Peripherin and Cooperates with Trk Receptor Signaling to Promote Neuronal Differentiation in PC12 Cells,” *J. Neurochem.*, vol. 67, no. 4, pp. 1365–1374, Oct. 1996, doi: 10.1046/j.1471-4159.1996.67041365.x.

[69] D.-Y. Choi *et al.*, “Fibroblast Growth Factor Receptor 3 Induces Gene Expression Primarily through Ras-independent Signal Transduction Pathways,” *Journal of Biological Chemistry*, vol. 276, no. 7, pp. 5116–5122, Feb. 2001, doi: 10.1074/jbc.M002959200.

[70] G. Cappelletti, M. G. Maggioni, C. Ronchi, R. Maci, and G. Tedeschi, “Protein tyrosine nitration is associated with cold- and drug-resistant microtubules in neuronal-like PC12 cells,” *Neurosci. Lett.*, vol. 401, no. 1–2, pp. 159–164, Jun. 2006, doi: 10.1016/j.neulet.2006.03.009.

[71] G. Tedeschi *et al.*, “Tyrosine Nitration is a Novel Post-translational Modification Occurring on the Neural Intermediate Filament Protein Peripherin,” *Neurochem. Res.*, vol. 32, no. 3, pp. 433–441, Feb. 2007, doi: 10.1007/s11064-006-9244-2.

[72] L. Cogli *et al.*, “Charcot–Marie–Tooth type 2B disease-causing RAB7A mutant proteins show altered interaction with the neuronal intermediate filament peripherin,” *Acta Neuropathol.*, vol. 125, no. 2, pp. 257–272, Feb. 2013, doi: 10.1007/s00401-012-1063-8.

[73] M. L. Styers, G. Salazar, R. Love, A. A. Peden, A. P. Kowalczyk, and V. Faundez, “**The Endo-Lysosomal Sorting Machinery Interacts with the Intermediate Filament Cytoskeleton**,” *Mol. Biol. Cell*, vol. 15, no. 12, pp. 5369–5382, Dec. 2004, doi: 10.1091/mbc.e04-03-0272.

[74] B. J. Gentil, J. R. McLean, S. Xiao, B. Zhao, H. D. Durham, and J. Robertson, “A two-hybrid screen identifies an unconventional role for the intermediate filament peripherin in regulating the subcellular distribution of the SNAP25-interacting protein, SIP30,” *J. Neurochem.*, vol. 131, no. 5, pp. 588–601, Dec. 2014, doi: 10.1111/jnc.12928.

[75] V. Muresan, C. Villegas, and Z. Ladescu Muresan, “Functional Interaction between Amyloid-β Precursor Protein and Peripherin Neurofilaments: A Shared Pathway Leading to Alzheimer’s Disease and Amyotrophic Lateral Sclerosis?,” *Neurodegener. Dis.*, vol. 13, no. 2–3, pp. 122–125, 2014, doi: 10.1159/000354238.

[76] L. Sunesson, U. Hellman, and C. Larsson, “Protein Kinase Cϵ Binds Peripherin and Induces Its Aggregation, Which Is Accompanied by Apoptosis of Neuroblastoma Cells,” *Journal of Biological Chemistry*, vol. 283, no. 24, pp. 16653–16664, Jun. 2008, doi: 10.1074/jbc.M710436200.

[77] D. Plantone *et al.*, “Brain neuronal and glial damage during acute COVID-19 infection in absence of clinical neurological manifestations,” *J. Neurol. Neurosurg. Psychiatry*, p. jnnp-2022-329933, Sep. 2022, doi: 10.1136/jnnp-2022-329933.

[78] D. Plantone *et al.*, “Elevated serum concentrations of GFAP in hereditary transthyretin amyloidosis since pre-symptomatic stages,” *J. Neurol.*, vol. 272, no. 5, p. 340, May 2025, doi: 10.1007/s00415-025-13072-6.

[79] E. Andersson *et al.*, “Blood and cerebrospinal fluid neurofilament light differentially detect neurodegeneration in early Alzheimer’s disease,” *Neurobiol. Aging*, vol. 95, pp. 143–153, Nov. 2020, doi: 10.1016/j.neurobiolaging.2020.07.018.

[80] S. Halbgebauer *et al.*, “Comparison of CSF and serum neurofilament light and heavy chain as differential diagnostic biomarkers for ALS,” *J. Neurol. Neurosurg. Psychiatry*, vol. 93, no. 1, pp. 68–74, Jan. 2022, doi: 10.1136/jnnp-2021-327129.

[81] A. L. Wojdała *et al.*, “Trajectories of CSF and plasma biomarkers across Alzheimer’s disease continuum: disease staging by NF-L, p-tau181, and GFAP,” *Neurobiol. Dis.*, vol. 189, p. 106356, Dec. 2023, doi: 10.1016/j.nbd.2023.106356.

[82] M. Watanabe *et al.*, “Serum GFAP and neurofilament light as biomarkers of disease activity and disability in NMOSD,” *Neurology*, vol. 93, no. 13, Sep. 2019, doi: 10.1212/WNL.0000000000008160.

[83] K. Koerbel *et al.*, “Evaluating the utility of serum NfL, GFAP, UCHL1 and tTAU as estimates of CSF levels and diagnostic instrument in neuroinflammation and multiple sclerosis,” *Mult. Scler. Relat. Disord.*, vol. 87, p. 105644, Jul. 2024, doi: 10.1016/j.msard.2024.105644.

[84] T. Kasai *et al.*, “Combined use of CSF NfL and CSF TDP-43 improves diagnostic performance in ALS,” *Ann. Clin. Transl. Neurol.*, vol. 6, no. 12, pp. 2489–2502, Dec. 2019, doi: 10.1002/acn3.50943.

[85] L. Álvarez-Sánchez *et al.*, “Assessment of Plasma and Cerebrospinal Fluid Biomarkers in Different Stages of Alzheimer’s Disease and Frontotemporal Dementia,” *Int. J. Mol. Sci.*, vol. 24, no. 2, p. 1226, Jan. 2023, doi: 10.3390/ijms24021226.

[86] E. Feneberg *et al.*, “Limited role of free TDP-43 as a diagnostic tool in neurodegenerative diseases,” *Amyotroph. Lateral Scler. Frontotemporal Degener.*, vol. 15, no. 5–6, pp. 351–356, Sep. 2014, doi: 10.3109/21678421.2014.905606.

[87] A. L. Wojdała *et al.*, “Trajectories of CSF and plasma biomarkers across Alzheimer’s disease continuum: disease staging by NF-L, p-tau181, and GFAP,” *Neurobiol. Dis.*, vol. 189, p. 106356, Dec. 2023, doi: 10.1016/j.nbd.2023.106356.

[88] T. Kasai *et al.*, “Combined use of CSF NfL and CSF TDP-43 improves diagnostic performance in ALS,” *Ann. Clin. Transl. Neurol.*, vol. 6, no. 12, pp. 2489–2502, Dec. 2019, doi: 10.1002/acn3.50943.

[89] G. Primiano *et al.*, “Comparative Analysis of <scp>SiMoA</scp> and Ella Immunoassay Platforms for Measuring Serum Neurofilament Light Chain Levels in <scp>ATTRv</scp> With Polyneuropathy and Presymptomatic Carriers,” *Eur. J. Neurol.*, vol. 32, no. 6, Jun. 2025, doi: 10.1111/ene.70215.

[90] A. Gauthier *et al.*, “Comparison of Simoa ™ and Ella ™ to assess serum neurofilament-light chain in multiple sclerosis,” *Ann. Clin. Transl. Neurol.*, vol. 8, no. 5, pp. 1141–1150, May 2021, doi: 10.1002/acn3.51355.

[91] M. Nötzel, L. I. Werder, T. Ziemssen, and K. Akgün, “Ella versus Simoa Serum Neurofilament Assessment to Monitor Treatment Response in Highly Active Multiple Sclerosis Patients,” *Int. J. Mol. Sci.*, vol. 23, no. 20, p. 12361, Oct. 2022, doi: 10.3390/ijms232012361.

[92] D. Vecchio *et al.*, “Serum and cerebrospinal fluid neurofilament light chains measured by SIMOA™, Ella™, and Lumipulse™ in multiple sclerosis naïve patients.,” *Mult. Scler. Relat. Disord.*, vol. 82, p. 105412, Feb. 2024, doi: 10.1016/j.msard.2023.105412.

[93] M. Truffi *et al.*, “Neurofilament-light chain quantification by Simoa and Ella in plasma from patients with dementia: a comparative study,” *Sci. Rep.*, vol. 13, no. 1, p. 4041, Mar. 2023, doi: 10.1038/s41598-023-29704-8.

[94] A. Gauthier *et al.*, “Comparison of Simoa ™ and Ella ™ to assess serum neurofilament-light chain in multiple sclerosis,” *Ann. Clin. Transl. Neurol.*, vol. 8, no. 5, pp. 1141–1150, May 2021, doi: 10.1002/acn3.51355.

[95] D. Plantone *et al.*, “CSF IL-6, GDF-15, GFAP and NfL levels in early Alzheimer disease: a pilot study,” *Ther. Adv. Neurol. Disord.*, vol. 18, Jan. 2025, doi: 10.1177/17562864251314773.

[96] J. E. Baulch, M. M. Acharya, S. Agrawal, L. A. Apodaca, C. Monteiro, and A. Agrawal, “Immune and Inflammatory Determinants Underlying Alzheimer’s Disease Pathology,” *Journal of Neuroimmune Pharmacology*, vol. 15, no. 4, pp. 852–862, Dec. 2020, doi: 10.1007/s11481-020-09908-9.

[97] S. Bhatia, R. Rawal, P. Sharma, T. Singh, M. Singh, and V. Singh, “Mitochondrial Dysfunction in Alzheimer’s Disease: Opportunities for Drug Development,” *Curr. Neuropharmacol.*, vol. 20, no. 4, pp. 675–692, Apr. 2022, doi: 10.2174/1570159X19666210517114016.

[98] P. Grant and H. C. Pant, “Neurofilament protein synthesis and phosphorylation,” *J. Neurocytol.*, vol. 29, no. 11–12, pp. 843–872, Nov. 2000, doi: 10.1023/A:1010999509251.

[99] A. Chiariello *et al.*, “The expression pattern of GDF15 in human brain changes during aging and in Alzheimer’s disease,” *Front. Aging Neurosci.*, vol. 14, Jan. 2023, doi: 10.3389/fnagi.2022.1058665.

[100] M. A. Beydoun *et al.*, “GDF15 and its association with cognitive performance over time in a longitudinal study of middle-aged urban adults,” *Brain Behav. Immun.*, vol. 108, pp. 340–349, Feb. 2023, doi: 10.1016/j.bbi.2022.12.015.

[101] M. A. Busche and B. T. Hyman, “Synergy between amyloid-β and tau in Alzheimer’s disease,” *Nat. Neurosci.*, vol. 23, no. 10, pp. 1183–1193, Oct. 2020, doi: 10.1038/s41593-020-0687-6.

[102] D. H. Kim *et al.*, “Effect of growth differentiation factor-15 secreted by human umbilical cord blood-derived mesenchymal stem cells on amyloid beta levels in in vitro and in vivo models of Alzheimer’s disease,” *Biochem. Biophys. Res. Commun.*, vol. 504, no. 4, pp. 933–940, Oct. 2018, doi: 10.1016/j.bbrc.2018.09.012.

[103] C. Carrillo-García *et al.*, “Growth/differentiation factor 15 promotes EGFR signalling, and regulates proliferation and migration in the hippocampus of neonatal and young adult mice,” *Development*, vol. 141, no. 4, pp. 773–783, Feb. 2014, doi: 10.1242/dev.096131.

[104] T. J. Cohen, V. M. Y. Lee, and J. Q. Trojanowski, “TDP-43 functions and pathogenic mechanisms implicated in TDP-43 proteinopathies,” *Trends Mol. Med.*, vol. 17, no. 11, pp. 659–667, Nov. 2011, doi: 10.1016/j.molmed.2011.06.004.

[105] J. R. Tollervey *et al.*, “Characterizing the RNA targets and position-dependent splicing regulation by TDP-43,” *Nat. Neurosci.*, vol. 14, no. 4, pp. 452–458, Apr. 2011, doi: 10.1038/nn.2778.

[106] J. Zhu, M. S. Cynader, and W. Jia, “TDP-43 Inhibits NF-κB Activity by Blocking p65 Nuclear Translocation,” *PLoS One*, vol. 10, no. 11, p. e0142296, Nov. 2015, doi: 10.1371/journal.pone.0142296.

[107] H. C. Karoly, C. J. Skrzynski, E. Moe, A. D. Bryan, and K. E. Hutchison, “Investigating Associations Between Inflammatory Biomarkers, Gray Matter, Neurofilament Light and Cognitive Performance in Healthy Older Adults,” *Front. Aging Neurosci.*, vol. 13, Sep. 2021, doi: 10.3389/fnagi.2021.719553.

[108] A. L. Marsland, P. J. Gianaros, S. M. Abramowitch, S. B. Manuck, and A. R. Hariri, “Interleukin-6 Covaries Inversely with Hippocampal Grey Matter Volume in Middle-Aged Adults,” *Biol. Psychiatry*, vol. 64, no. 6, pp. 484–490, Sep. 2008, doi: 10.1016/j.biopsych.2008.04.016.

[109] C. S. Nicolas *et al.*, “The role of JAK-STAT signaling within the CNS,” *JAKSTAT*, vol. 2, no. 1, p. e22925, Jan. 2013, doi: 10.4161/jkst.22925.

[110] H. Lin *et al.*, “p38 MAPK Is a Major Regulator of Amyloid Beta-Induced IL-6 Expression in Human Microglia,” *Mol. Neurobiol.*, vol. 59, no. 9, pp. 5284–5298, Sep. 2022, doi: 10.1007/s12035-022-02909-0.

[111] E. Razani, A. Pourbagheri-Sigaroodi, A. Safaroghli-Azar, A. Zoghi, M. Shanaki-Bavarsad, and D. Bashash, “The PI3K/Akt signaling axis in Alzheimer’s disease: a valuable target to stimulate or suppress?,” *Cell Stress Chaperones*, vol. 26, no. 6, pp. 871–887, Nov. 2021, doi: 10.1007/s12192-021-01231-3.

[112] M. P. Mattson and S. Camandola, “NF-κB in neuronal plasticity and neurodegenerative disorders,” *Journal of Clinical Investigation*, vol. 107, no. 3, pp. 247–254, Feb. 2001, doi: 10.1172/JCI11916.

[113] K. E. Prater, C. S. Latimer, and S. Jayadev, “Glial TDP-43 and TDP-43 induced glial pathology, focus on neurodegenerative proteinopathy syndromes,” *Glia*, vol. 70, no. 2, pp. 239–255, Feb. 2022, doi: 10.1002/glia.24096.

[114] E. Stomrud, O. Hansson, H. Zetterberg, K. Blennow, L. Minthon, and E. Londos, “Correlation of Longitudinal Cerebrospinal Fluid Biomarkers With Cognitive Decline in Healthy Older Adults,” *Arch. Neurol.*, vol. 67, no. 2, Feb. 2010, doi: 10.1001/archneurol.2009.316.

[115] M. Radanovic, C. A. Oshiro, T. Q. Freitas, L. L. Talib, and O. V. Forlenza, “Correlation between CSF biomarkers of Alzheimer’s disease and global cognition in a psychogeriatric clinic cohort,” *Brazilian Journal of Psychiatry*, vol. 41, no. 6, pp. 479–484, Dec. 2019, doi: 10.1590/1516-4446-2018-0296.

[116] D. Galasko *et al.*, “Assessment of CSF levels of tau protein in mildly demented patients with Alzheimer’s disease,” *Neurology*, vol. 48, no. 3, pp. 632–635, Mar. 1997, doi: 10.1212/WNL.48.3.632.

[117] D. Plantone *et al.*, “Elevated serum concentrations of GFAP in hereditary transthyretin amyloidosis since pre-symptomatic stages,” *J. Neurol.*, vol. 272, no. 5, p. 340, May 2025, doi: 10.1007/s00415-025-13072-6.

[118] Y. Sekijima, “Transthyretin-type cerebral amyloid angiopathy: a serious complication in post-transplant patients with familial amyloid polyneuropathy,” *J. Neurol. Neurosurg. Psychiatry*, vol. 86, no. 2, pp. 124–124, Feb. 2015, doi: 10.1136/jnnp-2014-308576.

[119] R. Taipa *et al.*, “Neuropathology of central nervous system involvement in TTR amyloidosis,” *Acta Neuropathol.*, vol. 145, no. 1, pp. 113–126, Jan. 2023, doi: 10.1007/s00401-022-02501-9.

[120] Z. Yang and K. K. W. Wang, “Glial fibrillary acidic protein: from intermediate filament assembly and gliosis to neurobiomarker,” *Trends Neurosci.*, vol. 38, no. 6, pp. 364–374, Jun. 2015, doi: 10.1016/j.tins.2015.04.003.

[121] Z. Yang and K. K. W. Wang, “Glial fibrillary acidic protein: from intermediate filament assembly and gliosis to neurobiomarker,” *Trends Neurosci.*, vol. 38, no. 6, pp. 364–374, Jun. 2015, doi: 10.1016/j.tins.2015.04.003.

[122] K. R. Jessen and R. Mirsky, “Signaling pathways that regulate glial development and early migration—Schwann cells,” in *Patterning and Cell Type Specification in the Developing CNS and PNS*, Elsevier, 2020, pp. 953–975. doi: 10.1016/B978-0-12-814405-3.00039-4.

[123] K. R. Jessen and R. Mirsky, “Schwann Cell Precursors; Multipotent Glial Cells in Embryonic Nerves,” *Front. Mol. Neurosci.*, vol. 12, Mar. 2019, doi: 10.3389/fnmol.2019.00069.

[124] M. Luigetti *et al.*, “Gastrointestinal Manifestations in Hereditary Transthyretin Amyloidosis: a Single-Centre Experience,” *Journal of Gastrointestinal and Liver Diseases*, vol. 29, no. 3, pp. 339–343, Sep. 2020, doi: 10.15403/jgld-2474.

[125] E. Galosi *et al.*, “Serum neurofilament light chain levels correlate with small fiber related parameters in patients with hereditary transthyretin amyloidosis with polyneuropathy (ATTRv-PN),” *Neurological Sciences*, vol. 45, no. 10, pp. 5023–5032, Oct. 2024, doi: 10.1007/s10072-024-07562-0.

[126] F. I. D. S. HORTAJDA S, “PORTUGUESE POLYNEURITIC FAMILIAL TYPE OF AMYLOIDOSIS.,” *Pathol Microbiol*.

[127] C. ANDRADE, “A PECULIAR FORM OF PERIPHERAL NEUROPATHY,” *Brain*, vol. 75, no. 3, pp. 408–427, 1952, doi: 10.1093/brain/75.3.408.

[128] A. L. Benedet *et al.*, “Differences Between Plasma and Cerebrospinal Fluid Glial Fibrillary Acidic Protein Levels Across the Alzheimer Disease Continuum,” *JAMA Neurol.*, vol. 78, no. 12, p. 1471, Dec. 2021, doi: 10.1001/jamaneurol.2021.3671.

[129] M. Santos-Galindo, E. Acaz-Fonseca, M. J. Bellini, and L. M. Garcia-Segura, “Sex differences in the inflammatory response of primary astrocytes to lipopolysaccharide,” *Biol. Sex Differ.*, vol. 2, no. 1, p. 7, Dec. 2011, doi: 10.1186/2042-6410-2-7.

[130] N. M. Conejo *et al.*, “Influence of gonadal steroids on the glial fibrillary acidic protein-immunoreactive astrocyte population in young rat hippocampus,” *J. Neurosci. Res.*, vol. 79, no. 4, pp. 488–494, Feb. 2005, doi: 10.1002/jnr.20372.

[131] C. Arias, A. Zepeda, K. Hernández-Ortega, P. Leal-Galicia, C. Lojero, and I. Camacho-Arroyo, “Sex and estrous cycle-dependent differences in glial fibrillary acidic protein immunoreactivity in the adult rat hippocampus,” *Horm. Behav.*, vol. 55, no. 1, pp. 257–263, Jan. 2009, doi: 10.1016/j.yhbeh.2008.10.016.

[132] S. K. Amateau and M. M. McCarthy, “Sexual Differentiation of Astrocyte Morphology in the Developing Rat Preoptic Area,” *J. Neuroendocrinol.*, vol. 14, no. 11, pp. 904–910, Nov. 2002, doi: 10.1046/j.1365-2826.2002.00858.x.

[133] L. Dion-Albert, L. Bandeira Binder, B. Daigle, A. Hong-Minh, M. Lebel, and C. Menard, “Sex differences in the blood–brain barrier: Implications for mental health,” *Front. Neuroendocrinol.*, vol. 65, p. 100989, Apr. 2022, doi: 10.1016/j.yfrne.2022.100989.

[134] F. Notturno, M. Capasso, A. Delauretis, M. Carpo, and A. Uncini, “Glial fibrillary acidic protein as a marker of axonal damage in chronic neuropathies,” *Muscle Nerve*, vol. 40, no. 1, pp. 50–54, Jul. 2009, doi: 10.1002/mus.21323.

[135] P. Benkert *et al.*, “Serum neurofilament light chain for individual prognostication of disease activity in people with multiple sclerosis: a retrospective modelling and validation study,” *Lancet Neurol.*, vol. 21, no. 3, pp. 246–257, Mar. 2022, doi: 10.1016/S1474-4422(22)00009-6.

[136] P. Benkert *et al.*, “Serum Glial Fibrillary Acidic Protein and Neurofilament Light Chain Levels Reflect Different Mechanisms of Disease Progression under B-Cell Depleting Treatment in Multiple Sclerosis,” *Ann. Neurol.*, vol. 97, no. 1, pp. 104–115, Jan. 2025, doi: 10.1002/ana.27096.

[137] D. Balschun *et al.*, “Interleukin-6: a cytokine to forget,” *The FASEB Journal*, vol. 18, no. 14, pp. 1788–1790, Nov. 2004, doi: 10.1096/fj.04-1625fje.

[138] T. E. Nelson *et al.*, “Altered synaptic transmission in the hippocampus of transgenic mice with enhanced central nervous systems expression of interleukin-6,” *Brain Behav. Immun.*, vol. 26, no. 6, pp. 959–971, Aug. 2012, doi: 10.1016/j.bbi.2012.05.005.

[139] A. F. Richwine *et al.*, “Architectural changes to CA1 pyramidal neurons in adult and aged mice after peripheral immune stimulation,” *Psychoneuroendocrinology*, vol. 33, no. 10, pp. 1369–1377, Nov. 2008, doi: 10.1016/j.psyneuen.2008.08.003.

[140] A. J. Kiliaan, I. A. C. Arnoldussen, and D. R. Gustafson, “Adipokines: a link between obesity and dementia?,” *Lancet Neurol.*, vol. 13, no. 9, pp. 913–923, Sep. 2014, doi: 10.1016/S1474-4422(14)70085-7.

[141] C. Zheng, X.-W. Zhou, and J.-Z. Wang, “The dual roles of cytokines in Alzheimer’s disease: update on interleukins, TNF-α, TGF-β and IFN-γ,” *Transl. Neurodegener.*, vol. 5, no. 1, p. 7, Dec. 2016, doi: 10.1186/s40035-016-0054-4.

[142] L. Thirumangalakudi *et al.*, “High cholesterol-induced neuroinflammation and amyloid precursor protein processing correlate with loss of working memory in mice,” *J. Neurochem.*, vol. 106, no. 1, pp. 475–485, Jul. 2008, doi: 10.1111/j.1471-4159.2008.05415.x.

[143] A. Neto, A. Fernandes, and A. Barateiro, “The complex relationship between obesity and neurodegenerative diseases: an updated review,” *Front. Cell. Neurosci.*, vol. 17, Nov. 2023, doi: 10.3389/fncel.2023.1294420.

[144] V. D. D’Agati *et al.*, “Obesity-related glomerulopathy: clinical and pathologic characteristics and pathogenesis,” *Nat. Rev. Nephrol.*, vol. 12, no. 8, pp. 453–471, Aug. 2016, doi: 10.1038/nrneph.2016.75.

[145] H. Zetterberg and K. Blennow, “From Cerebrospinal Fluid to Blood: The Third Wave of Fluid Biomarkers for Alzheimer’s Disease,” *Journal of Alzheimer’s Disease*, vol. 64, no. s1, pp. S271–S279, Jun. 2018, doi: 10.3233/JAD-179926.

[146] J. Bergman *et al.*, “Neurofilament light in CSF and serum is a sensitive marker for axonal white matter injury in MS,” *Neurol. Neuroimmunol. Neuroinflamm.*, vol. 3, no. 5, Oct. 2016, doi: 10.1212/NXI.0000000000000271.

[147] E. P. Thelin *et al.*, “Serial Sampling of Serum Protein Biomarkers for Monitoring Human Traumatic Brain Injury Dynamics: A Systematic Review,” *Front. Neurol.*, vol. 8, Jul. 2017, doi: 10.3389/fneur.2017.00300.

[148] R. D. Welch *et al.*, “Modeling the Kinetics of Serum Glial Fibrillary Acidic Protein, Ubiquitin Carboxyl-Terminal Hydrolase-L1, and S100B Concentrations in Patients with Traumatic Brain

Injury," *J. Neurotrauma*, vol. 34, no. 11, pp. 1957–1971, Jun. 2017, doi: 10.1089/neu.2016.4772.

[149] L. Papa *et al.*, "Time Course and Diagnostic Accuracy of Glial and Neuronal Blood Biomarkers GFAP and UCH-L1 in a Large Cohort of Trauma Patients With and Without Mild Traumatic Brain Injury," *JAMA Neurol.*, vol. 73, no. 5, p. 551, May 2016, doi: 10.1001/jamaneurol.2016.0039.

[150] I. Conceição *et al.*, "Early diagnosis of ATTR amyloidosis through targeted follow-up of identified carriers of *TTR* gene mutations*," *Amyloid*, vol. 26, no. 1, pp. 3–9, Jan. 2019, doi: 10.1080/13506129.2018.1556156.

[151] L. Turner-Stokes, A. Thu, H. Williams, R. Casey, H. Rose, and R. J. Siegert, "The Neurological Impairment Scale: reliability and validity as a predictor of functional outcome in neurorehabilitation," *Disabil. Rehabil.*, vol. 36, no. 1, pp. 23–31, Jan. 2014, doi: 10.3109/09638288.2013.775360.

[152] J.-M. Beaulieu, M. D. Nguyen, and J.-P. Julien, "Late Onset Death of Motor Neurons in Mice Overexpressing Wild-Type Peripherin," *J. Cell Biol.*, vol. 147, no. 3, pp. 531–544, Nov. 1999, doi: 10.1083/jcb.147.3.531.

[153] D. G. Leonard, J. D. Gorham, P. Cole, L. A. Greene, and E. B. Ziff, "A nerve growth factor-regulated messenger RNA encodes a new intermediate filament protein.," *J. Cell Biol.*, vol. 106, no. 1, pp. 181–193, Jan. 1988, doi: 10.1083/jcb.106.1.181.

[154] R. Romano, V. S. Del Fiore, and C. Bucci, "Role of the Intermediate Filament Protein Peripherin in Health and Disease," *Int. J. Mol. Sci.*, vol. 23, no. 23, p. 15416, Dec. 2022, doi: 10.3390/ijms232315416.

[155] J.-P. Julien and W. E. Mushynski, "Neurofilaments in Health and Disease," 1998, pp. 1–23. doi: 10.1016/S0079-6603(08)60823-5.

[156] J.-M. Beaulieu, J. Robertson, and J.-P. Julien, "Interactions between peripherin and neurofilaments in cultured cells: disruption of peripherin assembly by the NF-M and NF-H subunits," *Biochemistry and Cell Biology*, vol. 77, no. 1, pp. 41–45, Mar. 1999, doi: 10.1139/o99-003.

[157] C. M. Troy, N. A. Muma, L. A. Greene, D. L. Price, and M. L. Shelanski, "Regulation of peripherin and neurofilament expression in regenerating rat motor neurons," *Brain Res.*, vol. 529, no. 1–2, pp. 232–238, Oct. 1990, doi: 10.1016/0006-8993(90)90832-V.

[158] S. Keddie *et al.*, "Peripherin is a biomarker of axonal damage in peripheral nervous system disease," *Brain*, vol. 146, no. 11, pp. 4562–4573, Nov. 2023, doi: 10.1093/brain/awad234.

[159] D. Sabbatini *et al.*, "Evaluation of peripherin in biofluids of patients with motor neuron diseases," *Ann. Clin. Transl. Neurol.*, vol. 8, no. 8, pp. 1750–1754, Aug. 2021, doi: 10.1002/acn3.51419.

[160] M. Vizziello *et al.*, "TDP-43 seeding activity in the olfactory mucosa of patients with amyotrophic lateral sclerosis," *Mol. Neurodegener.*, vol. 20, no. 1, p. 49, Apr. 2025, doi: 10.1186/s13024-025-00833-0.

[161] E. Borberg *et al.*, "Digital seed amplification assay for TDP-43 aggregate quantification in CSF," Oct. 15, 2025. doi: 10.1101/2025.10.14.25338017.